Comparing Storage Duration in Hybrid Power Plants

Multi-Market Participation of Wind Power with Li-Ion Batteries and Liquid Piston CAES Considering Degradation

Master of Science Thesis

by

Werner Léon Kastelein

February 25, 2026

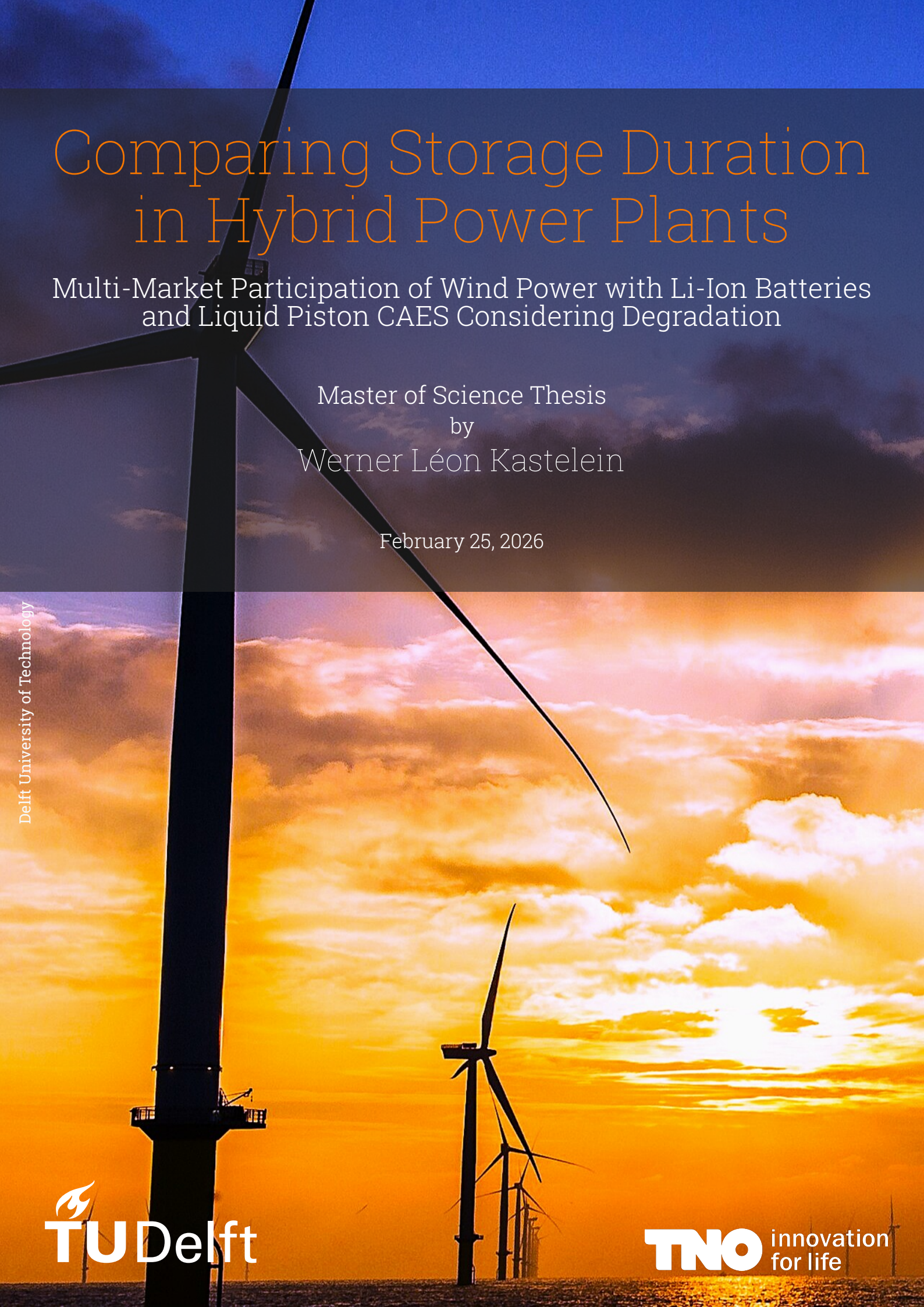

Delft University of Technology

TU Delft

TNO innovation for life

Comparing Storage Duration in Hybrid Power Plants

Multi-Market Participation of Wind Power with Li-Ion Batteries and Liquid Piston CAES Considering Degradation

by

Werner Léon Kastelein

to obtain the degree of Master of Science
in Sustainable Energy Technology at Delft University of Technology.

to be defended publicly at the Faculty of Aerospace Engineering
on March 11, 2026, at 14:00.

Thesis committee

Chair	Dr. ir. M.B. Zaaijer	Delft University of Technology
Supervisor	Dr. ir. J. Iori	Delft University of Technology
External examiner	Dr. ir. A. Jarquin Laguna	Delft University of Technology
Company supervisor	ir. M. Houwing	Netherlands Organisation for Applied Scientific Research
Company co-supervisor	ir. B.J. Klootwijk	Netherlands Organisation for Applied Scientific Research

An electronic version of this thesis is available at `http://repository.tudelft.nl/`.

MSc Sustainable Energy Technology,
Faculty Electrical Engineering, Mathematics and Computer Science, Delft University of Technology.

Abstract

Offshore wind is expected to become the largest energy source in the Netherlands. However, its economic viability has come under increasing pressure. Integrating energy storage with wind generation offers a potential solution by enhancing system flexibility and enabling additional revenues through multi-market participation. Hybrid Power Plants (HPPs) combine generation and storage technologies within a single system. This study investigates how the integration of short- and long-duration energy storage affects the profitability of wind-based HPPs operating across multiple electricity markets.

Short-duration lithium-ion (Li-ion) battery storage was compared with long-duration Liquid Piston Compressed Air Energy Storage (LPCAES). Lithium-ion batteries were evaluated while explicitly accounting for degradation, whereas LPCAES represents an emerging near-isothermal CAES technology with improved compression efficiency. Both technologies are evaluated across different energy capacities and charge/discharge rates within a multi-market framework, including participation in the day-ahead and automatic Frequency Restoration Reserve (aFRR) markets. Profitability is assessed using operational revenues and a Net Present Value analysis.

Results show that economic performance strongly depends on market conditions, storage sizing, degradation effects, and investment assumptions. Without degradation, Li-ion batteries generally outperform LPCAES in terms of profit due to higher efficiency and power capability. When degradation is considered, outcomes become year-dependent: LPCAES can achieve higher profitability under moderate price conditions and larger storage sizes, whereas Li-ion remains superior in high-price years. Overall, no single technology is universally optimal; the economically preferred option depends on the specific market environment and system configuration.

Preface

This thesis marks the completion of my MSc in Sustainable Energy Technology and brings an important phase of my academic journey to a close. The work presented here would not have been possible without the guidance, input, and support of many people along the way.

First, I would like to thank my supervisor, Jenna Iori, for her clear guidance, critical questions, and constructive feedback throughout the process. Her comments consistently helped to strengthen both the structure and the technical depth of this thesis.

I am grateful to TNO for offering me the opportunity to conduct this research within their organization and for providing access to valuable expertise and code. I would like to acknowledge my company supervisor and co-supervisor, Max Houwing and Bart Klootwijk, for their time and commitment, even during busy periods. Their flexibility, insights, and clear explanations were essential to the progress of this project. I also appreciate the constructive feedback and external perspective offered by Javier Fatou Gómez during our discussions.

My appreciation goes to Michiel Zaaijer for chairing my committee and for his valuable feedback during the midterm, which helped refine the direction and planning of this research. I would additionally like to thank Antonio Jarquin Laguna for his enthusiasm for the topic and his willingness to serve as an external examiner on my committee.

I am thankful to Daniel Buhagiar for sharing his knowledge and providing important insights into HPES/LP-CAES systems.

Also, I would like to acknowledge my family and friends for their continuous support throughout this period. A special word of appreciation goes to my girlfriend, who has always been there when I needed her, for her patience, encouragement, and the laughter along the way, especially during the most challenging periods of this thesis.

Finally, my deepest gratitude goes to my parents. Throughout my entire academic career, they have been my biggest supporters, always showing genuine interest and standing by me, both emotionally and financially. Without their commitment and belief in me, reaching this milestone would not have been possible.

Werner Léon Kastelein
Delft, February 2026

Contents

Nomenclature

Abbreviations

Abbreviation	Description
A-CAES	Adiabatic Compressed Air Energy Storage
aFRR	Automatic Frequency Restoration Reserve
BESS	Battery Energy Storage System
BRP	Balance Responsible Party
BSP	Balancing Service Provider
CAES	Compressed Air Energy Storage
CAPEX	Capital Expenditure
CESS	Chemical Energy Storage System
CR	Compression Ratio
CVaR	Conditional Value-at-Risk
DA	Day-Ahead (Market)
D-CAES	Diabatic Compressed Air Energy Storage
DoD	Depth of Discharge
ECESS	Electrochemical Energy Storage System
ECU	Energy Conversion Unit
EESS	Electric Energy Storage System
EFC	Equivalent Full Cycles
EMERGE	Energy Management systEm for Renewable Generation and storagE
EMS	Energy Management System
EOL	End of Life
E/P	Energy-to-Power (ratio)
FCR	Frequency Containment Reserve
FES	Flywheel Energy Storage
FRR	Frequency Restoration Reserve
HPES	Hydro-Pneumatic Energy Storage
HPP	Hybrid Power Plant
I-CAES	Isothermal Compressed Air Energy Storage
IDA	Intraday Auction
IDC	Intraday Continuous
ISP	Imbalance Settlement Period
KPI	Key Performance Indicator
LCOE	Levelized Cost of Electricity
LER	Limited Energy Reservoir
Li-ion	Lithium-Ion
LPCAES	Liquid Piston Compressed Air Energy Storage
MESS	Mechanical Energy Storage System
MILP	Mixed-Integer Linear Programming
mFRRda	Manual Frequency Restoration Reserve (Directly Activated)
MCP	Market Clearing Price
MRQ	Main Research Question
NaNiCl	Sodium–Nickel Chloride
NaS	Sodium–Sulfur
PCM	Phase Change Material
PBC	Physical Bilateral Contract
PCS	Pressure Containment System

Abbreviation	Description
PHS	Pumped Hydro Storage
PV	Photovoltaics
RES	Renewable Energy Sources
SCES	Supercapacitor Energy Storage
SEI	Solid Electrolyte Interphase
SMES	Superconducting Magnetic Energy Storage
SoC	State of Charge
SoH	State of Health
SQ	Sub-Question
STES	Sensible Thermal Energy Storage
TCS	Thermochemical Storage
TESS	Thermal Energy Storage System
TRL	Technology Readiness Level
TSO	Transmission System Operator
VPP	Virtual Power Plant
VRFB	Vanadium Redox Flow Battery
ZnBr	Zinc–Bromide

Symbols

Symbol	Description
b_t	Binary variable preventing simultaneous charge/discharge [-]
C	Specific cost of storage [€/kWh]
C_t	Total cost at time step t [€]
CR	Compression ratio P_c/P_0 [-]
ΔT	Time step duration [h]
ΔP	Pressure difference across the turbine [Pa]
E_{cap}	Energy capacity of the storage system [MWh]
E_P	Stored energy in LPCAES system [J]
$E_{\text{discharged}}$	Discharged energy [MWh]
$E_{\text{throughput},t}$	Energy charged or discharged at time step t [MWh]
f_d	Linear battery degradation rate [-]
L	Battery capacity loss [-]
M	Big-M constant for binary logic [-]
n	Polytropic index [-]
$P_{\text{(dis)charged}}$	Charging or discharging power [MW]
P_{export}	Exported power to the grid [MW]
$P_{\text{export,max}}$	Maximum export power to the grid [GW]
P_{import}	Imported power from the grid [MW]
$P_{\text{import,max}}$	Maximum import power from the grid [GW]
P_{in}, P_{out}	Charging and discharging power [MW]
$P_{\text{in,loss}}$, $P_{\text{out,loss}}$	Charging and discharging losses [MW]
$P_{\text{in,max}}$	Maximum charging power [MW]
P_{mid}	Mid-price between upward and downward regulation [€/MWh]
P_{net}	Net power from the storage system [MW]
$P_{\text{out,max}}$	Maximum discharging power [MW]
P_{turbine}	Turbine power output [W]
P_{up}	Balancing energy price for upward regulation [€/MWh]
P_{wind}	Wind power output [MW]
$P_{\text{wind,rated}}$	Rated wind power [GW]
Q	Volumetric flow rate [m^3/s]
$r_{\text{aFRR}\uparrow}$, $r_{\text{aFRR}\downarrow}$	Awarded up/down aFRR capacity [MW]
$r_{\text{aFRR}\uparrow,\text{req}}$, $r_{\text{aFRR}\downarrow,\text{req}}$	Required up/down aFRR capacity [MW]
$r_{\text{aFRR}\uparrow,\text{max}}$, $r_{\text{aFRR}\downarrow,\text{max}}$	Maximum up/down aFRR capacity [MW]
r_c	Charging C-rate [1/h]
r_d	Discharging C-rate [1/h]
R_t	Total revenue at time step t [€]
$R_{\text{DoD},j}$	Depth of discharge of cycle j [-]
$R_{\text{SoC},j}$	Mean state of charge of cycle j [-]
$R_{\text{count},j}$	Rainflow cycle count of cycle j [-]
SOC	State of Charge [%]
SoC^{final}, SoC^{init}	Final and initial State of Charge [%]
SoC^{max}, SoC^{min}	Maximum and minimum State of Charge [%]
T	Set of time steps in optimization horizon [-]
T_0	Ambient temperature [K]
t_{life}	Battery lifetime [years]
$\beta_t^{\uparrow}$, $\beta_t^{\downarrow}$	Activation factors for upward/downward regulation [-]
λ_{DA}	Day-ahead electricity price [€/MWh]
$\lambda_{\text{aFRR}\uparrow,\text{cap}}$, $\lambda_{\text{aFRR}\downarrow,\text{cap}}$	aFRR capacity prices [€/MW]
$\lambda_{\text{aFRR}\uparrow,\text{act}}$, $\lambda_{\text{aFRR}\downarrow,\text{act}}$	aFRR activation prices [€/MWh]
η	Round-trip efficiency [-]
η_c	Charging efficiency [-]
$\eta_{c,\text{CAES}}$, $\eta_{e,\text{CAES}}$	Compression and expansion efficiency of CAES [-]

Symbol	Description
η_{d}	Discharging efficiency [-]
η_{turbine}	Turbine efficiency [-]

1 Introduction

This chapter introduces the thesis by outlining its main topic and discussing the fundamental concepts and existing studies that collectively form the basis for the subsequent chapters.

1.1. Background

Offshore wind is becoming the Netherlands' largest source of electricity and a cornerstone of the national energy transition. Installed capacity is projected to reach approximately 40 GW by 2040, supplying around half of total electricity demand. As an intermediate milestone, the Dutch government aims to realize 21 GW of offshore wind capacity by 2032. However, as of 2025, only 4.7 GW is operational [1]. At the same time, the business case for offshore wind has weakened in recent years. Between 2020 and 2025, the levelized cost of energy (LCOE) for offshore wind increased by approximately 40%, driven by higher interest rates, inflation, and rising costs for materials, labor, and installation vessels. Meanwhile, demand for additional wind capacity has remained limited due to slower (industrial) electrification. This imbalance between supply and demand undermines the offshore wind business case, making developers more reluctant to invest and threatening the achievement of Dutch climate targets [2].

Integrating energy storage can strengthen the overall business case for offshore wind by unlocking additional revenue streams. In this context, Hybrid Power Plants (HPPs) present a promising approach. HPPs combine two or more co-located generation and storage technologies. In contrast, Virtual Power Plants (VPPs) are cloud-based systems that coordinate energy assets spread across different locations [3]. Specifically, HPPs combine technologies like wind turbines and solar photovoltaics (PV) with energy storage systems, such as batteries. An energy management system (EMS) determines whether electricity generated by PV or wind is supplied to the grid or stored in the storage system. It also decides when the storage system should be discharged, with the goal of maximizing the overall revenue of the HPP [4]. In addition, the EMS can also supply power to other components, such an electrolyzers for hydrogen production [5].

The flexibility of HPPs to dispatch energy on demand enables them to function similarly to conventional power plants [6], thereby improving supply–demand matching. Beyond this, in energy systems with high shares of renewable generation, such as the Netherlands, the variability of weather-dependent sources poses increasing balancing challenges. HPPs can help maintain grid stability by providing balancing energy, while also creating additional revenue opportunities through participation in balancing markets [7]. Furthermore, HPPs benefit from lower project costs by combining technologies to share permitting and siting processes, power electronics, and plant equipment [8].

1.2. Literature Review

Storage technologies vary significantly in their energy storage duration. Long-duration systems typically have higher power capacity costs (€/kW) but lower energy capacity costs (€/kWh) [9]. Due to their large-scale manufacturing capacity, the industry's extensive experience in production, and rapid

deployment capabilities, Li-ion batteries are among the leading candidates for short-term stationary energy storage [10]. Their use in grid applications is expected to grow significantly in the coming years. This scale-up holds substantial potential for further cost reductions. For instance, the cost of Li-ion battery packs for electric vehicles fell by 73% between 2010 and 2016, driven by factors such as expanded production capacity, improvements in battery materials, more competitive supply chains, and enhanced performance characteristics [11].

As outlined in Section 1.1, HPPs integrate generation and storage technologies and enable revenue stacking across multiple electricity markets. As will be discussed in Section 2.2.2 and [11], Lithium-ion batteries are particularly suited to certain balancing markets, whereas long-duration storage technologies such as Pumped Hydro Storage (PHS) and Compressed Air Energy Storage (CAES) are better aligned with others due to their operational characteristics.

[12] analyzes the optimal day-ahead self-scheduling of a wind power producer integrated with compressed air energy storage (CAES), accounting for uncertainties in wind generation and electricity prices. The study highlights that insufficient robustness can result in substantial additional costs when actual conditions deviate from forecasts. An optimal robustness level balances protection costs and realized benefits. The coordinated operation of wind and CAES outperforms separate operation in both deterministic and robust cases. Participation in balancing markets, however, is not included in the analysis.

In [13], a coordinated bidding framework for a hybrid power plant (HPP) integrating wind generation and compressed air energy storage (CAES) across the day-ahead, intraday, and balancing markets is presented. The approach is formulated as a risk-aware optimization problem that incorporates Conditional Value-at-Risk (CVaR) to limit financial risk while maximizing expected revenues and addressing wind power uncertainty. The results show that coordinated operation outperforms separate wind and CAES participation in terms of higher profits and improved risk management.

In addition, [14] studies the optimal bidding strategy of an HPP combining wind, battery storage, and CAES in the day-ahead and intraday markets. The model accounts for wind and price uncertainty, imbalance costs, battery degradation, and risk management using CVaR, and is formulated as a three-stage stochastic MILP. The coordinated operation of wind, BES, and CAES increases expected profit more than it improves CVaR. In other words, the strategy mainly improves average earnings but does not reduce the risk of very unfavorable outcomes to the same extent. The coordinated model provides the system with greater flexibility in the day-ahead and intraday markets and accepts higher downward imbalances to increase profit. When operating in a coordinated manner, the battery is used more intensively (deeper charging and discharging cycles), which increases its degradation cost. However, participation in balancing reserve markets is not considered.

[15] develops an optimal bidding strategy for a combined wind farm and pumped-hydro storage unit. The system participates in the day-ahead (DA) market and a physical bilateral contract (PBC), while accounting for imbalance penalties. A PBC is a direct agreement to deliver a fixed amount of electricity at a fixed price over a set period. he objective is to minimize imbalance costs, optimally allocate energy between the DA market and the PBC, and incorporate risk aversion using CVaR. The problem is formulated as a two-stage stochastic MILP model. Results show that coordinating wind with pumped-hydro storage mitigates wind uncertainty, as hydro generation can offset wind shortfalls or absorb excess production. High bilateral prices shift energy toward the PBC, reducing exposure to DA price volatility and stabilizing revenues. Greater risk aversion leads to more conservative DA offers to limit imbalance penalties. Finally, the integrated wind-hydro system achieves a better risk–return trade-off than standalone wind generation due to its operational flexibility.

Finally, [16] investigates the short-term self-scheduling of a HPP composed of a wind farm and a Li-ion battery participating in the Spanish DA and balancing markets, explicitly accounting for battery degradation costs. A MILP model is formulated to solve the problem. The results show that incorporating calendar aging significantly influences the battery's charging and discharging strategy, leading to lower State Of Charge levels to reduce degradation costs. When calendar aging is considered, revenues from both the DA and balancing markets decrease.

Existing literature demonstrates that several studies have examined the profitability of coupling wind energy with both Li-ion batteries and long-duration energy storage across multiple electricity markets.

However, a research gap remains, as no study has found that directly compared the profitability of short-duration Li-ion storage and long-duration storage technologies within the same optimization framework in a wind-based hybrid power plant (HPP) across multiple markets, while simultaneously accounting for different sizing configurations and degradation effects.

1.3. Research Questions

The proposed Main Research Question (MRQ) is:

How does the profit of hybrid power plants integrating either short- or long-duration storage compare across multiple electricity markets, considering storage sizing and degradation?

The accompanying Sub-Questions (SQs) are:

1. How does the integration of short- versus long-duration storage in hybrid power plants influence profitability across multiple electricity markets?
2. What is the relationship between the sizing of short- and long-duration storage systems and the profitability of hybrid power plants across multiple electricity markets?
3. How does the degradation characteristics of short- and long-duration storage affect profitability and the dispatch strategy of hybrid power plants?

1.4. Thesis Outline

This report is structured as follows. Chapter 2 introduces the technical background necessary to understand the study. Chapter 3 describes the applied methodology, while Chapter 4 presents the results. Chapter 5 discusses the findings, and Chapter 6 concludes the report and provides recommendations for further research.

2

Technical background

2.1. The Dutch electricity market

The electricity system, illustrated in Figure 2.1, is structured into three interconnected layers that represent different dimensions of the electricity market: the physical layer, the actors, and the institutional layer. The coming sections will explain these different layers.

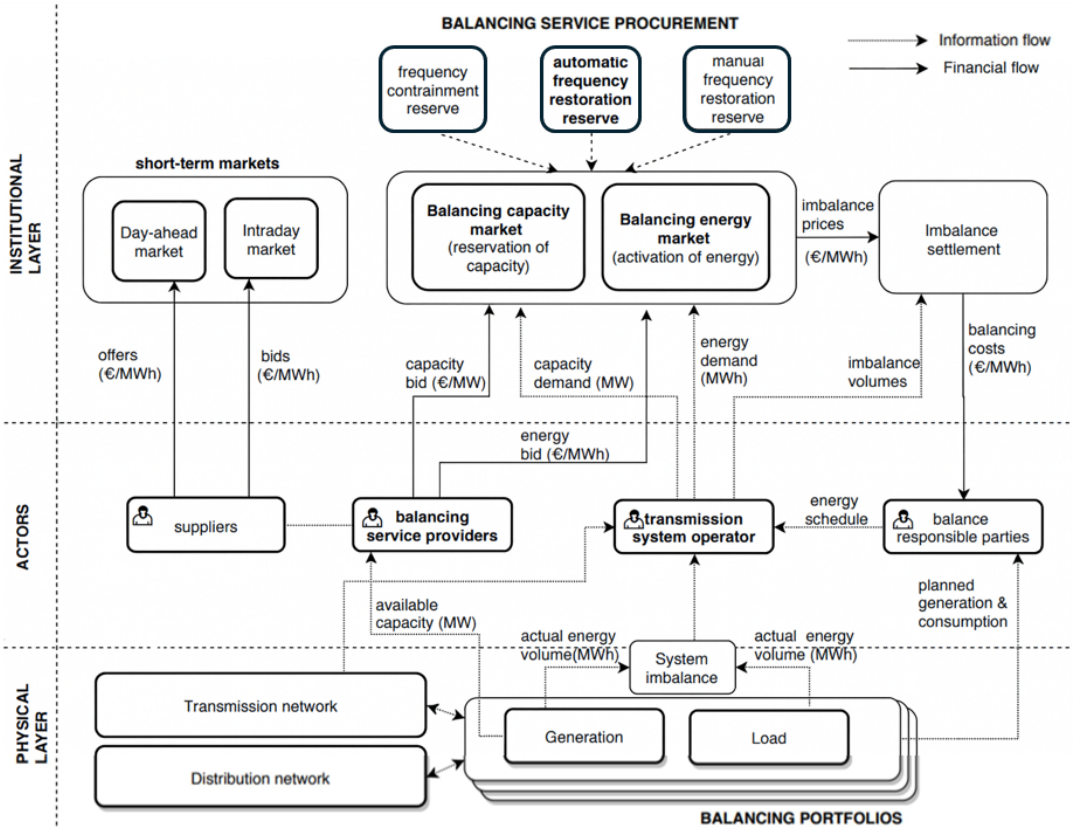

Figure 2.1: Overview of the Dutch electricity market, covering the physical infrastructure, key actors, market structures, and the flows of information and finances between them.
Adapted from [17].

2.1.1. Physical layer and actors

At the base of Figure 2.1 is the physical layer, which encompasses electricity generation and consumption (load). Maintaining a real-time balance between generation and consumption is essential but

challenging, often leading to system imbalances. Electricity generated flows through the high-voltage transmission network and is then distributed regionally through lower-voltage grids.

The next level is the actors layer, which comprises key market participants. Electricity suppliers, such as an HPP, produce electricity and must coordinate with the Transmission System Operator (TSO) to access the high-voltage grid. TSOs are responsible for planning, maintaining, and expanding the transmission infrastructure. In the Netherlands, this role is fulfilled by TenneT, which also collaborates with other European TSOs to enable the integration of a single European electricity market and facilitate cross-border electricity allocation. TSOs also play a crucial role in monitoring and correcting system imbalances. Balance Responsible Parties (BRPs) are financially accountable for ensuring that generation and consumption are balanced within each 15-minute Imbalance Settlement Period (ISP). They submit energy schedules to TenneT, indicating their planned generation and consumption. Finally, Balancing Service Providers (BSPs) supply balancing energy or capacity in real time to help stabilize the system [18].

2.1.2. Institutional layer

The institutional layer of Figure 2.1 is divided into two main market categories: the short-term markets, and the balancing market. These categories will be discussed in the following sections.

Short-term markets

The short-term markets, also known as spot markets, consist of the day-ahead and intraday markets. These platforms are crucial for managing real-time supply and demand, thereby ensuring system balance [19]. In the day-ahead market, a blind auction is held once per day, every day of the year. During this auction, trading occurs for all 24 hours of the following day. Market participants submit their orders before the order book closes at 12:00 CET. Suppliers offer a specific amount of capacity (in MW) at a designated price (€/MWh). This offering price typically reflects the marginal cost, the additional expense of producing one more MWh of electricity. The offers are sorted in merit order, from the lowest to the highest marginal cost, which forms the supply curve. Meanwhile, consumers submit bids indicating how much capacity they wish to purchase and the price they are willing to pay. These bids are ranked from highest to lowest, forming the demand curve. The market clearing price (MCP) is established at the intersection of supply and demand curve. This price applies uniformly to all accepted bids and offers for each delivery period [20]. In this competitive market, where both suppliers and consumers are price-takers and cannot influence the market price, suppliers maximize profit by selling electricity at marginal cost, while buyers maximize their utility by seeking the greatest value for their money. This results in the most efficient outcome, where low-cost suppliers produce electricity for those who value it most, thereby maximizing overall social welfare [21], see Figure 2.2. Note that starting in the fourth quarter of 2025, market clearing will occur every 15 minutes instead of hourly to better reflect fluctuations in renewable energy production [22].

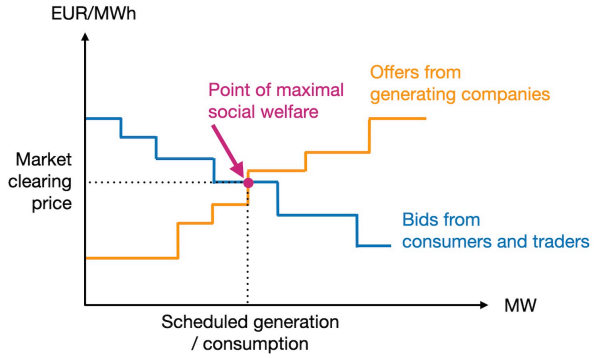

Figure 2.2: The market clearing process in the day-ahead market maximizes social welfare at the intersection of the supply and demand curves [23].

RES generally have very low marginal costs because they do not require fuel and have minimal operating expenses. In contrast, fossil fuel-based power plants, face higher marginal costs due to fuel

requirements. This cost advantage allows renewables to be dispatched earlier in the merit order. As a result, renewable energy can displace more expensive and more polluting fossil fuel plants, reducing overall generation costs and emissions [24]. The downside is that lower prices reduce revenues for all generators, but especially for renewables, since they depress prices most when they produce the most. This ”cannibalization” effect means that increasing RES capacity lowers market revenues and, in a free market, reduces the incentive to invest in new RES projects [25].

The intraday market opens at 15:00 CET, three hours after the closure of the day-ahead market. It is a trading platform where electricity is traded on a pay-as bid basis [26]. The intraday market helps achieve a more accurate balance between supply and demand. If a power plant unexpectedly experiences outage or wind and solar output exceed forecasts due to favorable weather, suppliers and consumers can adjust by trading electricity continuously. In other words, in the intraday market participants have the opportunity to correct deviations from their day-ahead schedules. A transaction is executed immediately when a buy order matches a sell order [27]. In 2025, alongside the intraday continuous market (IDC), a new intraday auction market (IDA) is introduced. This market allows electricity to be traded using a mechanism similar to the day-ahead market, featuring uniform pricing. Auctions are held multiple times per day and allow trading in hourly, 30-minute, and 15-minute time intervals. The new market provides an additional opportunity for market participants to adjust their positions from the day-ahead schedule and helps to reduce grid imbalance [28].

Balancing market

The balancing market is a mechanism designed to continuously maintain the equilibrium between electricity supply and demand [29]. The TSOs within Europe’s synchronous frequency area share joint responsibility for maintaining a stable frequency of 50 Hz. In the Netherlands, TenneT is responsible for maintaining the power system balance [30]. Any imbalance between electricity generation and consumption leads to deviations from this frequency. To manage this, every supplier or consumer connected to the grid must be associated with a BRP. Each BRP submits a commercial trade schedule to TenneT on a daily basis. TenneT verifies that the aggregated schedules of all BRPs balance out, meaning that total forecasted supply equals total forecasted demand for every ISP of the delivery day. On the delivery day itself, BRPs are expected to operate in line with their submitted schedules. If an imbalance arises, TenneT intervenes during the ISP to restore balance. After the delivery day, a financial settlement starts. Whether a BRP receives a payment from TenneT or is required to pay depends on the specific imbalance scenario and the corresponding regulation state.

TenneT uses different regulation states to determine imbalance prices:

- Regulation state 0 applies when there is no need for TenneT to activate any upward or downward reserves. In other words, despite deviations between what BRPs have scheduled and what actually occurs, the overall system remains balanced. This can happen when opposing deviations cancel each other out, or during special conditions like a blackout where the normal balancing mechanism is suspended. In this state, there is no formal balancing price derived from activated regulation. Instead, the imbalance price for BRPs is based on the mid-price.
- Regulation state +1 is used when there is a net shortage of electricity and TenneT must activate upward regulation to restore balance. In this case, the imbalance price is based on the upward regulation price. BRPs that have a shortage, contribute negatively to the system and must pay the upward price. Meanwhile, BRPs with a surplus help to correct the imbalance and are compensated at that same price.
- The opposite situation is represented by regulation state -1, where there is excess power in the system, and TenneT must activate downward regulation. Here, the imbalance price is based on the downward regulation price. Surplus BRPs worsen the imbalance by adding extra electricity to an already oversupplied system and therefore must pay this price. On the other hand, shortage BRPs, which withdraw more than scheduled, actually help correct the imbalance and are paid accordingly.
- In rare and more complex situations, regulation state 2 is used. This state applies when both upward and downward reserves are activated during the same ISP, or when the relationship between the regulation price and the mid-price requires special handling. For example, if the upward price is higher than or equal to the mid-price, then the upward price is used for settlements.

If it is lower, the mid-price is used instead. A similar rule applies to the downward regulation side. This mechanism ensures that imbalance prices reflect the real-time system conditions fairly, and prevent BRPs from benefiting from anomalies in price formation [30].

During ISP with	Imbalance position BRP	Imbalance price		Direction of payment
Regulation state 0	BRP shortage	$P_{mid}(+)$ $P_{mid}(-)$		BRP → TSO TSO → BRP
	BRP surplus	$P_{mid}(+)$ $P_{mid}(-)$		TSO → BRP BRP → TSO
Regulation state +1	BRP shortage	$P_{up}(+)$ $P_{up}(-)$		BRP → TSO BRP → TSO
	BRP surplus	$P_{up}(+)$ $P_{up}(-)$		TSO → BRP TSO → BRP
Regulation state -1	BRP shortage	$P_{down}(+)$ $P_{down}(-)$		BRP → TSO BRP → TSO
	BRP surplus	$P_{down}(+)$ $P_{down}(-)$		TSO → BRP TSO → BRP
Regulation state 2	BRP shortage	$P_{up} \geq P_{mid}$	$P_{up}(+)$ $P_{up}(-)$	BRP → TSO TSO → BRP
		$P_{up} < P_{mid}$	$P_{mid}(+)$ $P_{mid}(-)$	BRP → TSO TSO → BRP
	BRP surplus	$P_{down} \leq P_{mid}$	$P_{down}(+)$ $P_{down}(-)$	TSO → BRP BRP → TSO
		$P_{down} > P_{mid}$	$P_{mid}(+)$ $P_{mid}(-)$	TSO → BRP BRP → TSO

Table 2.1: Imbalance price and direction of payment per ISP, based on the regulation state and the BRPs imbalance position. The direction of payment depends on whether the TSO pays the BRP or the BRP pays the TSO. This is determined by the BRPs imbalance position (shortage or surplus) and the sign of the imbalance price, which can be positive $(+)$ or negative $(-)$. The imbalance prices are defined as follows: (P_{up}) is the balancing energy price for upward regulation, (P_{down}) is the balancing energy price for downward regulation, and (P_{mid}) is the mid-price [30].

BSPs supply balancing energy when activated by TenneT through contractual agreements. In addition to these contracted BSPs, other market participants without contracts may also submit bids to provide balancing energy. This open participation encourages price competition. The market operates on a marginal pricing principle. Bids for upward regulation are ordered from lowest to highest on the right-hand side of the merit order, while bids for downward regulation are ordered from highest to lowest on the left-hand side. These sorted bids together form the merit orders for upward and downward regulation, see Figure 2.3. The figure also displays the mid-price, calculated as the average of the highest activated downward bid and the lowest activated upward bid [30].

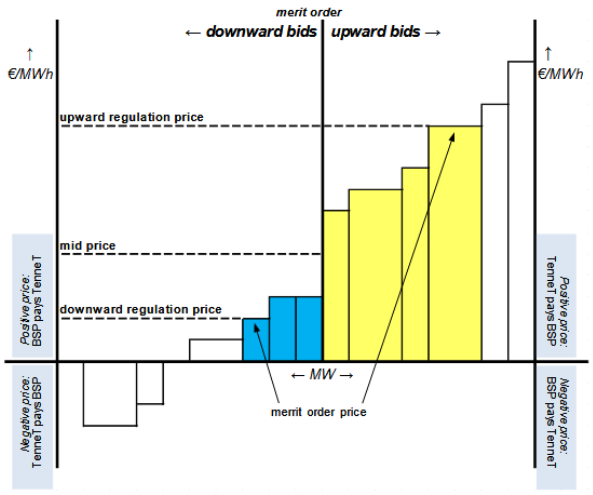

Figure 2.3: Merit order for upward and downward regulation. The upward regulation price is determined by the highest accepted upward bid, while the downward regulation price is set by the lowest accepted downward bid. The mid-price represents the average of these two regulation prices [30].

In case of imbalance, TenneT intervenes by regulating the grid either upward or downward. Upward regulation involves increasing electricity injections into the grid or reducing withdrawals. Conversely, downward regulation means decreasing injections or increasing withdrawals. These regulatory actions are categorized into different regulation states. Depending on whether their position of BRPs supports or hinders the grid balance, BRPs will either receive payment from TenneT or be required to pay an imbalance fee. This interaction ensures that market participants remain incentivized to balance their portfolios as accurately as possible, contributing to the overall stability of the electricity system [30]. A BRP may choose not to follow its scheduled plan if it anticipates that the resulting imbalance will help stabilize the overall electricity system. In this case, the BRP does not provide a formal balancing product on the market but can still receive the imbalance price from TenneT [26]. This approach is known as passive balancing.

Ancillary services

Ancillary services are essential for TSOs to ensure a reliable power supply. These services can be divided into four main categories: frequency control, voltage control, restoration of supply after a black-out, and operational management. Among these, balancing energy, or frequency control, is the most prominent. It is procured through the balancing market of Section 2.1.2, where balancing energy and reserves are traded, while the other services are usually secured through bilateral contracts between the TSO and generators [31]. There are three different types of frequency control services in the Netherlands.

Frequency Containment Reserve (FCR)

The Frequency Containment Reserve (FCR), previously known as ”primary reserve,” involves contracted BSPs that automatically respond to changes in the frequency of the grid [26]. FCR capacity is bid through a daily auction with a 4-hour resolution, where both upward and downward capacity are offered simultaneously (symmetrical bidding). The minimum bid size is 1 MW, with a bid increment of 1 MW. The FCR market is procured via a common merit order. TenneT can automatically activate the offered capacity when needed. Full activation must occur within 30 seconds, with the activation process starting in less than 2 seconds. For limited energy reservoirs (LERs), such as batteries, the power must be delivered for at least 15 minutes. For ”unlimited” sources, like gas plants, a longer delivery duration is required [32]. The average daily FCR capacity contracted in the Netherlands was 55 MW during the period 2019–2023, but it is expected to increase to 120 MW by 2033. According to Rabobank, despite relatively high prices, the FCR market is small and offers limited earning potential for flexible power providers [33].

automatic Frequency Restoration Reserve (aFRR)

The automatic Frequency Restoration Reserve (aFRR), formerly known as the ”secondary reserve”, is procured through the procedure described in Section 2.1.2. In daily 24-hour auctions, BSPs can submit bids for both upward and downward capacity at a specified price (€/MW). BSPs receive a capacity payment simply for being available, regardless of whether their reserve is actually activated by TenneT. This mechanism ensures that TenneT always has sufficient balancing capacity available for automatic activation. After being awarded a contract, BSPs must submit energy bids (€/MWh) for each 15-minute interval. Non-contracted BSPs may also submit bids to provide balancing energy [26]. Capacity bids are asymmetrical. The minimum bid size is 1 MW, with increments of 1 MW. The offered aFRR volume must have a ramp-up rate of at least 20% per minute, meaning the full capacity must be delivered within 5 minutes. The reaction time must be less than 30 seconds. The delivered power must cover at least the ISP, thus 15 minutes [34]. Between 2021 and 2024, the average daily aFRR capacity in the Netherlands was approximately 340 MW for upward regulation and 390 MW for downward regulation. This capacity is expected to increase significantly in the coming years. According to Rabobank, although contracted capacity prices are declining, high price volatility presents attractive opportunities for flexible power suppliers [33].

manual Frequency Restoration Reserve directly activated (mFRRda)

Formerly referred to as the ”tertiary reserve,” the manual Frequency Restoration Reserve directly activated (mFRRda) is activated manually by TenneT in cases of incidents or sustained power imbalances. To qualify as an mFRRda provider, a unit must be capable of delivering the contracted power continuously over the full 24-hour contract period [26]. Capacity bids for mFRRda are asymmetrical, with a

minimum bid size of 1 MW and increments of 1 MW. The maximum activation time is 15 minutes for upward capacity and 10 minutes for downward capacity. Once activated by TenneT, the contracted BSP must be able to deliver the full offered capacity continuously for at least one hour [35]. FRR (Frequency Restoration Reserve) auctions are conducted jointly, with both aFRR and mFRRda capacity bids evaluated in a single process. The awarding algorithm first ensures that the minimum required volumes of aFRR and total FRR are met, then selects the most cost-effective combination of aFRR and mFRRda to fulfill these requirements [34]. Note: If aFRR and mFRRda are delivered simultaneously, they must be provided via physically separate connections. This ensures the independent delivery of each service and allows TenneT to verify them individually [35]. Between 2021 and 2024, the average mFRRda capacity in the Netherlands was approximately 920 MW for upward regulation and 880 MW for downward regulation. This capacity is expected to increase significantly in the coming years. According to Rabobank, the price for upward capacity is relatively high and may remain that way. As a result, the mFRRda market presents a potentially attractive opportunity for providing upward capacity [33].

Overview ancillary services

Figure 2.4 shows how the three types of frequency control reserves play distinct roles in maintaining grid stability. The FCR acts first, providing an automatic response to arrest any immediate frequency deviation. Following this, the aFRR takes over to correct more significant imbalances and steer the frequency back to the nominal 50 Hz. For even greater disturbances that exceed the corrective capacity of FCR and aFRR, the mFRRda is deployed. A comparative overview of these reserves and their operational features can be found in Table 2.2.

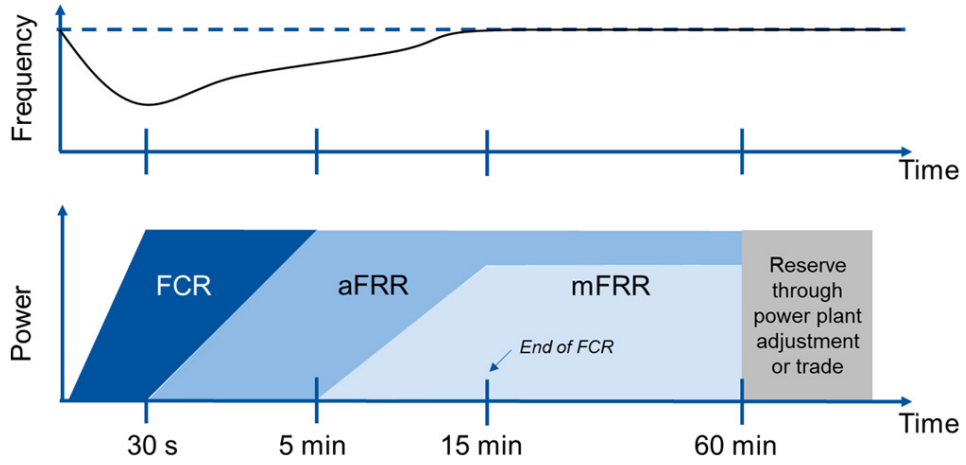

Figure 2.4: Timeline of reserve activation after a frequency deviation in the grid: FCR, aFRR, and mFRRda. [36].

Attribute	FCR	aFRR	mFRRda
Activation type	Automatic	Automatic	Manual
Reaction time	$<$2 s	$<$30 s	-
Activation time	$<$30 s	$<$5 min	$<$15 min (up), $<$10 min (down)
Min. volume	1 MW	1 MW	1 MW
Direction	Symmetrical	Asymmetrical	Asymmetrical
Bid resolution	1 MW	1 MW	1 MW
Duration	$\geq$15 min	$\geq$15 min	$\geq$1 h
Average capacity	$\sim$55 MW[a]	$\sim$340/390 MW[b]	$\sim$920/880 MW[b]

Table 2.2: Overview of Dutch frequency balancing markets [32, 34, 35, 37]. [a]Approximate average daily contracted capacity in the Netherlands (2019-2023) [33]. [b]Approximate average daily contracted upward/downward capacity in the Netherlands (2021–2024) [33].

2.2. Storage Technologies for Hybrid Power Plants

2.2.1. Overview of storage technologies

In general, energy storage technologies can be categorized into five groups: electrical (EESS), electrochemical (ECESS), mechanical (MESS), thermal (TESS), and chemical (CESS) energy storage systems [38]. In this section, the storage technologies suitable for integration into HPPs for this research are identified.

EESS technologies include capacitors, Supercapacitor Energy Storage (SCES), and Superconducting Magnetic Energy Storage (SMES). These systems typically have very short discharge durations, from milliseconds to a few minutes, and are better suited for power quality applications rather than grid-scale energy management. For instance, capacitors are generally used in small-scale applications with power ratings ranging from 200 kW to a few megawatts. Supercapacitors and SMES, despite their high power densities, are unsuitable for participation in energy or balancing markets due to their limited energy capacity and short-duration discharge [39] Therefore, they are not considered appropriate for integration into a HPP configuration in this work.

TESS technologies include Sensible Thermal Energy Storage (STES), latent heat using phase-change materials (PCM), and Thermochemical Storage (TCS). These systems are typically designed for applications where thermal energy is used directly. Depending on the storage medium and system configuration, discharge durations can range from several hours to days or even longer. Their relatively slow discharge rates and the need to convert thermal energy to electricity limit their effectiveness for grid services that require fast response. In addition, round-trip efficiencies for TESS are typically in the range of 60–70% [39]. Accordingly, they are excluded from using in HPP configurations in this work.

CESS technologies, such as hydrogen, are considered beyond the scope of this research and are therefore not included in the HPP configurations analyzed in this study. In HPP configurations that already include electrolyzers, hydrogen is typically either stored for long-term use or sold directly. Its reconversion to electricity, for example via fuel cells, results in lower overall efficiency and is generally less attractive compared to electrochemical storage.

For ECESS, viable technologies for usage in HPPs include lead-acid batteries, various lithium-ion (Li-ion) chemistries, sodium-nickel chloride (NaNiCl), sodium-sulfur (NaS), vanadium redox flow batteries (VRFB), and zinc-bromide (ZnBr) flow batteries [11].

For MESS, there are Flywheel Energy Storage (FES), Pumped Hydro Storage (PHS) and Compressed Air Energy Storage (CAES) are the most common [39]. Flywheels, are a natural fit for FCR because of their high power output, but their high self-discharge (roughly 15% per hour) makes them less suitable for integration in HPPs and impractical for energy trading on the balancing market [11]. Therefore, only PHS and CAES are considered realistic options.

Figure 2.5 provides an overview of the storage technologies considered and illustrates their performance in terms of power rating and discharge duration.

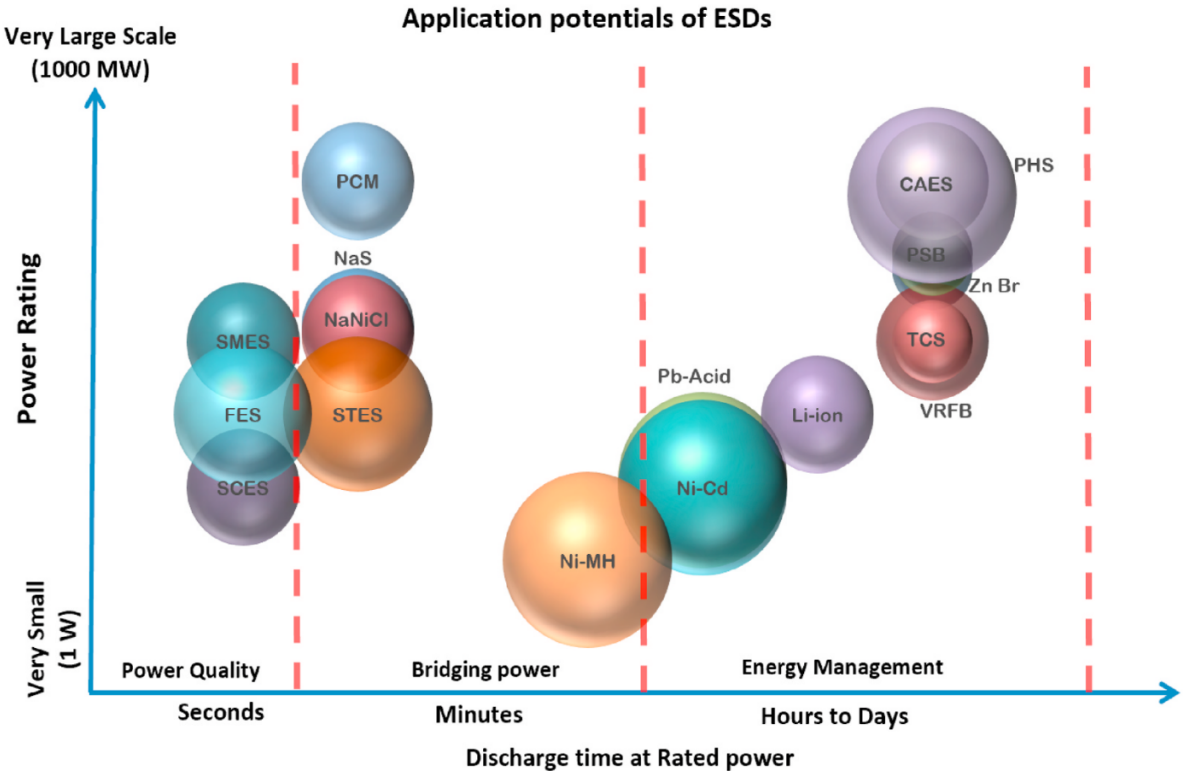

Figure 2.5: Overview of energy storage technologies categorized by system power rating and discharge time at rated power. The figure illustrates different storage types (electrochemical, electrical, mechanical, thermal, and chemical) and their application ranges. Adapted from [39].

2.2.2. Short- and long-duration storage choice and market participation

Building on the observations from Section 2.2.1, the range of feasible storage technologies is reduced to electrical energy storage systems (EESS), PHS, and CAES.

As illustrated in Figure 2.5, most EESS technologies, VRFB and ZnBr flow batteries, are characterized by relatively low power ratings and short discharge durations at rated power. In contrast, flow batteries, CAES, and PHS provide substantially higher power capacities and longer discharge times, making them more suitable for applications requiring sustained energy delivery.

As discussed in Section 1.2, Li-ion batteries have become the dominant and industry-standard solution for grid-connected and HPP systems. Owing to their high round-trip efficiency, technological maturity, and widespread commercial availability, Li-ion batteries are therefore selected as the short-duration storage technology in this study, instead of other EESS options.

Section 2.1.2 explains the different balancing markets. For these markets, Frequency Containment Reserve (FCR) provision typically requires storage technologies with an energy-to-power (E/P) ratio of approximately 1–1.5, reflecting short-duration, high-power operation. In contrast, Frequency Restoration Reserve (FRR) provision demands technologies capable of longer discharge durations, corresponding to E/P ratios greater than 5 [11].

PHS, CAES, VRFB and ZnBr flow batteries are generally better suited for Frequency Restoration Reserve (FRR) markets, as they offer moderate to long discharge durations at comparatively low energy-specific costs. In contrast, FCR requires very fast response times and high power dynamics. Lithium-ion batteries are particularly well suited for such applications due to their rapid controllability and high power capability. PHS may lack fine control and is often restricted to either pumping or generating mode, limiting flexibility. CAES involves complex energy conversion processes, making it less suitable for highly dynamic operation in the FCR market. Redox flow batteries exhibit inherent inertia due to their fluid-based operation and are therefore currently less suited for FCR [11].

In practice, PHS and CAES have decades of operational experience in FRR provision and are well

established in this role. Battery systems can also participate in FRR, especially within multi-market strategies. However, standalone operation dedicated exclusively to FRR may be less attractive economically because of higher energy-related costs. Although redox flow battery technologies have the technical potential to provide FRR services, their current cost level remains a limiting factor. Therefore, they are not selected as the long-duration storage technology in this work [11].

Between the PHS and CAES, CAES is generally more suitable for small to medium-scale HPP configurations, particularly due to its modular deployment potential, and therefore presents a promising option for multi-hour storage needs. CAES also features low self-discharge and a long operational lifespan [40]. Owing to these characteristics, CAES is selected in this work as the long-duration storage technology.

The choice of Li-ion and CAES is supported by [41], which identifies these technologies as the most suitable offshore storage options based on weighted KPIs across two renewable energy scenarios. This is particularly relevant given the strong growth potential of the offshore renewable energy sector [42]. Against this background, Liquid Piston (LP) technology has attracted increasing attention as a promising solution for advanced CAES systems, offering improved efficiency [43].

2.2.3. Storage terminology

Before discussing the specific technologies of Li-ion storage in Section 2.2.4 and (LP)CAES in Section 2.2.5, general terminology of energy storage technologies are first explained.

Depth of Discharge (DoD) describes the fraction of the nominal energy capacity that has been discharged:

$$\mathrm{DoD} = \frac{E_{\mathrm{discharged}}}{E_{\mathrm{cap}}} \times 100\%. \tag{2.1}$$

where $E_{\mathrm{discharged}}$ denotes discharged energy, and E_{cap} the nominal energy capacity.

A DoD of 0% corresponds to a fully charged storage module, whereas 100% DoD represents a fully discharged storage module. Depth of discharge is directly related to the State of Charge (SoC), defined as:

$$\mathrm{SoC} = 100\% - \mathrm{DoD}. \tag{2.2}$$

In practical operation, storage mediums are rarely fully charged and discharged in each cycle. Instead, they undergo irregular partial charge and discharge events. To quantify cumulative usage, these partial cycles are converted into Equivalent Full Cycles (EFC). One EFC corresponds to one complete charge and discharge cycle at 100% DoD. The total number of equivalent full cycles is calculated as:

$$\mathrm{EFC} = \frac{\sum_t E_{\mathrm{throughput},t}}{E_{\mathrm{cap}}}, \tag{2.3}$$

where $E_{\mathrm{throughput},t}$ denotes the charged or discharged energy during time step t, and E_{cap} is the nominal capacity. For example, two cycles at 50% DoD and four cycles at 25% DoD correspond to:

$$2 \times 0.5 + 4 \times 0.25 = 2\ \mathrm{EFC}. \tag{2.4}$$

The C-rate describes the charging or discharging power relative to the nominal energy capacity:

$$\text{C-rate} = \frac{P_{\text{(dis)charged}}}{E_{\mathrm{cap}}}, \tag{2.5}$$

where $P_{\text{(dis)charged}}$ denotes the charging or discharging power and E_{cap} the nominal energy capacity. The C-rate generally denotes the maximum charging or discharging power relative to the nominal energy

capacity of the battery system. For example, a C-rate of 0.5 implies that a full charge or discharge would require 2 hours, whereas a C-rate of 0.25 corresponds to 4 hours. In practice, the storage system may also operate below its rated C-rate, resulting in proportionally longer charging or discharging times.

2.2.4. Lithium-ion storage

Li-ion batteries offer a specific energy range of 75–250 Wh/kg, specific power of 150–315 W/kg, a service life of 5–15 years. Their high energy and power density contribute to compact designs, making them well-suited for fast-response and space-constrained applications [39]. The roundtrip efficiency is approximately 94% [11].

Despite this high efficiency, battery performance gradually declines over time. This degradation is commonly quantified by the State of Health (SoH), which reflects the gradual loss of available capacity as the battery ages. To track this degradation, the SoH is based on underlying aging mechanisms and degradation models. Repeated charge–discharge cycling accelerates this process through unwanted side reactions that reduce usable capacity and increase internal resistance [44].

At the core of these degradation processes lies the electrode–electrolyte interface, the region where lithium ions and electrons participate in charge-transfer reactions during charging and discharging. To achieve high energy density, the electrodes operate at very high potentials. However, at these extreme voltages the electrolyte is thermodynamically unstable and would normally continue to decompose. This instability is resolved through the formation of a protective layer. During the first few cycles, a small fraction of the electrolyte decomposes and forms a thin film on the negative electrode. This film, known as the solid electrolyte interphase (SEI), develops directly on the electrode surface and consists of a mixture of different decomposition products. Once formed, the SEI acts as a passivation layer: it limits further electrolyte degradation while still allowing lithium ions to pass through to the electrode. In this way, the SEI stabilizes the electrode-electrolyte interface, making reversible charging and discharging possible and enabling long-term cycling and extended battery lifetime [45].

Lithium-ion batteries exhibit accelerated degradation at both high and low SoC levels, corresponding to high and low voltages, due to increased side reactions and structural degradation mechanisms. Therefore, operation within a restricted SOC is recommended to ensure long service life, [44].

The capital expenditure (CAPEX) of the Li-ion battery system is calculated as

$$\text{CAPEX}_{\text{Li-ion}} = (c_{\text{E}} + c_{\text{P}} \cdot r_{\text{c}})\ E_{\text{cap}}, \tag{2.6}$$

where $c_{\text{E}} = 204.7$ €/kWh represents the energy-specific cost component and $c_{\text{P}} = 322.29$ €/kW the power-specific cost component. The resulting $\text{CAPEX}_{\text{Li-ion}}$ is expressed in euros (€). r_{c} is the C-rate and is given in h^{-1}, and E_{cap} denotes the installed battery energy capacity in kWh. A currency conversion factor of 0.85 €/$ is applied, in accordance with [46].

2.2.5. Compressed Air Energy storage

Compressed Air Energy Storage (CAES) stores electricity by using electrical power to drive compressors that increase the pressure of ambient air. The compressed air is then stored either in containers or in underground structures such as salt caverns.

The overall round-trip efficiency and the amount of recoverable energy in CAES systems are largely governed by the thermodynamic behavior of air during compression and expansion, which has led to the development of several distinct CAES concepts [43]:

- Diabatic CAES (D-CAES): Electrical energy is used to compress air and store it under pressure. The heat produced during compression is released to the surroundings and not recovered. Prior to expansion, the stored air must be reheated, typically by burning a fuel such as natural gas, in order to avoid excessive cooling during turbine expansion. This configuration represents the most mature and commercially deployed CAES technology.
- Adiabatic CAES (A-CAES): In this configuration, the thermal energy generated during compression is captured and stored, for example in a thermal energy storage system, and later reused to heat the air before expansion. By eliminating the need for external fuel input, adiabatic CAES can achieve higher overall efficiencies compared to diabatic systems.

- Isothermal CAES (I-CAES): This emerging approach aims to maintain the air temperature nearly constant throughout both compression and expansion. By minimizing temperature rises during compression and temperature drops during expansion, the need for fuel-based reheating is avoided. However, achieving near-isothermal behavior with conventional machinery is technically challenging, as it requires extremely effective heat transfer during both charging and discharging phases [43].

Against this background, Liquid Piston (LP) technology has gained increasing attention as a promising solution for advanced CAES systems. Liquid piston compressors compress a fixed gas volume through the controlled movement of a liquid column, usually water. Compared to conventional solid-piston compressors, liquid pistons significantly reduce mechanical friction and virtually eliminate gas leakage, resulting in improved compression efficiency. In addition, liquid piston concepts are particularly well suited for underwater or subsea CAES applications, where the surrounding water provides a large thermal reservoir that enhances heat transfer and supports near-isothermal operation [43].

Liquid Piston Compressed Air Energy Storage

Several liquid piston compressed air energy storage (LPCAES) concepts have been reported in the literature [43]. For offshore applications, certain designs take advantage of the non-linear pressure–volume relationship of compressed air. When a fixed mass of air experiences relatively small volume changes, the corresponding pressure and temperature variations remain moderate. As a result, the system operates with a relatively low compression ratio (CR). Combined with the direct thermal interaction with the surrounding seawater, acting effectively as an infinite heat sink, the heat generated during compression can be efficiently dissipated. Consequently, the compression and expansion processes can be approximated as quasi-isothermal [47].

During the charging phase, electrical energy drives a reversible hydraulic machine operating in pumping mode. Seawater is injected into the system, thereby compressing a pre-charged air volume into a reduced space. During discharge, the compressed air expands and forces the pressurized seawater back through the same hydraulic machine, which then operates in turbine mode to generate electricity. This operating principle is analogous to conventional pumped hydro storage, but without the geographical constraints associated with large elevation differences or upper reservoirs. The technology is therefore also referred to as Hydro-Pneumatic Energy Storage (HPES) [47]. ydro-pneumatic systems are generally classified as either open or closed gas cycle configurations. In a closed gas cycle. A schematic representation of a closed gas cycle hydro-pneumatic system is shown in Figure 2.7 [48].

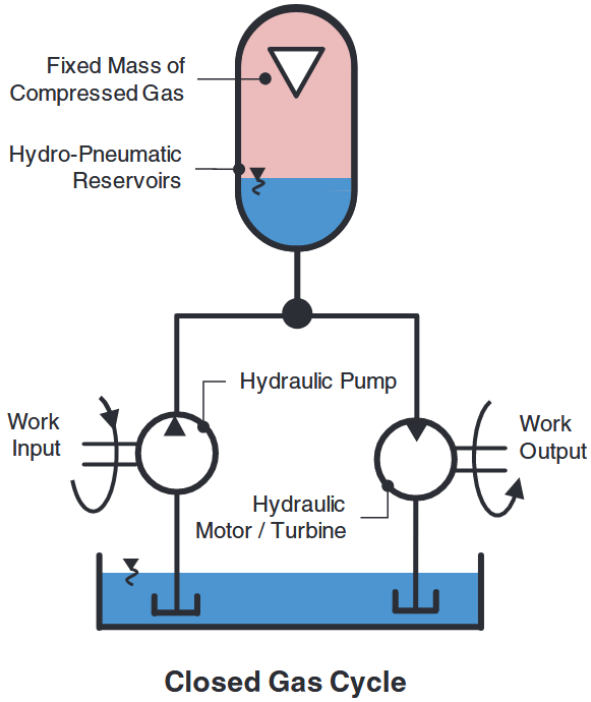

Figure 2.6: Schematic of a closed gas cycle hydro-pneumatic system. When electricity is supplied, a hydraulic pump compresses the fixed gas mass in the hydro-pneumatic reservoir. During discharge, the compressed gas expands, driving the liquid through a hydraulic turbine to generate electricity [48].

For offshore wind applications, a dual-chamber closed gas cycle hydro-pneumatic accumulator provides large-scale energy storage with an expected service life exceeding 25 years under standard offshore maintenance. The system comprises a pre-charged hydro-pneumatic liquid piston chamber connected to an external gas reservoir via a pneumatic line, see Figure 2.7 for a schematic. Here, pre-charged means that the gas is initially pressurized to a specified design pressure before operation. The external reservoir increases the total gas volume, thereby reducing pressure fluctuations and lowering the effective compression ratio. When fully charged, the remaining gas volume equals that of the external reservoir, such that the compression ratio is governed by the volume ratio of the two chambers. During operation, the hydro-pneumatic chamber has a variable mass due to changes in water volume, whereas the external reservoir contains a fixed gas mass. This separation enables flexible integration: the hydro-pneumatic unit can be installed on the seabed, while the buoyant gas reservoir can be positioned topside or integrated within a floating structure, interconnected by a pneumatic umbilical. The reduced effective pressure ratio limits heat generation during compression and improves thermodynamic efficiency [48].

At the start of compression, the accumulator contains only gas, occupying a total volume of $V_{A,0} + V_B$, where $V_{A,0}$ is the volume of the hydro-pneumatic chamber and V_B is the volume of the external reservoir, see Figure 2.7 As liquid is pumped into the lower chamber, the gas is compressed and its volume decreases until it equals V_B. The stored energy corresponds to the work done on the gas during this volume reduction from $V_{A,0} + V_B$ to V_B. This work is equal to the area under the pressure-volume curve and represents the energy storage potential. Consequently, a relatively large amount of energy can be stored even within a limited operating pressure range [48].

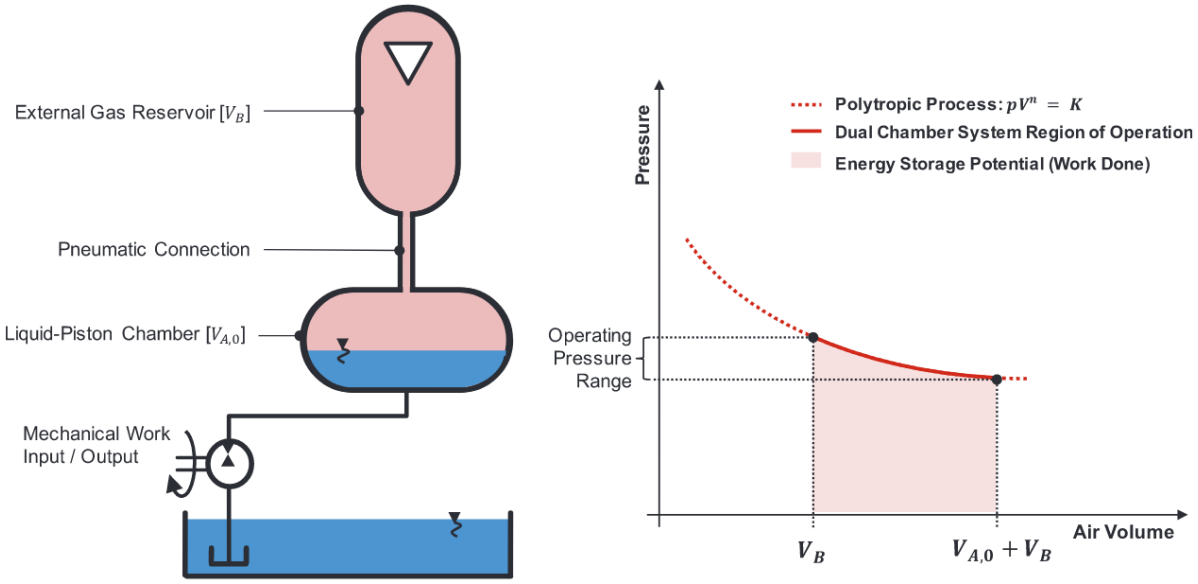

Figure 2.7: Schematic of a dual-chamber closed gas cycle hydro-pneumatic system (left). On the right, the corresponding pressure–volume curve is shown, illustrating the energy storage potential obtained by compressing the air from a volume of $V_{A,0} + V_B$ to V_B, thereby increasing the pressure [48].

The estimated capital expenditure (CAPEX) of the LPCAES system is calculated as

$$\text{CAPEX}_{\text{LPCAES}} = (c_{\text{E}} + c_{\text{P}} \cdot r_{\text{c}})\ E_{\text{cap}}, \tag{2.7}$$

where $c_{\text{E}} = 230$ €/kWh represents the energy-specific cost component and $c_{\text{P}} = 2300$ €/kW the power-specific cost component. The resulting $\text{CAPEX}_{\text{LPCAES}}$ is expressed in euros (e). Tr_{c} is the C-rate and is given in h^{-1}, and E_{cap} denotes the installed storage capacity in kWh. This CAPEX represents an indicative estimate, as LPCAES is still at a low technology readiness level (TRL). The assumed cost level is based on correspondence with an LPCAES technology provider. Publicly available cost data are limited, since the technology has not yet been deployed at commercial scale [48].

To structure this estimate, the total CAPEX is divided into two main components: the Pressure Containment System (PCS) and the Energy Conversion Unit (ECU). The PCS stores the pressurized fluids and therefore scales with the energy capacity (E_{cap}, kWh). In contrast, the ECU converts electricity to hydraulic power during charging and back during discharging, and thus scales with the power rating, which is determined by the C-rate (r_{c}). Consequently, ECU costs primarily depend on the power rating of the reversible pump–turbine configuration, while PCS costs are driven by the required storage capacity [48].

This distinction highlights how design choices influence system sizing. The energy capacity can be increased by enlarging the volume of the external gas reservoir on the seabed, i.e., by scaling the PCS. In contrast, the power-related characteristics are limited by thermodynamic constraints. Based on discussions with an LPCAES technology provider, C-rates below $0.25\ \text{h}^{-1}$ (corresponding to discharge durations longer than 4 hours) are considered feasible. At higher C-rates, the process departs from quasi-isothermal behavior due to insufficient time for heat transfer. Based on discussions with an LPCAES technology provider, discharge durations of 4 hours or longer are therefore considered a realistic and technically feasible design range.

The instantaneous turbine power output during expansion is given by:

$$P_{\text{turbine}} = \Delta P\ Q\ \eta_{\text{turbine}}, \tag{2.8}$$

where ΔP is the pressure difference across the turbine, Q is the volumetric flow rate, and η_{turbine} is the turbine efficiency.

Since the pressure decreases during expansion, the turbine power output also declines if the flow rate is kept constant; hence, the system does not inherently operate at constant power. However, by adjusting the flow rate, a constant power output can be maintained. A round-trip efficiency of approximately 70% [47] is assumed for the LPCAES system.

Operationally, LPCAES behaves similarly to a battery, with negligible switching time between charging and discharging. However, unlike electrochemical storage, cycling degradation can be neglected. Although cyclic loading may in principle reduce the fatigue life of the PCS, typically a steel pipeline, these components are designed for several hundred thousand cycles, far exceeding the expected number of cycles over the operational lifetime. The pump and motor require routine maintenance, including periodic replacement of consumables such as bearings and lubrication. These interventions do not reduce the storage capacity and are not cycle-dependent. Therefore, they are not considered a source of capacity degradation.

3

Methodology

3.1. EMERGE

TNO's Energy Management systEm for Renewable Generation and storagE (EMERGE) [49] is a Python optimization framework designed to model and simulate the operation of HPPs. The model integrates renewable energy generation (such as wind and solar PV) with energy storage systems and optimizes their joint operation across multiple electricity markets.

By using historical meteorological data, EMERGE generates forecasts of renewable generation profiles. These forecasts are then used in a Mixed-Integer Linear Programming (MILP) optimization to identify the most profitable operational strategy for the HPP as a whole. Each asset (generation and storage) is represented by a linearized model, and the optimizer produces time series of optimal setpoints for every asset at a 15-minute resolution, corresponding to one ISP [50].

The model supports a multi-market revenue stacking strategy by allowing simultaneous participation in the day-ahead and aFRR markets. This setup enables the evaluation of the economic performance of HPPs under different storage configurations and market conditions.

Section 3.1 documents the set of equations underlying the EMERGE model, which were developed before the start of this research [49].

3.1.1. Model structure

Optimization in EMERGE is performed for a 24-hour period, divided into 96 time steps of 15 minutes. At each time step $t \in T$, the model jointly optimizes wind dispatch, battery operation, and market participation in the day-ahead and aFRR markets. The objective is to maximize the daily operational profit of the HPP. Multi-day simulations are performed by solving the optimization problem separately for each day. There is no direct link between consecutive days, except for the imposed initial and final State of Charge (SoC) conditions.

3.1.2. Mathematical formulation

The hybrid power plant is modeled in discrete time. Let

$$T = \{1, \ldots, N\}$$

denote the set of time steps with duration ΔT.

At each time step, the operator decides how to:

- charge or discharge the battery,
- offer aFRR reserve capacity,
- import from or export power to the grid,
- curtail wind production via a dispatch factor S_t^{wind}.

The objective is to maximize total profit over the optimization horizon.

3.1.3. Decision variables

The decision variables are defined for every $t \in T$:

P_t^{in}	Battery charging power [W]	(3.1)
P_t^{out}	Battery discharging power [W]	(3.2)
SoC_t	State of charge [-]	(3.3)
$r_t^{\text{aFRR}\uparrow}$	Upward aFRR reserve capacity [W]	(3.4)
$r_t^{\text{aFRR}\downarrow}$	Downward aFRR reserve capacity [W]	(3.5)
$P_t^{\text{import}},\ P_t^{\text{export}}$	Grid exchange power [W]	(3.6)
b_t	Binary variable preventing simultaneous charge/discharge	(3.7)
S_t^{wind}	Wind dispatch (curtailment) factor $[0, 1]$	(3.8)

The binary variable b_t ensures that the battery cannot charge and discharge at the same time. The usable wind power after curtailment is denoted P_t^{wind}.

The decision vector is

$$\mathbf{x} := \left\{ P_t^{\text{in}}, P_t^{\text{out}}, SoC_t, r_t^{\text{aFRR}\uparrow}, r_t^{\text{aFRR}\downarrow}, P_t^{\text{import}}, P_t^{\text{export}}, b_t, S_t^{\text{wind}} \right\}_{t \in T}.$$

3.1.4. Input parameters

The model uses the following parameters:

E_{cap}	Storage energy capacity [Wh]	(3.9)
$r_{\text{c}},\ r_{\text{d}}$	Maximum charging/discharging C-rates [1/h]	(3.10)
$\eta_{\text{c}},\ \eta_{\text{d}}$	Charging/discharging efficiencies [-]	(3.11)
$SoC^{\min},\ SoC^{\max}$	State of Charge limits [-]	(3.12)
$SoC^{\text{init}},\ SoC^{\text{final}}$	Initial and final state of charge	(3.13)
C_{MC}	Marginal degradation cost [€/kWh]	(3.14)
$P_t^{w,\text{pred}}$	Forecasted normalized wind profile $[0, 1]$	(3.15)
$P^{\text{wind,rated}}$	Installed wind capacity [W]	(3.16)
λ_t^{DA}	Day-ahead electricity price	(3.17)
$\lambda_t^{\text{aFRR},\uparrow,res},\ \lambda_t^{\text{aFRR},\downarrow,res}$	aFRR reservation prices	(3.18)
$\lambda_t^{\text{aFRR},\uparrow,act},\ \lambda_t^{\text{aFRR},\downarrow,act}$	aFRR activation prices	(3.19)
$\beta_t^{\uparrow},\ \beta_t^{\downarrow}$	Activation ratios	(3.20)
$r^{\text{aFRR}\uparrow,\max},\ r^{\text{aFRR}\downarrow,\max}$	Maximum reserve capacities [W]	(3.21)
M	Big-M constant	(3.22)

The maximum charging and discharging powers follow from the C-rates:

$$\begin{aligned} P^{\text{in,max}} &= r_{\text{c}} E_{\text{cap}}, \\ P^{\text{out,max}} &= r_{\text{d}} E_{\text{cap}}. \end{aligned} \tag{3.23}$$

3.1.5. Objective function

At each time step, revenue consists of:

- Day-ahead energy sales,
- aFRR capacity payments,
- aFRR activation payments.

$$\begin{aligned} R_t = {} & \lambda_t^{DA} P_t^{\text{export}} \\ & + \lambda_t^{\text{aFRR},\uparrow,res} r_t^{\text{aFRR}\uparrow} + \lambda_t^{\text{aFRR},\downarrow,res} r_t^{\text{aFRR}\downarrow} \\ & + \lambda_t^{\text{aFRR},\uparrow,act} \beta_t^{\uparrow} r_t^{\text{aFRR}\uparrow} \quad + \lambda_t^{\text{aFRR},\downarrow,act} \beta_t^{\downarrow} r_t^{\text{aFRR}\downarrow}. \end{aligned} \tag{3.24}$$

Storage marginal cost is proportional to total throughput:

$$C_t = \left(P_t^{\text{in}} + P_t^{\text{out}}\right) C_{\text{MC}} \Delta T. \tag{3.25}$$

The total profit is therefore

$$\max_{\mathbf{x}} \quad \sum_{t \in T} (R_t - C_t) \tag{3.26}$$

3.1.6. Constraints

The constraints ensure physical feasibility and market consistency.

1. Wind power after curtailment

$$P_t^{\text{wind}} = S_t^{\text{wind}} P_t^{w,\text{pred}} P^{\text{wind,rated}} \qquad \forall t \in T. \tag{3.27}$$

2. Power limits and mutual exclusivity

$$0 \le P_t^{\text{in}} \le P^{\text{in,max}} \qquad \forall t \in T, \tag{3.28}$$

$$0 \le P_t^{\text{out}} \le P^{\text{out,max}} \qquad \forall t \in T, \tag{3.29}$$

$$P_t^{\text{in}} \le M b_t \qquad \forall t \in T, \tag{3.30}$$

$$P_t^{\text{out}} \le M(1 - b_t) \qquad \forall t \in T. \tag{3.31}$$

3. State of Charge dynamics

$$SOC_t = SOC_{t-1} + \frac{P_t^{\text{in}} - P_t^{\text{out}} - \beta_t^{\uparrow} r_t^{\text{aFRR}\uparrow} + \beta_t^{\downarrow} r_t^{\text{aFRR}\downarrow}}{E_{\text{cap}}} \Delta T \qquad \forall t \in T. \tag{3.32}$$

$$SoC^{\min} \le SoC_t \le SoC^{\max} \qquad \forall t \in T. \tag{3.33}$$

$$SoC_0 = SoC^{\text{init}}, \qquad SoC_T \ge SoC^{\text{final}}. \tag{3.34}$$

4. aFRR capacity limits

$$0 \le r_t^{\text{aFRR}\uparrow} \le r^{\text{aFRR}\uparrow,\max} \qquad \forall t \in T, \tag{3.35}$$

$$0 \le r_t^{\text{aFRR}\downarrow} \le r^{\text{aFRR}\downarrow,\max} \qquad \forall t \in T. \tag{3.36}$$

5. Power feasibility under activation

$$P_t^{\text{out}} - P_t^{\text{in}} + r_t^{\text{aFRR}\uparrow} \le P^{\text{out,max}} \eta_{\text{d}} \qquad \forall t \in T, \tag{3.37}$$

$$P_t^{\text{in}} - P_t^{\text{out}} + r_t^{\text{aFRR}\downarrow} \le P^{\text{in,max}} \eta_{\text{c}} \qquad \forall t \in T. \tag{3.38}$$

6. SoC feasibility under full activation

$$SoC_t E_{\text{cap}} - r_t^{\text{aFRR}\uparrow} \Delta T \geq SoC^{\min} E_{\text{cap}} \qquad \forall t \in T, \tag{3.39}$$
$$SoC_t E_{\text{cap}} + r_t^{\text{aFRR}\downarrow} \Delta T \leq SoC^{\max} E_{\text{cap}} \qquad \forall t \in T. \tag{3.40}$$

7. Power balance

$$P_t^{\text{wind}} + P_t^{\text{out}} - P_t^{\text{in}} + P_t^{\text{import}} = P_t^{\text{export}} \qquad \forall t \in T. \tag{3.41}$$

8. Variable domains

$$0 \leq S_t^{\text{wind}} \leq 1 \qquad \forall t \in T, \tag{3.42}$$
$$P_t^{\text{import}},\ P_t^{\text{export}} \geq 0 \qquad \forall t \in T, \tag{3.43}$$
$$b_t \in \{0, 1\} \qquad \forall t \in T. \tag{3.44}$$

3.1.7. Mathematical formulation

The final mathematical formulation of the optimization problem is:

Let $T = \{1, \ldots, N\}$ denote the set of time steps.

The vector of decision variables is defined as

$$\mathbf{x} := \left\{ P_t^{\text{in}}, P_t^{\text{out}}, SoC_t, r_t^{\text{aFRR}\uparrow}, r_t^{\text{aFRR}\downarrow}, P_t^{\text{import}}, P_t^{\text{export}}, b_t, S_t^{\text{wind}} \right\}_{t \in T}. \tag{3.45}$$

The profit maximization problem is formulated as

$$\begin{aligned}
\max_{\mathbf{x}} \quad & \sum_{t \in T} \Pi_t(\mathbf{x}) \\
\text{s.t.} \quad & P_t^{\text{wind}} = S_t^{\text{wind}} P_t^{w,\text{pred}} P^{\text{wind,rated}} && \forall t \in T \\
& 0 \leq P_t^{\text{in}} \leq r_{\text{c}} E_{\text{cap}} && \forall t \in T \\
& 0 \leq P_t^{\text{out}} \leq r_{\text{d}} E_{\text{cap}} && \forall t \in T \\
& P_t^{\text{in}} \leq M b_t && \forall t \in T \\
& P_t^{\text{out}} \leq M(1 - b_t) && \forall t \in T \\
& SoC_t = SoC_{t-1} + \frac{P_t^{\text{in}} - P_t^{\text{out}} - \beta_t^{\uparrow} r_t^{\text{aFRR}\uparrow} + \beta_t^{\downarrow} r_t^{\text{aFRR}\downarrow}}{E_{\text{cap}}} \Delta T && \forall t \in T \\
& SoC^{\min} \leq SoC_t \leq SoC^{\max} && \forall t \in T \\
& SoC_0 = SoC^{\text{init}} \\
& SoC_T \geq SoC^{\text{final}} \\
& 0 \leq r_t^{\text{aFRR}\uparrow} \leq r^{\text{aFRR}\uparrow,\max} && \forall t \in T \\
& 0 \leq r_t^{\text{aFRR}\downarrow} \leq r^{\text{aFRR}\downarrow,\max} && \forall t \in T \\
& P_t^{\text{out}} - P_t^{\text{in}} + r_t^{\text{aFRR}\uparrow} \leq r_{\text{d}} E_{\text{cap}} \eta_{\text{d}} && \forall t \in T \\
& P_t^{\text{in}} - P_t^{\text{out}} + r_t^{\text{aFRR}\downarrow} \leq r_{\text{c}} E_{\text{cap}} \eta_{\text{c}} && \forall t \in T \\
& SoC_t E_{\text{cap}} - r_t^{\text{aFRR}\uparrow} \Delta T \geq SoC^{\min} E_{\text{cap}} && \forall t \in T \\
& SoC_t E_{\text{cap}} + r_t^{\text{aFRR}\downarrow} \Delta T \leq SoC^{\max} E_{\text{cap}} && \forall t \in T \\
& P_t^{\text{wind}} + P_t^{\text{out}} - P_t^{\text{in}} + P_t^{\text{import}} = P_t^{\text{export}} && \forall t \in T \\
& 0 \leq S_t^{\text{wind}} \leq 1,\ P_t^{\text{import}} \geq 0,\ P_t^{\text{export}} \geq 0 && \forall t \in T \\
& b_t \in \{0, 1\} && \forall t \in T.
\end{aligned} \tag{3.46}$$

3.2. Simulation framework

3.2.1. EMERGE model overview

This study employs the EMERGE simulation framework to analyze the profit-maximizing operation of wind-based HPPs equipped with either Li-ion battery storage or LPCAES. Within EMERGE, Li-ion battery storage was already implemented. Its operation is represented using the generic storage model formulation in EMERGE, which is described in Section 3.1.7. This model captures the temporal evolution of the state of charge (SoC) as well as charging and discharging processes through a set of technology-agnostic equations.

In contrast, the LPCAES concept introduced in Section 2.2.5 was not previously available in EMERGE and was implemented as part of this work. Since LPCAES can be described using the same generic storage formulation, its integration does not require changes to the underlying model structure. Instead, the technology is characterized by a distinct set of parameters, including energy capacity, charging and discharging efficiencies, maximum charging and discharging rates, marginal operating costs, and minimum and maximum SoC limits. By defining these technology-specific inputs, LPCAES is added as an additional storage option within the EMERGE framework.

3.2.2. Input data

Wind data

Wind power profiles are sourced from Renewables.ninja [51] and are based on the data from [52]. The data rely on the MERRA-2 (global) dataset, assuming a hub height of 135 m and the GE Haliade-X 12-220 turbine model. The original data have an hourly time step. These values are rescaled to a 15-minute resolution to meet the requirements of EMERGE. A correction factor of 0.88 is applied to represent losses due to cabling and wind farm wake effects.

Market data

The market data used was obtained from the ENTSO-E Transparency Platform [53]. An overview of the market data inputs and associated time resolutions used in the simulations is provided in Table 3.1.

Table 3.1: Overview of market data inputs in EMERGE from [53].

Market	Variable	Unit	Time Resolution
aFRR	Activation price (up & down)	€/MWh	15 min (ISP)
	Activated energy (up & down)	MWh	15 min (ISP)
	Offered capacity (up & down)	MW	15 min (ISP)
	Capacity price (up & down)	€/MW	Daily
Day-ahead	Day-ahead electricity price	€/kWh	Hourly

Market and wind data for the years 2022, 2023, and 2024 were sourced and can be provided as inputs to EMERGE. For each simulation run, a single year is selected, and EMERGE is executed using the corresponding market price data and wind generation profiles for that year.

3.2.3. Simulation setup and execution

The simulation is configured following a structured sequence:

1. **Year selection**
   First, the simulation year is selected to ensure that the appropriate market data and wind generation profiles are used as inputs.
2. **aFRR participation**
   Next, it is specified whether the system participates in the aFRR market. This choice affects both the operational strategy and the resulting profits.
3. **Storage configuration**
   The inclusion of an energy storage system is then determined. If storage is selected, either a Li-ion battery or an LPCAES system can be chosen. Each technology is characterized by technology-specific parameters, including minimum and maximum SoC limits and charging and discharging

efficiencies. For each storage system, the energy capacity, maximum charging and discharging rate, and marginal operating costs (€/kWh) can be defined.

For each simulation run, EMERGE provides outputs at the imbalance settlement period (ISP) level, including wind farm power output, electricity imports from and exports to the grid, storage charging and discharging power, the storage system SoC, total profit, and revenues generated from participation in the aFRR market. Since EMERGE optimizes for profit maximization, the input data are provided on a daily basis, and the model is executed sequentially for each day. The daily results are subsequently aggregated over the selected simulation period. However, continuity of the storage system's SoC is enforced, whereby the final SoC of each day is carried over as the initial SoC of the subsequent day.

3.3. Battery degradation

3.3.1. Degradation model implementation

Lithium-ion batteries experience capacity loss over their lifetime. To incorporate this effect into EMERGE, the methodology and code provided by [4] were used.

This framework builds upon the empirically validated degradation model introduced by [54]. The model applies a rainflow cycle-counting algorithm to a State of Charge time series, decomposing it into individual charge–discharge cycles that are then used to estimate degradation [55]. The algorithm produces the following outputs for each identified load cycle: (i) the cycle amplitude, (ii) the cycle mean value, (iii) the cycle count, equal to 0.5 for a half cycle and 1 for a full cycle, (iv) the start time of the cycle, and (v) the end time of the cycle.

These outputs are subsequently used to derive degradation-relevant stress metrics. For each load cycle j, the cycle amplitude is interpreted as the depth of discharge ($R_{\mathrm{DoD},j}$), the cycle mean value represents the average state of charge ($R_{\mathrm{SoC},j}$), and the rainflow cycle count is used as the cycle weighting factor ($R_{\mathrm{count},j}$). This is done for all identified cycles $j = 1, \ldots, n_R$. The battery age at the j-th load cycle is represented by $t_{\mathrm{c},j}$ [4, 54].

The linear degradation rate f^d in Eq. (3.47) depends on stress models associated with the depth of discharge (S_{DoD}), the battery age (S_{t_c}), the state of charge (S_{SoC}), and the cell temperature in kelvin (S_{T_c}). The degradation rate is given by

$$f^d = \sum_{j=1}^{n_R} \left(\left(S_{\mathrm{DoD},j} + S_{t_c,j} \right) S_{\mathrm{SoC},j} S_{T_c,j} \right) R_{\mathrm{count},j}, \tag{3.47}$$

where the individual stress factors are defined as

$$S_{\mathrm{DoD},j} = \left(k_{\delta 1} R_{\mathrm{DoD},j}^{k_{\delta 2}} + k_{\delta 3} \right)^{-1}, \tag{3.48}$$

$$S_{t_c,j} = k_t \, t_{c,j}, \tag{3.49}$$

$$S_{\mathrm{SoC},j} = e^{(k_\sigma (R_{\mathrm{SoC},j} - \sigma_{\mathrm{ref}}))}, \tag{3.50}$$

$$S_{T_c,j} = \begin{cases} e^{\left(k_T \frac{(T_{c,j} - T_{\mathrm{ref}}) T_{\mathrm{ref}}}{T_{\mathrm{ref}}} \right)} & \text{if } T_{c,j} > T_{\mathrm{ref}} \\ 1 & \text{if } T_{c,j} \leq T_{\mathrm{ref}}, \end{cases} \tag{3.51}$$

with model parameters: $k_{\delta 1} = 1.4 \times 10^5$, $k_{\delta 2} = -5.01 \times 10^{-1}$, $k_{\delta 3} = -1.23 \times 10^5$, $\sigma_{\mathrm{ref}} = 0.5$, $k_T = 6.93 \times 10^{-2}$, $T_{\mathrm{ref}} = 293.15$ K, and $k_t = 4.14 \times 10^{-10}$, which are empirically derived [4].

In EMERGE, the effect of temperature is ignored, so $T_{\mathrm{c}} = T_{\mathrm{ref}} = 293.15$ K,

Battery capacity loss however does not evolve linearly with accumulated stress. Therefore, the linear degradation measure f^d is mapped to the loss of capacity L using nonlinear expressions that represent two distinct aging regimes. The first regime corresponds to the early-life *new-battery* phase dominated by solid-electrolyte interphase (SEI) formation, while the second regime represents the *used-battery* phase. The formation mechanism of the SEI is described in Section 2.2.4.

For the new-battery regime, the loss of capacity is calculated for each cycle according to

$$L = 1 - \alpha e^{-\beta f^d} - (1-\alpha)e^{-f^d}, \tag{3.52}$$

and this expression is evaluated cumulatively as f^d evolves over the SoC sequence.

Once the loss of capacity reaches the transition threshold $L_1 = 0.92$, corresponding to a state of health (SoH) of 92%, the model switches to the used-battery regime. The value of the linear degradation rate at this switching point is denoted $f^{d'}$, and the corresponding loss of capacity is denoted L'. For all subsequent cycles, L is updated using a second nonlinear expression that ensures continuity at the transition point.

The complete loss-of-capacity model can therefore be written as

$$L = \begin{cases} 1 - \alpha e^{-\beta f^d} - (1-\alpha)e^{-f^d}, & \text{if } L \le L_1, \\ 1 - (1-L')\, e^{-\left(f^d - f^{d'}\right)}, & \text{if } L > L_1. \end{cases} \tag{3.53}$$

where α = 0.0575, β = 121, and L_1 = 0.92.

The loss of capacity L is thus time-dependent through its dependence on $f^d(t)$. The degraded battery energy capacity is given by

$$\mathrm{E}_{\mathrm{cap}}(t) = \mathrm{E}_{\mathrm{cap,new}}\left[1 - L(t)\right]. \tag{3.54}$$

After processing the full SoC time series, the final value $L(t_{\mathrm{final}})$ represents the total accumulated capacity loss of the battery [4].

The code used for battery degradation in EMERGE is based on the implementation provided in this section, developed by [4], with two slight adjustments. First, the SoC time series produced by EMERGE has a temporal resolution of 15 minutes, whereas the standard rainflow counting algorithm assumes hourly data; therefore, an appropriate time-scale conversion is applied. In addition, the GitLab implementation of Eq. (3.47) applies an extra factor of 0.7, thereby reducing the calculated cycle-induced degradation. However, this factor is not consistent with [54], and its justification is unclear. Therefore, to ensure consistency with [54], the factor is omitted in EMERGE.

3.3.2. Degradation model usage

After running a full-year simulation in EMERGE using the selected input data, a yearly SoC time series is obtained. This SoC time series is used as input to the battery degradation model to estimate the resulting loss in usable capacity. To represent consecutive years of operation, the same yearly SoC profile is then repeated, and the degradation model is applied again after each repetition, thereby accumulating degradation over time. This iterative process continues until the battery state of health (SoH) falls below a predefined threshold, at which point the battery is considered to have reached its end of life (EOL), following the same approach as adopted in [4]. Continued operation beyond this point may lead to increased safety risks and potential accident scenarios.

In general, battery EOL is assumed to occur when the maximum available capacity decreases to 80of the nominal capacity [56], although alternative thresholds such as 70% are also commonly used in the literature [4]. To nevertheless obtain a more precise estimate of the battery lifetime, the final year in which the SoH crosses the EOL threshold is approximated using an average daily degradation rate, allowing interpolation to a more accurate lifetime value.

Figure 3.1 illustrates the degradation trajectory of a representative battery configuration. The SoH gradually decreases over time due to capacity fade. For this specific configuration, assuming an EOL threshold of 70% minimum SoH, the calculated lifetime is 6.1 years. The transition at 92% SoH, marking

the change from the new-battery phase to the used-battery phase as defined in Equation 3.53, is also indicated.

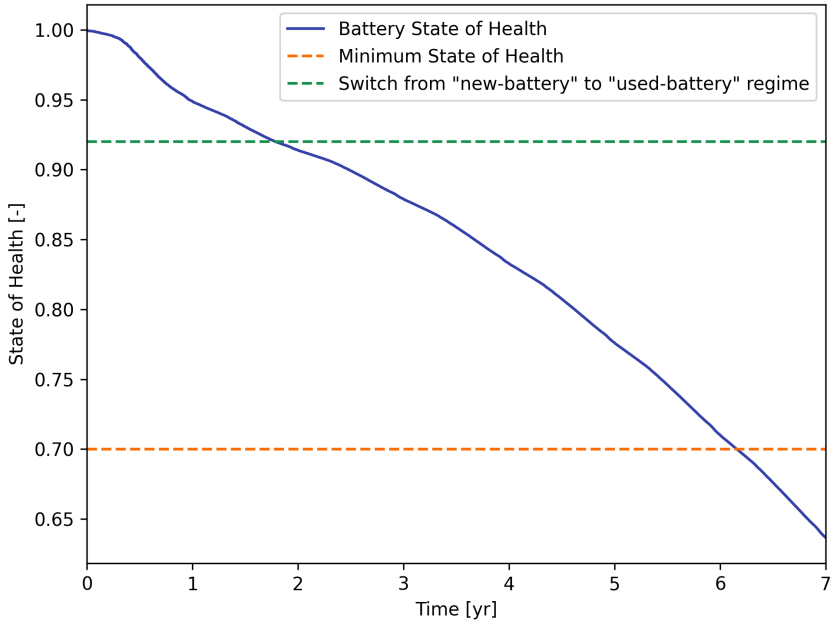

Figure 3.1: State of Health (SoH) of a battery configuration as a function of capacity degradation. The battery is assumed to reach End-of-Life (EOL) when the minimum SoH declines to 70%. At 92% SoH, the battery transitions from the new-battery phase to the used-battery phase, resulting in a change in the capacity degradation behavior.

The number of cycles experienced by the battery over a year is determined using a rainflow cycle-counting algorithm. From this analysis, the Equivalent Full Cycles (EFC) are computed by combining the cycle count and depth of discharge for all identified load cycles. The total number of EFC over the battery lifetime is given by

$$\mathrm{EFC} = t_{\mathrm{life}} \sum_{j=1}^{n_R} R_{\mathrm{count},j} R_{\mathrm{DoD},j}, \tag{3.55}$$

where $R_{\mathrm{count},j}$ denotes the cycle count (equal to 0.5 for a half cycle and 1 for a full cycle), $R_{\mathrm{DoD},j}$ is the depth of discharge associated with load cycle j, and t_{life} is the battery lifetime in years.

Given the total number of EFC until EOL, marginal degradation costs can be estimated by distributing the battery replacement costs over the total energy throughput during the battery lifetime. Since one EFC consists of one full discharge and one full charge, it accounts for two energy throughputs. The replacement cost of battery cells is assumed to be 210 $/kWh [46], which corresponds to 178.50 €/kWh assuming an exchange rate of 0.85 €/$. The marginal degradation cost is then calculated as

$$MC_{\mathrm{deg}} = C_{\mathrm{MC}} = \frac{c_{\mathrm{repl}}}{2EFC} \tag{3.56}$$

where $\mathrm{MC}_{\mathrm{deg}}$ is expressed in €/kWh, c_{repl} denotes the battery replacement cost of 178.50 €/kWh, and *EFC* is the total number of equivalent full cycles over the battery lifetime.

Finally, the degradation model is directly integrated into EMERGE, allowing the battery energy capacity E_{cap} to be updated during the simulation. EMERGE is operated on a daily optimization horizon over a full year, with profit maximization performed for each day. At the end of every day, the SoC trajectory is recorded, the corresponding capacity loss is calculated, and the available energy capacity is updated accordingly. This updated capacity is then used as an input for the optimization of the next day.

The SoC is treated as a continuous state variable, such that the final energy content of the battery at the end of one day becomes the initial energy content for the next day. However, since SoC is defined as the ratio of stored energy to the current usable capacity, the numerical SoC value cannot be carried

over directly when the capacity changes due to degradation. Instead, continuity is enforced in terms of the absolute stored energy in the battery. Accordingly, the state of charge at the beginning of day $d+1$ is computed as

$$\mathrm{SoC}_{d+1}^{\mathrm{init}} = \frac{\mathrm{SoC}_{d}^{\mathrm{final}}\, E_{\mathrm{cap},d}}{E_{\mathrm{cap},d+1}}, \tag{3.57}$$

which ensures that the energy content at the end of day d is preserved when transitioning to day $d+1$, despite changes in the usable battery capacity due to degradation.

In Eq. (3.57), $\mathrm{SoC}_{d+1}^{\mathrm{init}}$ denotes the SoC at the beginning of day $d+1$, and $\mathrm{SoC}_{d}^{\mathrm{final}}$ denotes the SoC at the end of day d. The variable $E_{\mathrm{cap},d}$ represents the available battery energy capacity at the end of day d, while $E_{\mathrm{cap},d+1}$ denotes the updated energy capacity at the start of day $d+1$ after accounting for degradation.

3.3.3. Net Present Value

When evaluating an investment, cash flows usually occur at different moments in time. Here, a cash flow is defined as the net amount of money entering or leaving a project in a given period, denoted as R_t for time period t. Because money has a time value, amounts can only be compared when they are expressed at the same point in time. A euro received today is generally worth more than a euro received in the future, as it can be invested to earn a return over time [57], although this relationship depends on assumptions such as positive discount rates and stable economic conditions.

If the interest rate is r, a cash flow can be moved forward in time by multiplying it by $(1+r)$. This is called compounding. To move a future cash flow back to today, it must be divided by $(1+r)$. This is called discounting.

In investment analysis, all future cash flows are converted to their present value. The Net Present Value (NPV) is defined as the sum of all discounted net cash flows over the project lifetime:

$$\mathrm{NPV} = \sum_{t=1}^{T} \frac{R_t}{(1+r)^t} - \mathrm{CAPEX}, \tag{3.58}$$

where R_t denotes the net cash flow in period t, T is the project lifetime, and r is the discount rate. It is assumed that the capital expenditure (CAPEX) occurs at $t=0$ (year 0) and is therefore not subject to discounting.

If the NPV is positive, the project generates more value than the required return and can be considered financially attractive [57].

In this work, a project lifetime of 25 years is assumed. Since EMERGE is simulated for a single year, the resulting annual cash flow is assumed to repeat over the project lifetime and is therefore accounted for once per year in the NPV calculation.

To isolate the economic value of storage, the wind-only configuration is used as a baseline. This ensures that only the additional revenues attributable to the storage system are assessed.

The NPV of the wind-plus-storage configuration is defined as:

$$\mathrm{NPV}_{\mathrm{wind+storage}} = \sum_{t=1}^{T} \frac{R_{\mathrm{w+s},t}}{(1+r)^t} - \mathit{CAPEX}_{\mathrm{wind}} - \mathit{CAPEX}_{\mathrm{storage}}, \tag{3.59}$$

where $R_{\mathrm{w+s},t}$ denotes the annual cash flow of the hybrid power plant with wind and storage in year t, r is the discount rate, and T is the project lifetime (25 years).

Similarly, the NPV of the wind-only configuration is given by:

$$\mathrm{NPV}_{\mathrm{wind\text{-}only}} = \sum_{t=1}^{T} \frac{R_{\mathrm{w},t}}{(1+r)^t} - \mathit{CAPEX}_{\mathrm{wind}}, \tag{3.60}$$

where $R_{\mathrm{w},t}$ denotes the annual cash flow of the hybrid power plant with only wind in year t.

The NPV of the storage system is then defined as:

$$\mathrm{NPV}_{\mathrm{storage}} = \mathrm{NPV}_{\mathrm{wind+storage}} - \mathrm{NPV}_{\mathrm{wind\text{-}only}}. \tag{3.61}$$

By subtracting the wind-only case, all wind-related capital expenditures cancel out. The resulting expression therefore represents the net economic contribution of storage:

$$\mathrm{NPV}_{\mathrm{storage}} = \sum_{t=1}^{T} \frac{R_{\mathrm{w+s},t} - R_{\mathrm{w},t}}{(1+r)^t} - \mathit{CAPEX}_{\mathrm{storage}}. \tag{3.62}$$

This formulation ensures that the comparison between lithium-ion batteries and LPCAES reflects only their incremental value addition to the wind asset. Wind CAPEX is excluded from the comparison, as it is identical across storage configurations.

3.4. Case study

3.4.1. Introduction

Within this framework, the *Nederwiek* area covers approximately 600 km^2 and has a planned total capacity of 6 GW. It borders the United Kingdom's section of the North Sea and comprises three zones: *Nederwiek I*, *II*, and *III*, each with a capacity of 2 GW. *Nederwiek I* includes two sites, *I–A* and *I–B*, each planned for 1 GW [58], and will be connected to the mainland through an underground high-voltage cable system with a total transmission capacity of 2 GW [59]. In Appendix A, the location of the *Nederwiek* area is shown.

The site *Nederwiek (Zuid) kavel I–B* is located approximately 95 km offshore [60]. Its position within the overall roadmap is shown in Figure A.1 in Appendix A. This study focuses on site *I–B* only, for which one of the two 1 GW high-voltage connections is assumed to be available.

Input parameters

This *Nederwiek (Zuid) kavel I–B* site serves as an example for analyzing the integration of offshore wind with energy storage in HPP configuration. The modeled HPP consists of a 1 GW offshore wind farm coupled with an energy storage system connected to the Dutch electricity grid. The system is constrained by the maximum import and export capacities, while also being capable of participating in the aFRR market. The corresponding input parameters are summarized in Table 3.2.

Table 3.2: System input parameters for the case study.

Parameter	Symbol	Value
Maximum export power to the grid	$P^{\mathrm{export,max}}$	1 GW
Maximum import power from the grid	$P^{\mathrm{import,max}}$	1 GW
Rated wind power	$P^{\mathrm{wind,rated}}$	1 GW
Initial State of Charge	SoC^{init}	50 [%]
Required upward capacity	$r^{\mathrm{aFRR}\uparrow,\mathrm{req}}$	0 MW
Required downward capacity	$r^{\mathrm{aFRR}\downarrow,\mathrm{req}}$	0 MW
Maximum upward capacity	$r^{\mathrm{aFRR}\uparrow,\mathrm{max}}$ [33]	35 MW
Maximum downward capacity	$r^{\mathrm{aFRR}\downarrow,\mathrm{max}}$ [33]	40 MW

The maximum upward ($r^{\mathrm{aFRR}\uparrow,\mathrm{max}}$) and downward ($r^{\mathrm{aFRR}\downarrow,\mathrm{max}}$) capacities listed in Table 3.2 are set to approximately 10% of the average daily aFRR capacity in the Dutch electricity market [33]; see Section 2.1.2 for further details.

The storage-specific parameters for the Li-ion battery and LPCAES systems are given in Tables 3.3 and 3.4, respectively.

Table 3.3: Input parameters for Li-ion battery storage.

Parameter	Symbol	Value
Charging efficiency	η_{c} [11]	94 [%]
Discharging efficiency	η_{d} [11]	94 [%]
Minimum state of charge	SoC^{min}	10 [%]
Maximum state of charge	SoC^{max}	90 [%]

Table 3.4: Input parameters for LPCAES storage.

Parameter	Symbol	Value
Charging efficiency	η_{c} [47]	70 [%]
Discharging efficiency	η_{d} [47]	70 [%]
Minimum state of charge	SOC^{min}	0 [%]
Maximum state of charge	SOC^{max}	100 [%]

Profitability of short- and long-duration storage

In Section 4.1, a wind farm with a rated power of 1 GW is considered. Simulations are performed using the input data listed in Tables 3.3, 3.4, and 3.5. At this stage, the remaining free design variables are the storage energy capacity (E_{cap}) and the maximum charge and discharge rates (r_{c} and r_{d}). A storage power capacity equal to 20% of the wind farm's rated power is selected, corresponding to 200 MW. For the Li-ion system, a maximum (dis)charging rate of $r_{\mathrm{c}} = r_{\mathrm{d}} = 0.5$ is assumed, resulting in an energy capacity (E_{cap}) of 400 MWh. For the LPCAES system, the same power capacity of 200 MW is used; however, a lower maximum (dis)charging rate of $r_{\mathrm{c}} = r_{\mathrm{d}} = 0.125$ is assumed, and the corresponding energy capacity (E_{cap}) amounts to 1600 MWh.

To allow for a fair comparison of different power-to-energy ratios, two additional cases are simulated: a 1600 MWh Li-ion system and a 400 MWh LPCAES system. At this stage, the marginal costs of the storage technologies are set to 0.00 €/kWh.

In total, the EMERGE model is run for four storage configurations: two Li-ion battery cases and two LPCAES cases, each evaluated at energy capacities of 400 MWh and 1600 MWh. Simulations are conducted for the years 2022, 2023, and 2024, resulting in 12 storage cases (3 years × 4 configurations), plus an additional three simulations without storage. The objective of this section is to obtain an initial estimate of the profitability of short- versus long-duration storage across multiple electricity markets. Here, the operational profits are compared, referring to the profit generated by the HPP through market participation. This is defined, per time step, as the net cash flow obtained from total revenues minus marginal operating costs. In this analysis, the marginal operating costs are assumed to be zero.

Sizing of short- and long-duration storage

In Section 4.2, the influence of storage size and C-rate on profitability is analyzed. By selecting a simulation year, enabling or disabling aFRR participation, choosing a storage technology, and defining a grid of storage capacities and maximum (dis)charge rates, heat maps are generated to illustrate output parameters (e.g., operational profit) for each configuration over the selected year. The (dis)charge rates are expressed in terms of the C-rate and are assumed to be symmetric for charging and discharging.

For lithium-ion batteries, the considered energy capacities correspond to 10–50% of the installed wind capacity of 1 GW, resulting in a power range of 100–500 MW. The assumed C-rates span from 0.1 to 0.5 h^{-1}, corresponding to storage durations between 10 h and 2 h. The C-rate is discretized into 17 steps of 0.025, which includes representative durations such as 2 h (0.5), 4 h (0.25), 5 h (0.2), ~ 6 h (0.175), 8 h (0.125), and 10 h (0.1). Combining the selected C-rates and capacities results in storage sizes ranging from 200 MWh (100 MW at 0.5 h^{-1}) to 5000 MWh (500 MW at 0.1 h^{-1}). The energy capacity is discretized into 13 steps of 400 MWh, yielding a grid of $13 \times 17 = 221$ Li-ion configurations.

For LPCAES, only C-rates less than or equal to 0.25 h^{-1} are considered, as the technology requires a minimum storage duration of approximately 4 h to ensure quasi-isothermal operation (see Sec-

tion 2.2.5). Consequently, the C-rate range is limited to 0.1–0.25 h^{-1}, corresponding to storage durations between 10 h and 4 h. Using the same energy capacity range of 200–5000 MWh, this translates to power capacities of 50–500 MW, or 5–50% of the wind capacity. The C-rate range is discretized into 7 steps of 0.025, and together with the 13 energy capacity steps, this results in a total of $13 \times 7 = 91$ LPCAES configurations.

The missing LPCAES configurations within the grid range of 0.25–0.5 and storage capacities of 200–500 MWh are nevertheless included in the heat maps and indicated by a hatched pattern, allowing the overall figure layout and comparison across both storage technologies to be preserved. To obtain smoother visualizations, the data were upsampled using linear interpolation, increasing the grid resolution by a factor of four. In addition, contour lines were overlaid to improve readability and to emphasize key trends in the results.

Using all the different options described in the previous sections, the following simulations will be run:

Year	Sim.	Storage technology	Daily degr.	Marginal degradation costs	aFRR
2024	1	No storage	N/A	N/A	N/A
	2	Lithium-ion	No	No	No
	3	Lithium-ion	No	No	Yes
	4	LPCAES	N/A	N/A	No
	5	LPCAES	N/A	N/A	Yes
	6	Lithium-ion	No	Yes (EoL 70%, MC_{deg} via Sim. 2)	No
	7	Lithium-ion	No	Yes (EoL 70%, MC_{deg} via Sim. 3)	Yes
	8	Lithium-ion	Yes	Yes (EoL 70%, MC_{deg} via Sim. 2)	No
	9	Lithium-ion	Yes	Yes (EoL 80%, MC_{deg} via Sim. 3)	Yes
	10	Lithium-ion	Yes	Yes (EoL 70%, MC_{deg} via Sim. 3)	Yes
	11	Lithium-ion	Yes	Yes (EoL 60%, MC_{deg} via Sim. 3)	Yes
2023	12	No storage	N/A	N/A	N/A
	13	Lithium-ion	No	No	Yes
	14	Lithium-ion	Yes	Yes (EoL 70%, MC_{deg} via Sim. 13)	Yes
	15	LPCAES	N/A	N/A	Yes
2022	16	No storage	N/A	N/A	N/A
	17	Lithium-ion	No	No	Yes
	18	Lithium-ion	Yes	Yes (EoL 70%, MC_{deg} via Sim. 17)	Yes
	19	LPCAES	N/A	N/A	Yes

Table 3.5: Overview of simulation cases. N/A denotes not applicable. "Daily degr." indicates whether daily battery capacity updates due to degradation are implemented. "MC_{deg} via Sim. k" indicates that the marginal degradation cost is calculated using Eq. 3.56, based on the degradation results obtained from simulation k. Different End-of-Life State of Health thresholds are considered in the marginal cost calculation, affecting both the marginal degradation costs and the resulting battery lifetime. "aFRR" indicates whether the storage technology participates in the aFRR market; if not, it operates exclusively in the day-ahead market.

In this section, simulation cases 1, 2, 3, 4, 5, 12, 13, 15, 16, 17, and 19 from Table 3.5 are compared.

Degradation effects on short- and long-duration storage

In Section 4.3, the remaining simulation cases listed in Table 3.5, which explicitly account for storage degradation, are analyzed to assess the impact of degradation on profitability.

Also, Net Present Values (NPV) analyses will be performed. Battery degradation costs are included directly in the annual cash flows and are therefore implicitly accounted for in the NPV calculation. A discount rate of $r = 7\%$ is adopted, consistent with common practice in energy techno-economic analyses [61]. Additionally, values of 5% and 9% are evaluated to examine the sensitivity of the results to the discount rate.

4

Results

4.1. Profitability of short- and long-duration storage

4.1.1. Operational profits of different storage configurations

Figure 4.1 presents the operational profits for all simulated configurations over the years 2022–2024, as described in Section 3.4.1, including a reference case without storage. For each storage technology, two energy capacities (400 MWh and 1600 MWh) are evaluated. For both capacities, participation is analyzed under two market strategies: participation in the day-ahead market only and combined participation in the day-ahead and aFRR markets.

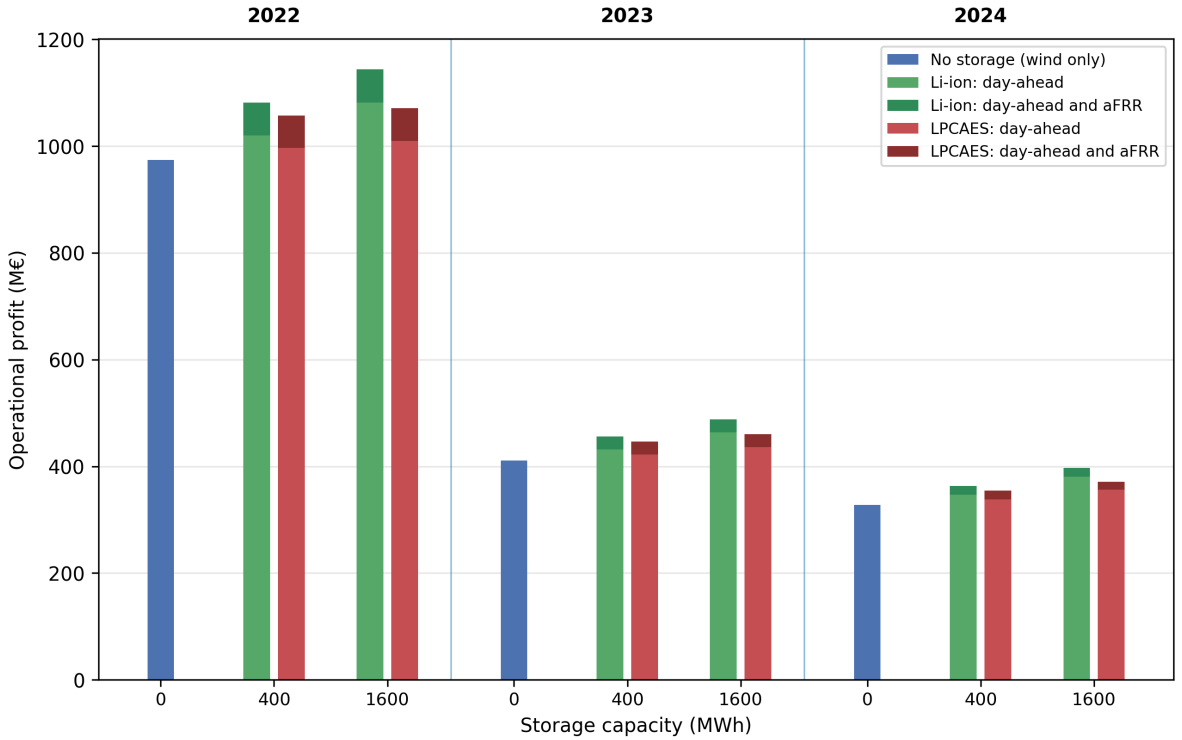

Figure 4.1: Operational profits (in million €) for HPP configurations comprising wind-only operation, Li-ion storage (400 MWh and 1600 MWh), and LPCAES (400 MWh and 1600 MWh), under two market strategies, namely day-ahead only and combined participation in the day-ahead and aFRR markets, over the years 2022, 2023, and 2024.

Across all years, the no-storage configuration results in the lowest operational profit, whereas all wind-plus-storage configurations achieve higher operational profits. Absolute profits are highest in 2022,

followed by 2023 and 2024, a pattern that is consistent across storage technologies, capacities, and market participation options, as shown in Figure 4.1. The observed trend is driven by differences in day-ahead electricity prices.

The average day-ahead price was 0.0773 €/kWh in 2024, 0.0958 €/kWh in 2023, and 0.2412 €/kWh in 2022. Operational profits in the no-storage case in 2023 exceed those of 2024 by roughly 25%, closely mirroring the 24% higher average day-ahead price in 2023. In 2022, operational profits are approximately 197% higher than in 2024, which aligns with the substantially elevated price levels observed in that year. The high electricity prices observed in 2022 can largely be explained by the sharp increase in natural gas prices. After the COVID-19 pandemic, energy demand recovered rapidly as economic activity resumed. However, gas markets remained tight, with relatively low storage levels and significantly reduced deliveries from Russia, particularly following the outbreak of the war in Ukraine [62].

Because natural gas-fired power plants frequently act as the marginal producers in the European electricity market, as described in Section 2.1.2, gas prices often influence the wholesale electricity price. As a result, the increase in gas prices translated directly into higher electricity prices across the market [62].

Figure 4.2 highlights the impact of storage integration, using the wind-only case as the baseline. The figure shows the absolute increase in operational profit achieved by the storage technologies compared to the wind-only reference case for each year.

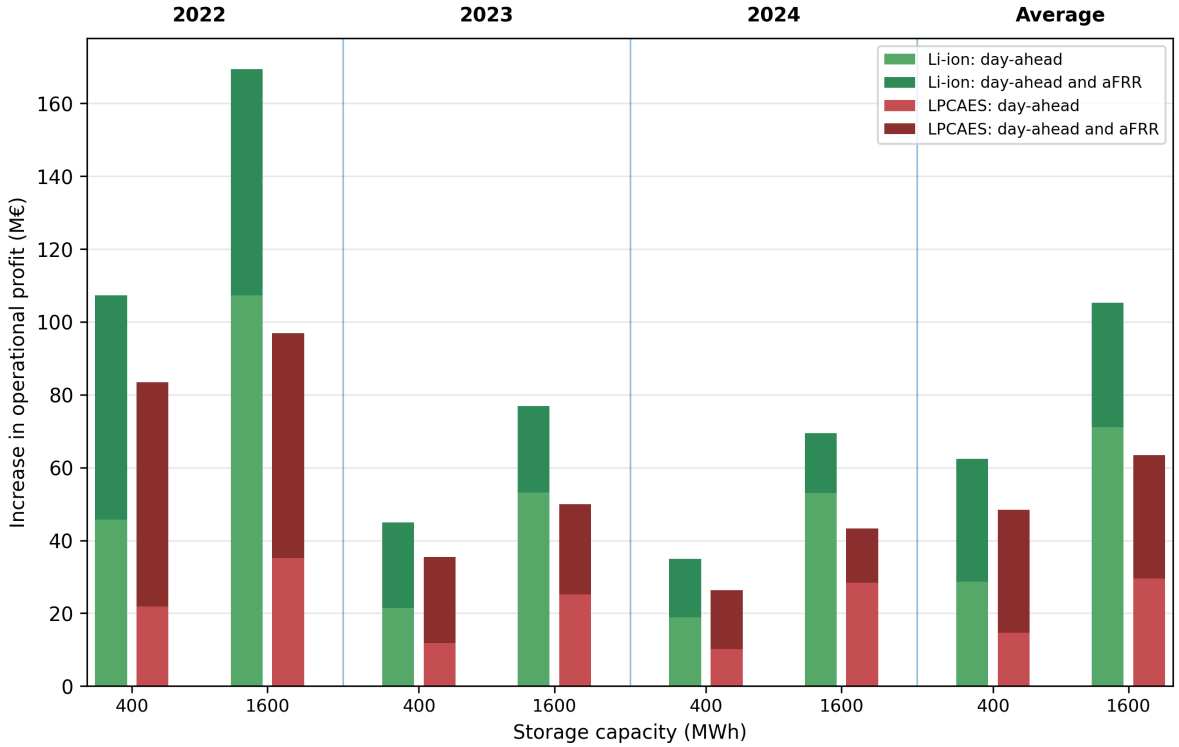

Figure 4.2: Increase in operational profit (in million €) relative to the wind-only reference case (blue bar) shown in Figure 4.1, for the years 2022, 2023, and 2024, for Li-ion (400 MWh and 1600 MWh) and LPCAES (400 MWh and 1600 MWh) HPP configurations participating in the day-ahead and aFRR markets.

As shown in Figure 4.2, the following trends can be identified when the wind-only case is used as the baseline.

Day-ahead market performance

For identical storage capacities, Li-ion storage achieves a larger increase in operational profit than LPCAES in the day-ahead market in all analyzed years. For the 400 MWh configuration, the profit increase of Li-ion exceeds that of LPCAES by 109% in 2022, 81% in 2023, and 85% in 2024. For the

1600 MWh configuration, the relative difference is even more pronounced, amounting to 205% in 2022, 111% in 2023, and 87% in 2024. Hence, Li-ion consistently delivers substantially higher day-ahead profit increases, with the largest relative gaps observed in 2022 and for the 1600 MWh system.

These differences are primarily driven by the technical characteristics of the storage technologies. Li-ion exhibits charging and discharging rates of $r_{\mathrm{c}} = r_{\mathrm{d}} = 0.5\,\mathrm{h}^{-1}$, whereas LPCAES is limited to $r_{\mathrm{c}} = r_{\mathrm{d}} = 0.125\,\mathrm{h}^{-1}$. Since maximum charging and discharging powers scale proportionally with these rates (see Equation 3.23), Li-ion can provide substantially higher power relative to its energy capacity. A higher C-rate enables faster responses to short-term price signals: the system can discharge larger volumes during price peaks and charge more during low or negative price periods. This flexibility allows Li-ion to capture short-lived price spreads more effectively, which is particularly valuable in volatile years such as 2022.

LPCAES also has lower charging and discharging efficiencies (η_{c} and η_{d}) than Li-ion (0.70 compared to 0.94). This means that a larger share of the input electricity is lost during charging and discharging. As a result, part of the electricity that is stored is lost and cannot be sold later. This means that the system earns less money from buying electricity at low prices and selling it at high prices, which reduces the profits from day-ahead trading.

Increasing the storage capacity from 400 MWh to 1600 MWh enhances day-ahead profits for both technologies. For Li-ion, this expansion leads to relative profit increases of 135% in 2022, 149% in 2023, and 181% in 2024. For LPCAES, the corresponding increases amount to 61% in 2022, 114% in 2023, and 179% in 2024. Larger energy capacity allows more energy to be shifted across time, thereby increasing arbitrage potential. However, the benefit of capacity expansion is amplified when combined with a high C-rate, which explains the particularly strong scaling observed for Li-ion systems.

Impact of aFRR participation

Participation in the aFRR market further increases operational profit for all configurations. The incremental aFRR profit, defined as the difference between the day-ahead-only case and the combined day-ahead plus aFRR case, is very similar across technologies and storage sizes. For the 400 MWh configuration, the additional aFRR profit amounts to 62 M€ in 2022, 24 M€ in 2023, and 16 M€ in 2024 for both technologies. For the 1600 MWh configuration, the corresponding values are likewise about 62 M€ in 2022, around 24 M€ in 2023 (23.8 M€ for Li-ion and 24.7 M€ for LPCAES), and roughly 15–17 M€ in 2024 (16.5 M€ for Li-ion and 14.9 M€ for LPCAES).

The limited variation in incremental aFRR profit between storage sizes is explained by the technical caps imposed on reserve provision. The maximum upward and downward aFRR capacities are restricted to:

$$r^{\mathrm{aFRR}\uparrow,\mathrm{max}} = 35\ \mathrm{MW} \quad \text{and} \quad r^{\mathrm{aFRR}\downarrow,\mathrm{max}} = 40\ \mathrm{MW}$$

as specified in Table 3.2. These limits apply equally to all configurations and cap the reservable power independently of installed energy capacity. Once a system can reliably provide 35–40 MW while respecting SoC constraints, increasing the energy capacity from 400 MWh to 1600 MWh does not increase the amount of reserve that can be offered. As a result, capacity-related profits do not scale with storage size.

aFRR remuneration consists of capacity payments (€/MW) and activation energy payments (€/MWh) (see Section 2.1.2). In the present results, total aFRR profit is dominated by the capacity component. Since the maximum reserve power is the same for all configurations and all systems are able to provide this amount, the total aFRR revenues end up at nearly the same level for both technologies and storage sizes. For the 400 MWh LPCAES configuration in 2023 and 2024, the incremental aFRR profit even exceeds the additional profit from day-ahead trading alone. This does not imply that aFRR is inherently more profitable than arbitrage. LPCAES has a low C-rate and lower efficiency, which limits how much it can earn in the day-ahead market. It cannot charge and discharge as quickly as Li-ion, and part of the stored energy is lost. This reduces its arbitrage profits. In the aFRR market, revenues mainly depend on how much reserve power (MW) can be offered. As long as the system can provide the required reserve and keep its SoC within the allowed range, efficiency plays a smaller role. Therefore, aFRR revenues make up a larger share of the total profit for LPCAES, particularly at smaller energy capacities.

The remaining small differences between technologies and storage sizes (within approximately ±1 M€) arise from activation-induced energy exchanges, efficiency losses, and the State of Charge management required to guarantee continuous reserve availability. These interactions slightly affect the coordination between day-ahead dispatch and balancing provision, but their quantitative impact remains limited because overall aFRR revenues are largely determined by the capped capacity remuneration.

The remaining small differences between technologies and storage sizes (within about ±1 M€) result from the interaction between day-ahead trading and aFRR provision. When aFRR is activated, the SoC changes, which can slightly alter the optimal day-ahead dispatch compared to the day-ahead-only case. In addition, efficiency losses during activation differ between technologies.

4.1.2. Storage dispatch in EMERGE

This section examines the operational behavior of EMERGE. Using 9 March 2024 as an illustrative example, the 1600 MWh storage configurations operating exclusively in the day-ahead market (see Section 4.1.1) are analyzed. The day-ahead prices, grid import and export power, wind park generation, as well as the charging, discharging, and SoC of the storage systems are presented in Figure 4.3.

As shown in Figure 4.3, both storage configurations follow the same overall price-driven operating strategy. During the morning, until approximately 11:00h, day-ahead prices are positive and the electricity generated by the wind farm is directly exported to the grid. When prices turn negative around midday, electricity is imported instead of exported, as buying power at negative prices generates revenue. At the same time, wind generation is curtailed, since exporting electricity under negative prices would incur costs. Both Li-ion and LPCAES therefore charge during these hours.

Around 14:00h, the storage systems reach their upper SoC limits. From that point onward, no further charging occurs, and the systems remain at the maximum SoC until prices increase sufficiently to make discharging economically attractive. During the high-price hours in the late afternoon and evening, both technologies discharge and export electricity to the grid.

Although the general strategy is similar, important differences arise from the technical characteristics of the two storage technologies. Around 12:00–13:00h, the Li-ion system already switches from charging to exporting, while LPCAES continues charging for a longer period. This is primarily due to the higher C-rate of Li-ion ($0.5\ h^{-1}$), compared to LPCAES ($0.125\ h^{-1}$). The higher C-rate allows Li-ion to charge and discharge at higher power, enabling it to reach its upper SoC limit faster and to react more quickly to short-term price changes. Under the assumption of perfect price foresight in the model, this power flexibility becomes particularly valuable. Since price developments are known in advance, the systems optimize their schedules accordingly. The Li-ion system can briefly export electricity at slightly negative prices around 12:00–13:00h to create additional storage headroom. This allows it to import larger volumes later when prices become even more negative. Due to its lower C-rate, LPCAES cannot adjust its charging strategy as quickly and is therefore less able to exploit short-term price fluctuation.

Another structural difference concerns the usable SoC range. Li-ion operates between 10–90% SoC, whereas LPCAES can use the full 0–100% range. This restriction reduces the usable energy capacity of Li-ion. However, Li-ion has a significantly higher round-trip efficiency (94%) than LPCAES (70%). As a result, a larger share of imported electricity can be converted into exported electricity, which improves its arbitrage performance despite the narrower SoC window.

During the evening peak-price period, both systems discharge from full capacity down to their minimum SoC in order to maximize revenues for that day. Electricity export is capped at 1000 MW, and both technologies operate at their maximum discharge power during the highest price hours. It can be observed that LPCAES discharges at a higher power than Li-ion. This is a direct consequence of its lower efficiency: to deliver the same net export of 1000 MW to the grid, LPCAES must generate a higher gross output. Consequently, it depletes its stored energy more quickly and reaches its minimum SoC earlier than Li-ion.

Small charging and discharging actions before 11:00h and between 14:00 and 17:00h are related to the model implementation in EMERGE. The grid export is constrained to be constant on an hourly basis, whereas wind generation data are provided in 15-minute intervals. The storage system compensates for short-term fluctuations in wind generation to maintain a constant hourly export level.

When the storage systems also participate in the aFRR market, part of the power and energy capacity must be reserved. This reduces the capacity available for day-ahead arbitrage and constrains the SoC trajectory, since sufficient room must be maintained during the contracted availability periods (see Section 2.1.2). If activated, the reserved capacity leads to additional energy exchanges, further affecting the SoC evolution.

Finally, degradation reduces the available storage capacity over time, limiting the amount of energy that can be charged and discharged. In addition, marginal degradation costs decrease the net profit in each timestep, as using the storage system is no longer cost-free.

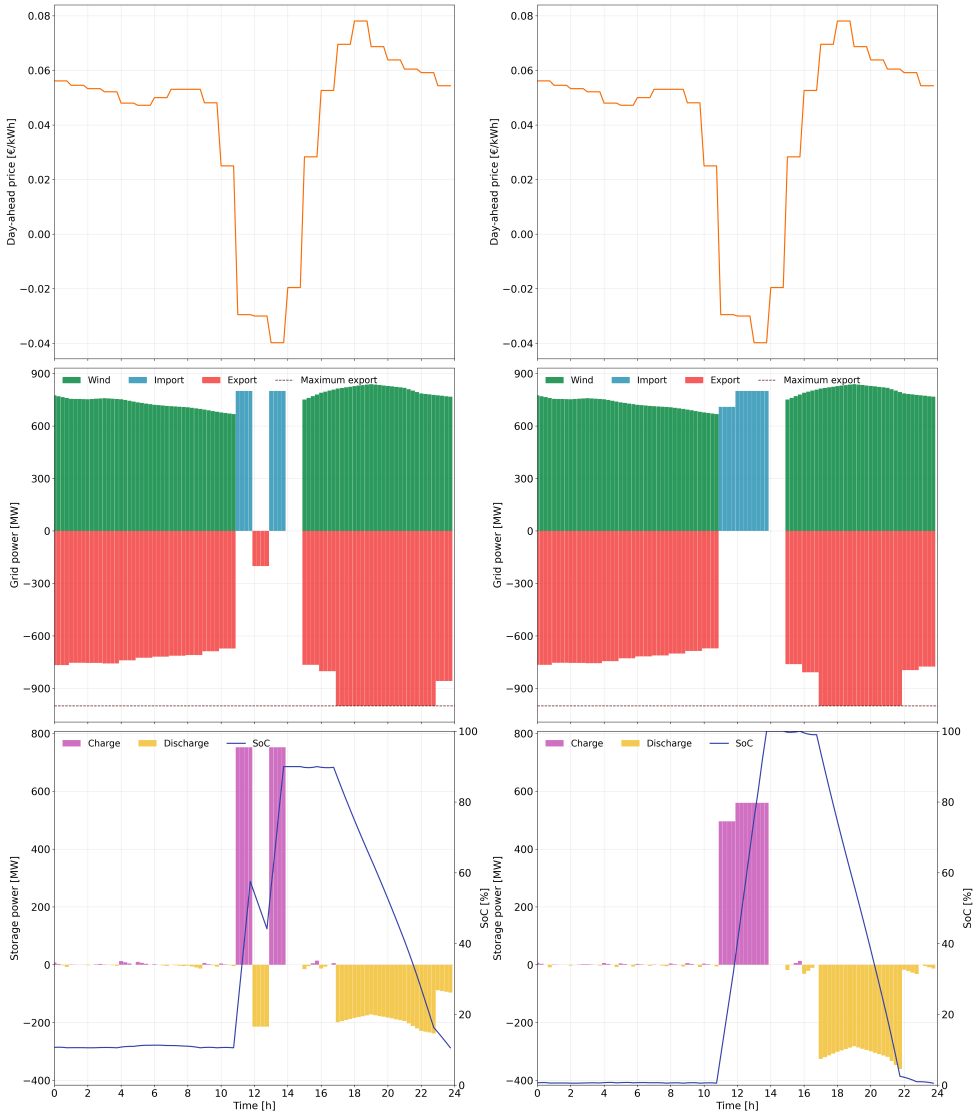

Figure 4.3: Overview of the HPP operation on 9 March 2024 in the day-ahead market. The left column presents the wind farm combined with Li-ion storage, while the right column shows the wind farm combined with LPCAES. For both configurations, an energy capacity of 1600 MWh is assumed. The maximum C-rate is set to 0.5 for Li-ion and 0.125 for LPCAES. The first row depicts the day-ahead electricity price in €/kWh throughout the day. The second row shows the power flows in MW, including grid import and export and the maximum export power, as well as the wind farm output, which is identical for both configurations. The third row illustrates the storage operation, presenting the charging and discharging power in MW together with the state of charge (SoC) of the respective storage technology.

4.2. Sizing of short- and long-duration storage

In Figure 4.4, the operational profits of four different storage configurations in 2024 are shown. For all configurations no marginal degradation costs are assumed.

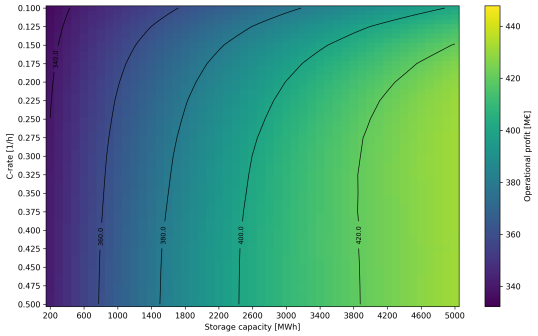

(a) Operational profits of a wind park combined with Li-ion battery storage, excluding marginal degradation costs and operating exclusively in the day-ahead market.

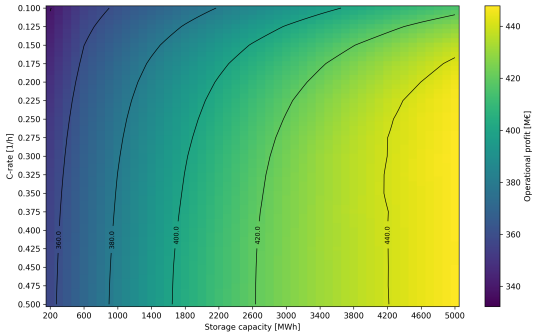

(b) Operational profits of Li-ion battery storage, excluding marginal degradation costs, with participation in both the day-ahead and the aFRR markets.

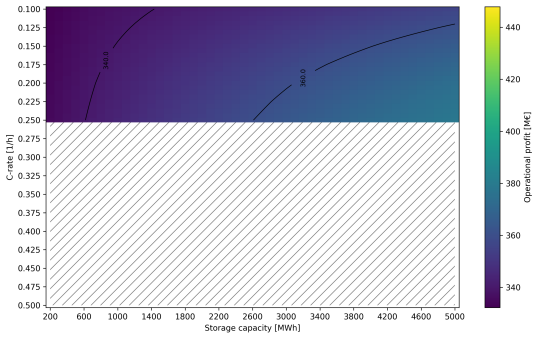

(c) Operational profits of a wind park combined with LPCAES, excluding marginal degradation costs and operating exclusively in the day-ahead market.

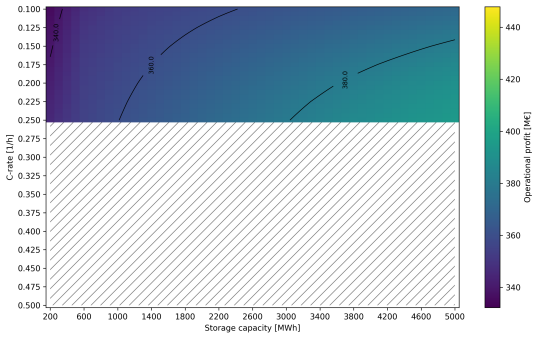

(d) Operational profits of LPCAES, excluding marginal degradation costs, with participation in both the day-ahead and the aFRR markets.

Figure 4.4: Operational profits (million €) of a 1 GW wind farm combined with different storage technologies, storage capacities, and C-rates in 2024.

Figure 4.4a presents the Li-ion battery configurations operating exclusively in the day-ahead market. When participation in the aFRR market is enabled (Figure 4.4b), operational profits increase for all storage capacities and C-rates. Accordingly, participation in the aFRR market leads to consistently higher operational revenues than operation in the day-ahead market alone. The same trend is observed for the LPCAES configurations. Comparing Figures 4.4c (without aFRR) and 4.4d (with aFRR) shows that participation in the aFRR market also increases operational profits for LPCAES. However, profit levels remain lower than for Li-ion across most configurations.

This effect is clearly illustrated in Figure 4.5, which shows the relative change in operational profits (in %) of the different configurations compared to the Li-ion day-ahead reference case (Figure 4.4a).

For Li-ion (Figure 4.5b), participation in the aFRR market increases operational profit for all configurations. Beyond roughly 600 MWh, the relative increase stabilizes at around 4%. This occurs because the technical limits for aFRR provision are reached: the maximum upward and downward reserve capacities are capped, as described in Section 4.1.1. For smaller storage capacities and lower C-rates, these caps cannot yet be fully utilized, resulting in a smaller profit increase. As shown in Figure 4.4, the maximum additional profit obtainable from aFRR provision is approximately 20 M€. Once the reserve capacity limit is reached, further increases in energy capacity do not increase aFRR revenues. The same mechanism applies to LPCAES (Figures 4.4c and 4.4c). The maximum additional profit from aFRR participation is similar, as reserve remuneration primarily depends on the contracted MW and the same capacity caps apply, independent of storage technology.

Without aFRR participation (Figure 4.5c), LPCAES generates lower operational profits than Li-ion for all configurations. This difference is mainly driven by the lower round-trip efficiency of LPCAES, which reduces arbitrage revenues in the day-ahead market. The effect becomes more pronounced at larger storage capacities because a bigger system can (dis)charge more energy to profit from price differences. Since LPCAES has a lower efficiency, it loses more energy in each cycle. With larger energy volumes, these losses increase, which reduces arbitrage revenues compared to Li-ion.

When LPCAES participates in the aFRR market (Figure 4.5d), its operational profits exceed those of the Li-ion day-ahead reference case for smaller storage capacities (up to approximately 1000 MWh). At small capacities, the arbitrage potential in the day-ahead market is limited for both technologies. By additionally providing aFRR capacity, LPCAES generates extra revenue from reserve reservation, which is sufficient to surpass the profits of Li-ion operating only in the day-ahead market, despite Li-ion's higher efficiency. For larger capacities, however, Li-ion benefits more strongly from its higher efficiency in day-ahead arbitrage. The higher arbitrage revenues achieved by Li-ion therefore dominate the comparable aFRR income, resulting in higher overall profits than LPCAES as the energy capacity increases.

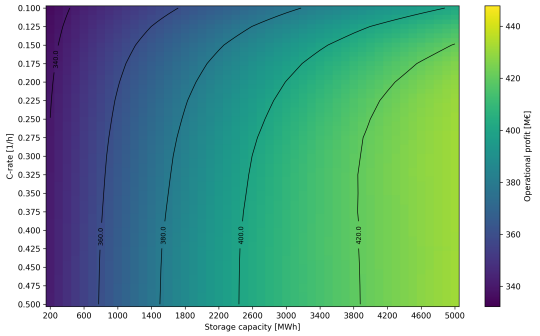

(a) Operational profits of a wind park combined with Li-ion battery storage, excluding marginal degradation costs and operating exclusively in the day-ahead market.

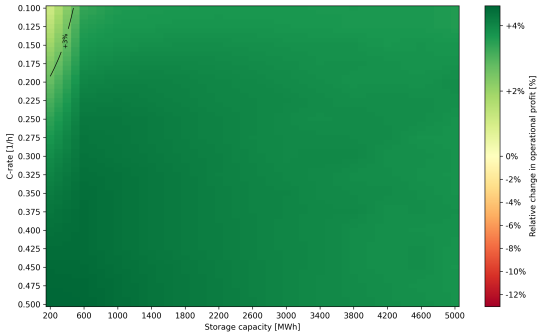

(b) Relative change in operational profits of Li-ion battery storage, excluding marginal degradation costs, with participation in both the day-ahead and the aFRR markets.

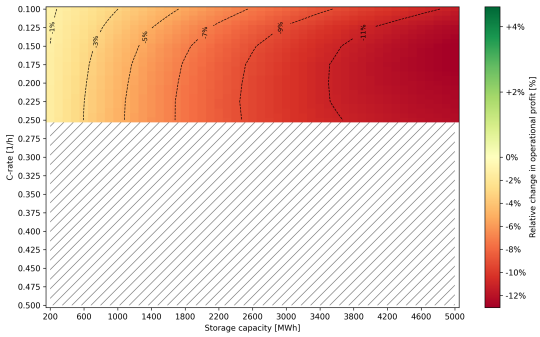

(c) Relative change in operational profits of a wind park combined with LPCAES and operating exclusively in the day-ahead market.

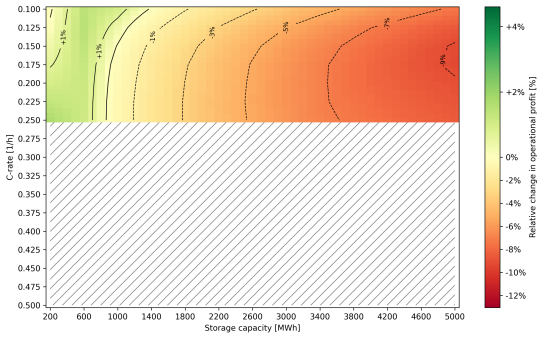

(d) Relative change in operational profits of LPCAES, with participation in both the day-ahead and the aFRR markets.

Figure 4.5: Relative change in operational profits (%) of a 1 GW wind farm in 2024 combined with different storage technologies, storage capacities, and C-rates, compared to the reference case shown in Figure 4.5a.

Figures 4.4 and 4.5 are based on wind generation and price data for 2024. Figure 4.6 presents the operational profits of the wind farm using input data for 2022 and 2023 and compares these results with those for 2024.

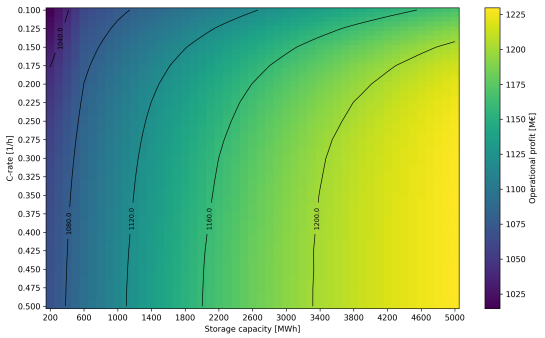

(a) Operational profits of Li-ion battery storage, excluding marginal degradation costs, with participation in both the day-ahead and the aFRR markets in 2022.

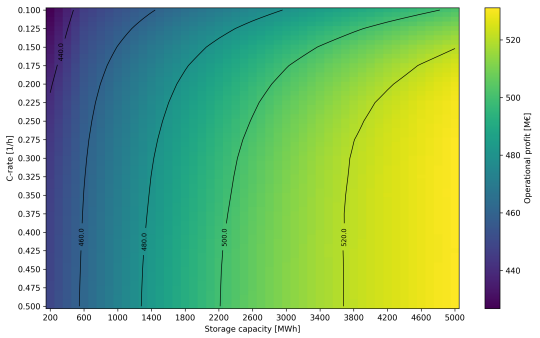

(b) Operational profits of Li-ion battery storage, excluding marginal degradation costs, with participation in both the day-ahead and the aFRR markets in 2023.

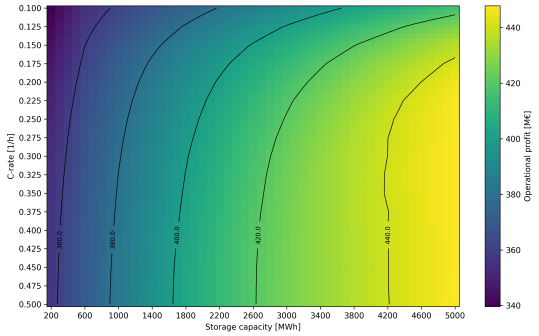

(c) Operational profits of Li-ion battery storage, excluding marginal degradation costs, with participation in both the day-ahead and the aFRR markets in 2024.

Figure 4.6: Operational profits (million €) of a 1 GW wind farm combined with Li-ion battery storage for different storage capacities and C-rates in 2022, 2023, and 2024.

Figure 4.6 shows that, in all three years, the operational profits of the Li-ion battery increase with higher storage capacities and higher C-rates. A larger energy capacity allows the system to store more electricity during low-price periods and discharge more during high-price periods. This increases the total energy volume that can be shifted over time, directly raising arbitrage revenues. The C-rate determines the maximum charging and discharging power. A higher C-rate allows the storage technology to respond more quickly and trade larger power volumes over short high- or low-price periods. The contour lines indicate that, at lower C-rates, a larger energy capacity is required to achieve the same operational profit. In other words, limited power capability must be compensated by increased storage size to reach comparable profit levels.

Although this general trend is consistent across all years, the absolute profit levels differ substantially. As shown in Figure 4.6a, operational profits in 2022 are significantly higher than in the following years. Profits in 2023 (Figure 4.6b) remain above those in 2024 (Figure 4.6c), while 2024 exhibits the lowest operational profits. The differences in price levels across the years are explained in Section 4.1.1.

Figures 4.4 and 4.5 present the results for 2024, comparing Li-ion in day-ahead-only operation with Li-ion and LPCAES configurations that additionally participate in the aFRR market. The same comparison is carried out for 2022 and 2023. Although absolute profit levels vary due to different price conditions, the qualitative patterns remain unchanged: when no marginal degradation costs are considered, Li-ion achieves higher operational profits than LPCAES across all configurations. The corresponding results are shown in Figure B.1 for 2022 and in Figure B.2 for 2023 in Appendix B.

4.3. Degradation effects on short- and long-duration storage

In this section, degradation effects are incorporated into the analysis. Section 4.3.1 presents the battery lifetimes for different configurations and End-of-Life (EoL) State of Health (SoH) thresholds, and examines the impact of marginal degradation costs and daily capacity degradation on the operational profits of the battery configurations in EMERGE. Section 4.3.2 provides a Net Present Value (NPV) analysis comparing wind coupled with Li-ion storage under degradation to LPCAES.

4.3.1. Degradation of hybrid power plant configuration with Li-ion storage

Lifetimes and Equivalent Full Cycles

Figure 4.7 illustrates how different End-of-Life (EoL) criteria, defined at varying State of Health (SoH) thresholds within the implemented degradation model, affect the resulting battery lifetime and the total number of Equivalent Full Cycles (EFC). The analysis is based on battery configurations simulated using weather and market data from 2024.

Figure 4.7 shows that lowering the EoL threshold from 80% to 60% (SoH) increases the estimated lifetime of the battery configurations. The lifetime rises from approximately 4–6 years at 80% SoH to about 6–10 years at 60% SoH. A similar trend is observed in the total number of EFC, which increases on average from roughly 2000 cycles at 80% SoH to around 2500 cycles at 70% and about 3000 cycles at 60%. This increase follows directly from the definition of the EoL criterion: a lower SoH threshold permits a larger amount of cumulative degradation before the battery is considered to have reached EoL.

As can be seen in Figure 4.7a, 4.7c and 4.7e, the shortest lifetimes occur for configurations with a small storage capacity and a high C-rate. In this case, the battery can charge and discharge at high power relative to its energy capacity, resulting in many (partial) cycles within a short period. Consequently, the accumulated EFC increase rapidly, and the EoL threshold is reached relatively early.

As storage capacity increases and/or the C-rate decreases, the cycling intensity is reduced. A larger energy capacity means that the same energy throughput corresponds to fewer equivalent full cycles, while a lower C-rate limits the maximum charge and discharge power. Both effects slow down the annual accumulation of EFC and therefore extend the operational lifetime.

If the storage capacity remains small but the C-rate increases, the battery is able to respond more aggressively to price signals, which increases cycling frequency and accelerates degradation. Conversely, increasing the storage capacity at a constant C-rate generally reduces the number of EFC per year, as the same dispatched energy represents a smaller fraction of the total capacity. This reduces relative cycling intensity and increases lifetime.

Despite these differences in annual cycling intensity, the total number of EFC reached at EoL is relatively similar across most configurations (Figures 4.7b, 4.7d, and 4.7f). This follows directly from Equation 3.55, where the lifetime EFC is defined by the product of the operational lifetime t_{life} and cumulative normalized energy throughput, expressed as $\sum_{j=1}^{n_R} R_{\mathrm{count},j} R_{\mathrm{DoD},j}$. For a fixed SoH threshold, end-of-life is reached once the total accumulated degradation equals the allowable capacity loss. In configurations where cycling degradation is the dominant aging mechanism, a higher annual cycling intensity increases the yearly degradation rate and therefore reduces t_{life}. Conversely, a lower annual cycling intensity decreases the degradation rate and extends t_{life}. Because lifetime is inversely related to the annual cycling-induced degradation, the product of annual EFC (the total lifetime EFC at EoL) remains approximately constant across these configurations.

The main exception is the combination of low storage capacity and low C-rate. In this case, limited power capability constrains market participation and reduces cycling activity, leading to a lower annual normalized energy throughput $\sum_{j=1}^{n_R} R_{\mathrm{count},j} R_{\mathrm{DoD},j}$. As a result, cycling degradation contributes less to total capacity fade, and calendar aging (the time-dependent degradation term in Equation 3.49) becomes relatively more significant. Since calendar degradation accumulates with time rather than throughput, the battery can reach the SoH threshold after a certain period even with comparatively few accumulated EFC. This explains why the total EFC at EoL is lower for this specific configuration. A detailed breakdown of the degradation components is provided in Section 3.3.

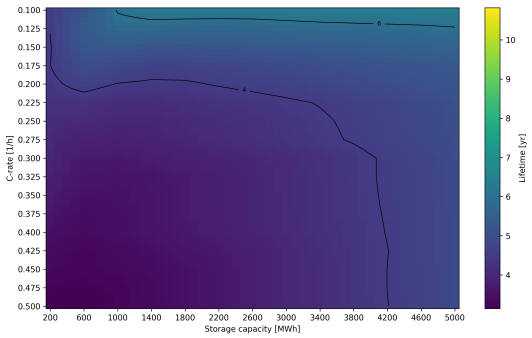

(a) Battery lifetimes with End-of-Life defined at 80% State of Health.

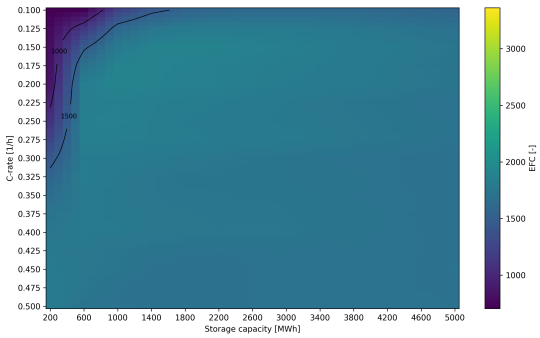

(b) Equivalent Full Cycles with End-of-Life defined at 80% State of Health.

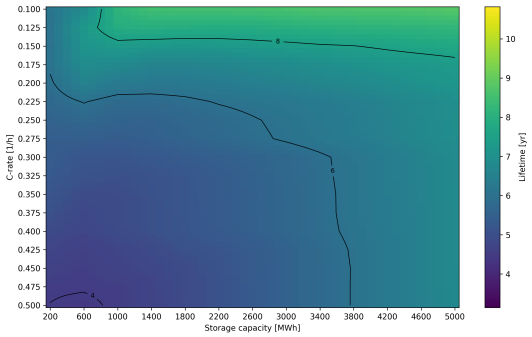

(c) Battery lifetimes with End-of-Life defined at 70% State of Health.

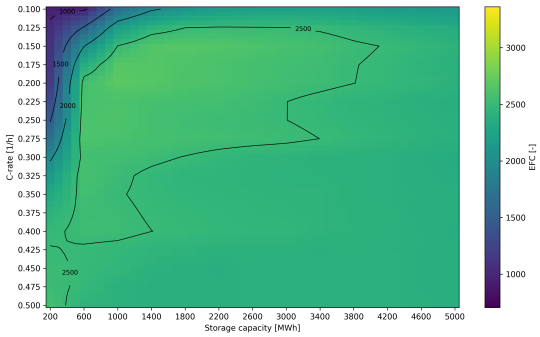

(d) Equivalent Full Cycles with End-of-Life defined at 70% State of Health.

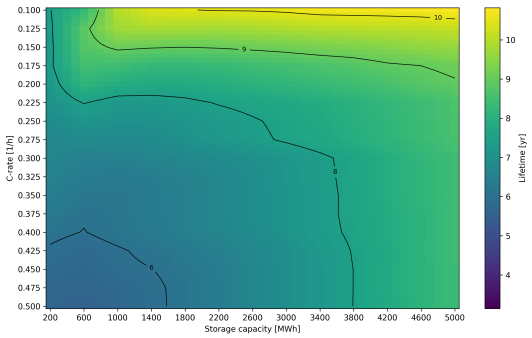

(e) Battery lifetimes with End-of-Life defined at 60% State of Health.

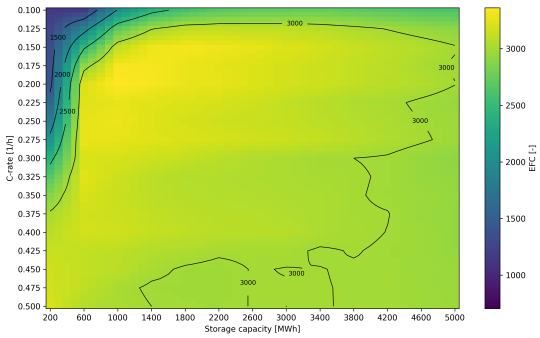

(f) Equivalent Full Cycles with End-of-Life defined at 60% State of Health.

Figure 4.7: Estimated battery lifetimes for different End-of-Life (EoL) State of Health (SoH) thresholds (80%, 70%, and 60%), shown as a function of storage capacity and C-rate. The corresponding total number of Equivalent Full Cycles (EFC) for each SoH threshold is also presented as a function of storage capacity and C-rate. The simulations are performed for a 1 GW wind farm combined with Li-ion battery storage, including marginal degradation costs, daily degradation, and with participation in both the day-ahead and aFRR markets in 2024.

Marginal degradation costs and daily capacity degradation

For the following simulations as the reference case, EoL is defined at a SoH threshold of 70%. Figure 4.8 subsequently illustrates the impact of including marginal degradation costs on operational profits.

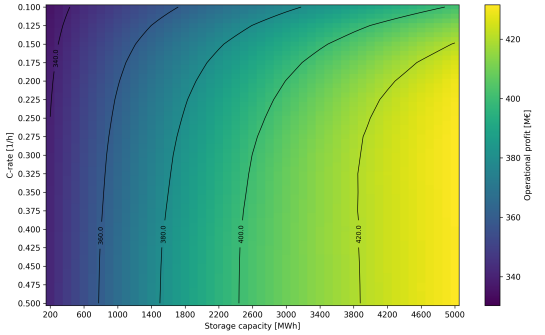

(a) Operational profits of Li-ion battery storage without marginal degradation costs, without daily capacity degradation, and operating exclusively in the day-ahead market.

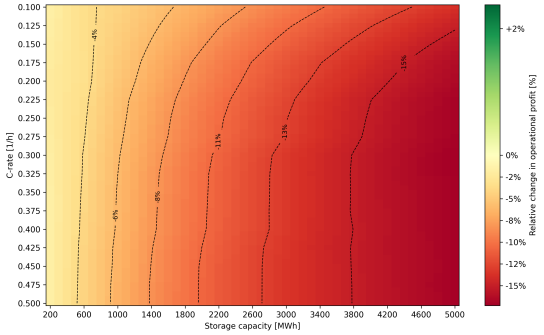

(b) Relative change in operational profits of a wind park combined with Li-ion battery storage with marginal degradation costs, without daily capacity degradation, and operating exclusively in the day-ahead market.

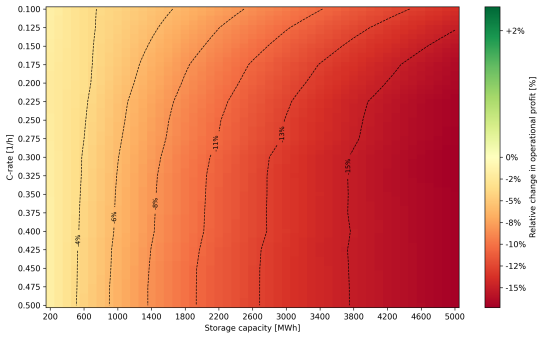

(c) Relative change in operational profits of a wind park combined with Li-ion battery storage with marginal degradation costs, with daily capacity degradation, and operating exclusively in the day-ahead market.

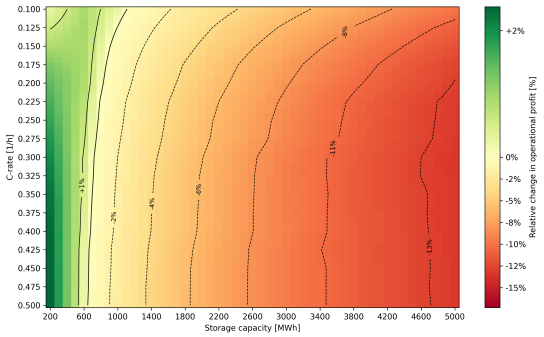

(d) Relative change in operational profits of a wind park combined with Li-ion battery storage with marginal degradation costs, without daily capacity degradation, and with participation in both the day-ahead and the aFRR markets.

Figure 4.8: Relative change in operational profits (%) of a 1 GW wind farm in 2024 combined with Li-ion battery storage in 2024 for different configurations with and without aFRR participation, marginal degradation costs (with End-of-Life defined at 70% State of Health), and daily capacity degradation, compared to the reference case shown in Figure 4.8a.

Figure 4.8a is the same configuration as in Figure 4.4a. When marginal degradation costs in are included (Figure 4.8b), operational profits decrease. According to Equation 3.56, the marginal degradation cost (€/kWh) is defined as a constant divided by the number of EFC. As shown in Figure 4.7d, the total number of EFC is approximately constant across most configurations, except for the combination of low C-rate and low energy capacity. Consequently, the marginal degradation cost per unit of throughput is nearly identical for the majority of configurations. From Equation 3.25, the degradation cost incurred in each timestep depends on the battery power flow. For a fixed C-rate, a larger energy capacity results in a higher power rating. As a result, the absolute power flows increase with storage size, which also leads to higher degradation costs. However, Figure 4.8b shows that along a contour line corresponding to a fixed reduction in operational profit, a lower C-rate requires a larger energy capacity to reach the same profit decrease. This is because a lower C-rate limits the maximum charging and discharging power. As a result, the power flow through the battery is lower, leading to less energy throughput and therefore lower degradation costs compared to a higher C-rate.

A comparison between Figures 4.8b and 4.8c indicates that including daily capacity degradation has only a limited effect on operational profits in this analysis. This is because EMERGE is simulated for a single year, while the available capacity is reduced gradually on a daily basis, as described in Section 3.3.2. Since the capacity loss accumulates slowly over time, its impact on profits remains relatively small within the one-year simulation horizon. A multi-year simulation would be required to

fully capture the long-term economic effects of capacity fade.

Furthermore, comparing Figures 4.8c and 4.8d shows that enabling participation in the aFRR market increases operational profits, even when marginal degradation costs are included. Although aFRR revenues are capped, as discussed in Sections 4.1.1 and 4.2, they provide an additional revenue stream on top of day-ahead arbitrage. For storage capacities up to approximately 600 MWh, the additional profit from aFRR participation is sufficient to offset the marginal degradation costs, resulting in higher total profits than in the case without marginal degradation costs and with participation in the day-ahead market only (Figure 4.8a).

Different End-of-Life thresholds and input years

As stated, an SoH threshold of 70% is selected as the reference case, in line with common practice in the literature [4], see Section 3.3.2. Continued operation beyond this point may lead to increased safety risks and potential accident scenarios [56]. To illustrate the impact of alternative EoL thresholds, Figure C.1 in Appendix C presents the operational profits for different SoH limits. Figures C.1b and C.1c show that lowering the SoH threshold from 80% to 60% increases operational profits. As shown in Figure 4.7, a lower EoL threshold results in a higher number of achievable EFC in the lifetime, which directly affects Equation 3.56 by reducing the marginal degradation cost and thereby increasing profits.

As described in Section 4.3.1, for a fixed C-rate, increasing the energy capacity raises the power rating and thus the absolute power flows, leading to higher degradation costs. Conversely, a lower C-rate limits power throughput and thus associated degradation costs. Therefore, to reach the same profit reduction, configurations with a lower C-rate require a larger energy capacity, as can be seen in Figure C.1.

In Appendix C, Figure C.2 shows the corresponding battery lifetimes and lifetime EFC values for the input years 2022, 2023, and 2024 at the same 70% SoH threshold. Figures C.2e and C.2f are identical to Figures 4.7c and 4.7d, respectively, as they are generated from the same underlying simulation results. Minor visual differences between these contour plots arise from the plotting function's automatic selection of colour scales and contour levels. These graphical settings affect how the data surface is displayed, which can lead to small shifts in contour lines or label placements, even though the numerical results are identical.

Figure C.2 further shows that, across all considered years, the distribution of battery lifetimes at a fixed EoL threshold of 70% SoH remains consistent. The lifetime EFC pattern is likewise similar, with most configurations reaching approximately 2400 equivalent full cycles. This indicates that degradation is primarily driven by cumulative cycling rather than by the specific yearly input data.

Comparison of Li-ion, including degradation, and LPCAES

The operational profit of a wind farm combined with Li-ion battery storage, including marginal degradation costs, daily degradation, with participation in both the day-ahead and the aFRR markets, is compared against LPCAES with aFRR participation for the years 2022 - 2024 in Figure 4.9.

The patterns in Figures 4.9d and 4.9f are highly comparable, whereas Figure 4.9b shows a different distribution. A comparison of Figures 4.9b and 4.9f shows that for small storage configurations (below approximately 600 MWh), LPCAES is less profitable than Li-ion.

As discussed in Section 4.3.1, degradation costs in each timestep depend on the instantaneous battery power flow (Equation 3.25). For a fixed C-rate, a larger energy capacity implies a higher power rating, resulting in greater absolute power flows and therefore higher degradation costs per timestep. As the energy capacity increases, these rising degradation costs gradually offset the efficiency advantage of Li-ion (94%) compared to LPCAES (70%). Consequently, the relative advantage of LPCAES, which does not incur marginal degradation costs, becomes more pronounced for larger storage sizes.

Along a contour of equal profit difference, a lower C-rate requires a larger energy capacity to reach the same relative profit increase of LPCAES over Li-ion. The reason is that a lower C-rate limits the maximum charging and discharging power, thereby reducing energy throughput and the associated degradation costs. To achieve a comparable absolute level of degradation cost (and thus a similar relative profit advantage for LPCAES), the system must compensate by increasing the energy capacity.

For very low C-rates, the total lifetime EFC is generally lower due to the limited power capability, which restricts cycling intensity (see Figure 4.7). As a result, marginal degradation costs are slightly lower for these configurations, meaning that degradation has a smaller impact on operational profits. Consequently, a smaller LPCAES capacity is required to obtain the same relative profit increase.

An important exception is the combination of low C-rate and low energy capacity. As shown in Figure 4.7d, these configurations results in a lower lifetime EFC. Because both power capability and cycling activity are limited, the battery accumulates fewer equivalent full cycles before reaching the SoH threshold. According to Equation 3.56, a lower lifetime EFC leads to lower marginal degradation costs per unit of throughput. In this case, the efficiency advantage of Li-ion dominates, allowing it to outperform LPCAES despite the inclusion of degradation costs.

Figure 4.9b shows a different pattern than the other years. In 2022, day-ahead prices are high enough that the round-trip efficiency advantage of Li-ion outweighs the effect of marginal degradation costs. As a result, degradation plays a smaller role in relative profitability. As storage capacity increases, more energy can be shifted between periods of low and high prices, which increases arbitrage revenues. Because larger price differences increase the value of efficiency, Li-ion outperforms LPCAES more clearly at higher energy capacities. Although degradation costs rise with higher throughput, they remain small compared to the high arbitrage revenues in 2022. The contour lines show that at lower C-rates, a larger energy capacity is needed to achieve the same profit increase. Since lower C-rates limit charging and discharging power, this must be compensated by higher storage capacity to reach similar profit levels.

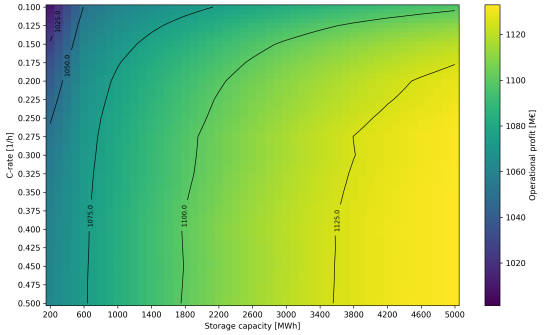

(a) Operational profits of the 1 GW wind park combined with Li-ion battery storage, including marginal degradation cost, with daily degradation, and with participation in both the day-ahead and the aFRR markets in 2022.

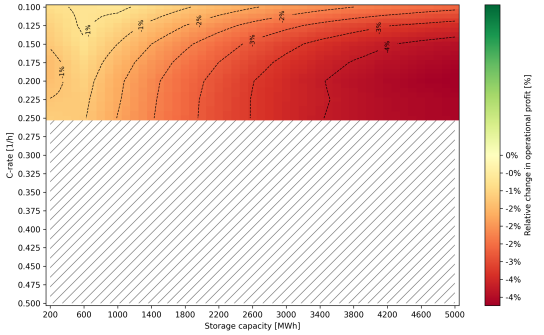

(b) Relative change in operational profit (%) of the 1 GW wind park with LPCAES compared to the reference case in Figure 4.9a, with participation in both the day-ahead and the aFRR markets in 2022.

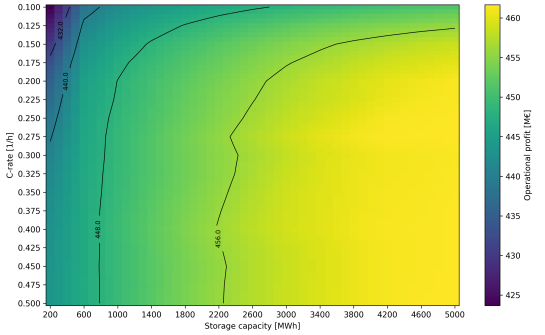

(c) Operational profits of the 1 GW wind park combined with Li-ion battery storage, including marginal degradation cost, with daily degradation, and with participation in both the day-ahead and the aFRR markets in 2023.

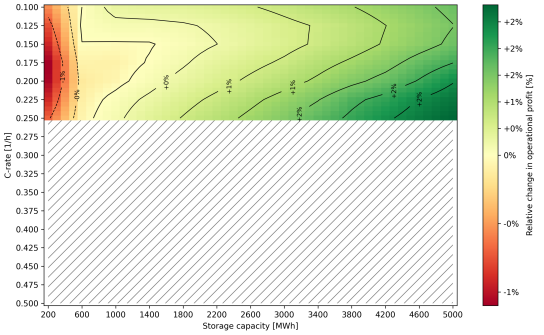

(d) Relative change in operational profit (%) of the 1 GW wind park with LPCAES compared to the reference case in Figure 4.9c, with participation in both the day-ahead and the aFRR markets in 2023.

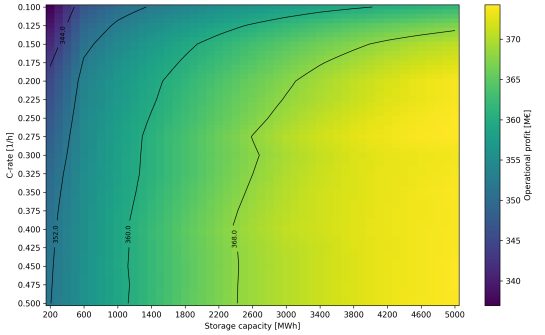

(e) Operational profits of the 1 GW wind park combined with Li-ion battery storage, including marginal degradation cost, with daily degradation, and with participation in both the day-ahead and the aFRR markets in 2024.

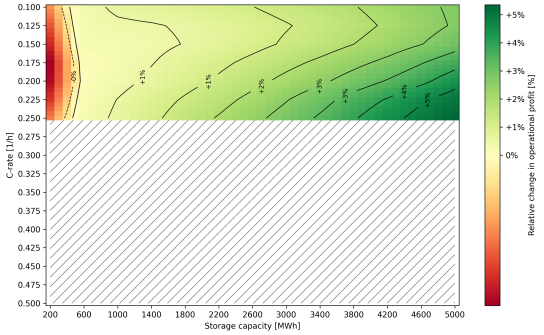

(f) Relative change in operational profit (%) of the 1 GW wind park with LPCAES compared to the reference case in Figure 4.9e, with participation in both the day-ahead and the aFRR markets in 2024.

Figure 4.9: Operational profit (million €) and relative profit difference (%) of a 1 GW wind farm combined with Li-ion battery storage and LPCAES for different storage capacities and C-rates in 2022, 2023 and 2024, relative to their Li-ion reference cases.

4.3.2. Net Present Value analysis

Figures 4.10 and 4.11 present the Net Present Value (NPV) analysis of the wind farm combined with Li-ion storage and LPCAES for 2024. For both technologies, the NPV decreases with increasing discount rate (r) and increasing energy capacity. A positive NPV is only obtained for relatively small storage sizes.

According to Equations 2.6 and 2.7, the total CAPEX is determined by the energy capacity E_{cap} and the C-rate r_{c}. The energy capacity scales with both the energy-specific cost component (c_{E}) and the power-specific cost component (c_{P}), whereas the C-rate only scales the power-related cost. As a result, increasing energy capacity has a stronger impact on total CAPEX than increasing the C-rate. Since both c_{E} and c_{P} are higher for LPCAES than for Li-ion, LPCAES exhibits higher overall investment costs.

For both technologies, the combination of large energy capacity and high C-rate leads to the most negative NPV due to high upfront investment. Conversely, very small systems with low C-rates have low CAPEX but generate insufficient operational revenues to offset the investment. The highest NPV values are therefore achieved for small energy capacities combined with relatively high C-rates, as this configuration allows the system to capture short-term price variations while keeping total investment moderate.

Operationally, Figure 4.9f shows that for identical C-rates and capacities, LPCAES can achieve higher operating profits than Li-ion when marginal degradation costs are included. However, due to its higher CAPEX, fewer LPCAES configurations result in a positive NPV.

When assessed purely on NPV, smaller energy capacities are preferred, and higher C-rates are advantageous for small systems. These conclusions, however, depend on the assumed market conditions. Under different price dynamics or wind patterns, larger capacities and higher C-rates may provide additional flexibility and improve long-term profitability.

Appendix D presents the NPV results for 2022 and 2023. The general trends remain the same, but in 2023 more configurations achieve a positive NPV due to higher day-ahead prices. In 2022, exceptionally high prices result in positive NPVs for nearly all Li-ion configurations, except at a discount rate of $r = 9\%$ combined with large energy capacity and high C-rate. For LPCAES in 2022, substantially fewer configurations are profitable. As shown earlier in Figure 4.9b, LPCAES already achieves lower operational profits than Li-ion in that year. When this is combined with its higher CAPEX, it results in fewer positive-NPV configurations relative to Li-ion.

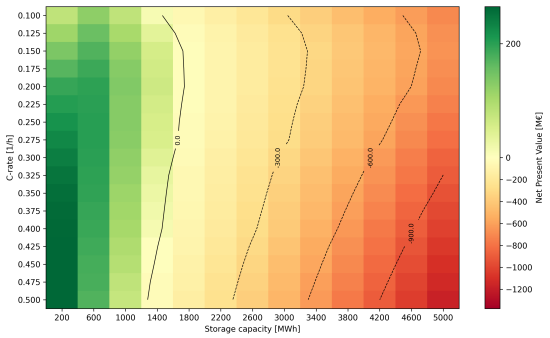

(a) NPV for wind with Li-ion storage, with $r = 5\%$

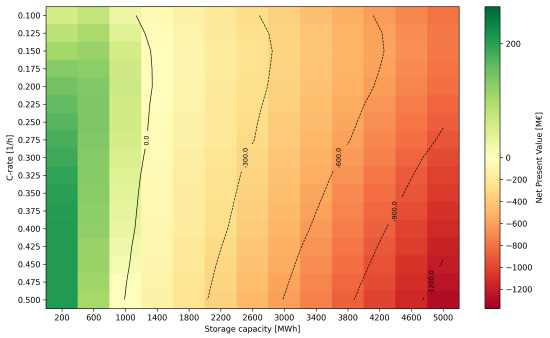

(b) NPV for wind with Li-ion storage, with $r = 7\%$

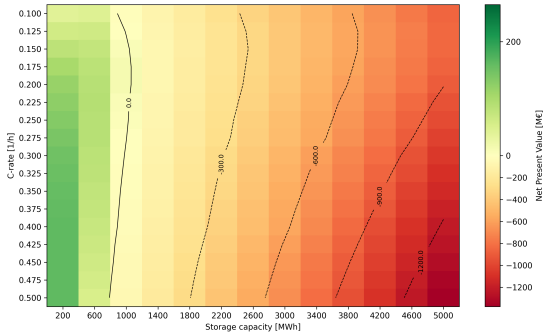

(c) NPV for wind with Li-ion storage, with $r = 9\%$

Figure 4.10: Net Present Value (NPV) analysis of a 1 GW wind farm with Li-ion storage across different energy capacities and C-rates, including marginal degradation costs and daily degradation, participation in day-ahead and aFRR markets, based on 2024 data and evaluated at various discount rates.

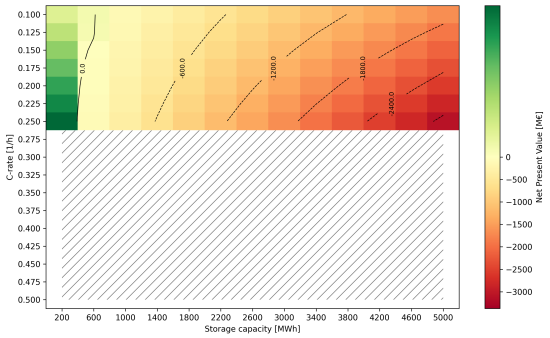

(a) NPV for wind with LPCAES, with $r = 5\%$

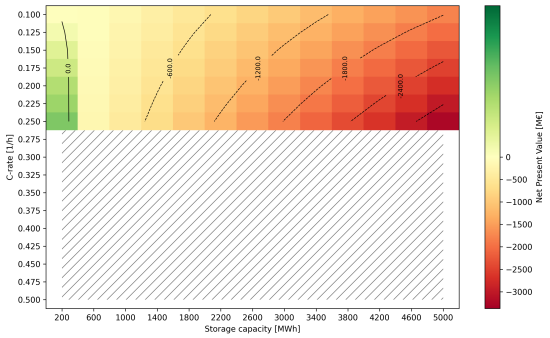

(b) NPV for wind with LPCAES, with $r = 7\%$

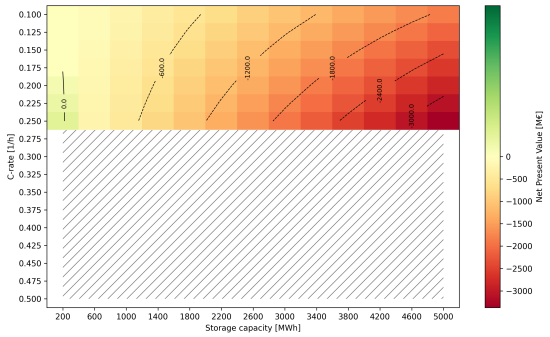

(c) NPV for wind with LPCAES, with $r = 9\%$

Figure 4.11: Net Present Value (NPV) analysis of a 1 GW wind farm with LPCAES storage across different energy capacities and C-rates, with participation in day-ahead and aFRR markets, based on 2024 data and evaluated at various discount rates.

5

Discussion

The results indicate that the relative performance of Li-ion and LPCAES depends strongly on the assumed C-rate, degradation, and the selected market year. Section 5.1 discusses these findings.

5.1. Discussion

5.1.1. Operational profits while neglecting degradation

In the specific scenario where a maximum (dis)charge rate of $r_c = r_d = 0.5$ h^{-1} is assumed for Li-ion and $r_c = r_d = 0.125$ h^{-1} for LPCAES, Li-ion achieves higher operational profits when degradation is not considered. This result is driven by the combination of a higher C-rate and a higher round-trip efficiency for Li-ion under these particular parameter settings. A higher C-rate increases the power capability, allowing more energy to be dispatched during periods with favorable market prices. Likewise, larger storage capacities enable higher energy volumes to be shifted over time. Under zero marginal costs and while neglecting capital investments, both higher C-rates and larger energy capacities therefore increase the revenue potential for both technologies.

Although participation in the aFRR market increases total operational profits compared to day-ahead-only operation, its relative impact on the comparison between technologies is limited. The maximum reserve capacity is identical for all configurations, and both technologies can provide this capacity, noting that ramping requirements for aFRR are not implemented in EMERGE. Consequently, total aFRR revenues are nearly equal across technologies and storage sizes.

Across all market years, Li-ion remains more profitable than LPCAES when degradation is neglected, and this advantage increases with storage capacity due to the higher efficiency.

5.1.2. Impact of degradation

When marginal degradation costs and daily capacity degradation are included for Li-ion, the comparison changes.

The degradation model is cycle-dependent, and for sufficiently large systems (around 600 MWh), the lifetime Equivalent Full Cycles (EFC) are comparable across most configurations. However, the total degradation cost per time step scales with absolute energy throughput. For a fixed C-rate, larger energy capacities higher power dispatch and therefore higher absolute degradation costs

When degradation is included and both technologies are evaluated at identical C-rates and energy capacities, the relative performance becomes dependent on the selected market year. Under the 2023 and 2024 market conditions, LPCAES becomes more profitable as energy capacity increases, whereas in 2022 Li-ion remains the more profitable option at higher capacities. This difference is driven by the higher average day-ahead price level in 2022, which increases the relative value of round-trip efficiency compared to marginal degradation costs. This demonstrates that the relative performance of both technologies is highly sensitive to market price levels.

5.1.3. Net Present Value considerations

When evaluated using NPV, smaller system configurations tend to appear more economically attractive, primarily due to their lower upfront capital expenditure (CAPEX), assuming the investment occurs in year 0 and future cash flows are discounted. However, this outcome depends strongly on: the assumed discount rate, the selected market year and the technology-specific CAPEX assumptions.

The preferred system size depends on market conditions. Higher price volatility increases the value of flexibility, potentially favoring larger storage capacities and higher C-rates. In contrast, under more stable price conditions, smaller configurations may be economically optimal due to lower investment costs.

It is important to emphasize that LPCAES is an emerging technology with a lower Technology Readiness Level (TRL). CAPEX and efficiency assumptions are therefore uncertain. In contrast, Li-ion CAPEX is based on established systems. Moreover, the Li-ion system is assumed to be onshore, whereas LPCAES is modeled as an offshore technology. If Li-ion were deployed offshore, its CAPEX could increase significantly, potentially altering the comparison. Since EMERGE is simulated for only a single year, the resulting annual cash flow is assumed to repeat over the entire project lifetime. However, if EMERGE were simulated over a longer time horizon, ongoing daily capacity degradation for Li-ion would accumulate and likely lead to greater profit reductions over time.

5.1.4. Modeling assumptions and limitations

Several simplifying assumptions influence the interpretation of the results. No OPEX values are included for either technology, and perfect foresight of market prices is assumed in the optimization. Furthermore, the analysis is limited to participation in the day-ahead and aFRR markets. These assumptions simplify the modeling framework but may affect the absolute profitability levels and the relative comparison between technologies under more realistic operating conditions. In practice, dispatch decisions and profitability are affected by uncertainty in market prices and renewable generation, as well as forecasting errors. The current analysis assumes perfect foresight, whereas real-world operation is subject to deviations between expected and realized conditions. Such deviations may lead to suboptimal dispatch, unnecessary cycling, imbalance penalties, or reduced revenue capture. Incorporating stochastic input data would therefore allow for a more realistic assessment of cycling behavior and improve the evaluation of the robustness of the economic comparison between Li-ion and LPCAES under practical operating conditions.

5.1.5. Dispatch behavior and market participation

The hybrid power plant dispatch is determined through joint optimization of renewable generation and storage operation. The objective is to maximize operational profit by allocating energy between: direct market sales, storage charging and discharging, and ancillary service provision.

For Li-ion batteries, marginal degradation costs are included in the optimization and therefore influence dispatch decisions. Each charging and discharging action contributes to cycle-dependent degradation, represented as a cost per unit of energy throughput. As a result, the model tends to dispatch the battery only when expected revenues are sufficiently high to cover both efficiency losses and degradation costs. This introduces a profitability threshold and likely leads to more selective operation during high-price periods. In contrast, LPCAES is modeled without cycle-dependent degradation costs. Its dispatch is therefore mainly driven by market price differences and technical constraints. Due to its longer discharge duration, it is expected to be more suited to longer-term energy shifting rather than short, high-frequency operation. These structural differences are expected to result in different dispatch patterns. Li-ion is likely to prioritize high-value, short-duration arbitrage. LPCAES, in contrast, may operate more continuously when sustained price differences support longer discharge periods.

It is important to further assess how participation in additional ancillary service markets influences degradation and long-term profitability. Providing services such as FCR or mFRRda alongside day-ahead arbitrage and aFRR can increase the frequency and depth of charging and discharging. While the marginal degradation cost per cycle is defined by the assumed lifetime EFC, a higher operational intensity accelerates the accumulation of equivalent full cycles. This may shorten the effective calendar lifetime of the battery and lead to earlier replacement, thereby affecting overall project economics.

Furthermore, as outlined in Section 2.2.2, Li-ion is theoretically well suited for participation in the FCR market, while CAES is more appropriate for the mFRRda market. Whether LPCAES can successfully participate in these markets remains uncertain. It should also be noted that ramping characteristics for the aFRR market are not implemented in EMERGE, which limits the assessment of LPCAES participation under realistic operational constraints.

6

Conclusions and Recommendations

The Main Research Question (MRQ) of this work, as stated in Section 1.3, is:

How does the profit of hybrid power plants integrating either short- or long-duration storage compare across multiple electricity markets, considering storage sizing and degradation?

Section 6.1 answers the MRQ by addressing the Sub-Questions (SQs). Section 6.2 provides recommendations for future work.

6.1. Conclusions

- **SQ1: How does the integration of short- versus long-duration storage in hybrid power plants influence profitability across multiple electricity markets?**

  The integration of both short-duration (Li-ion) and long-duration (LPCAES) storage increases the operational flexibility and revenue potential of hybrid power plants compared to renewable generation alone. Participation in both the day-ahead and aFRR markets increases total profits relative to day-ahead-only operation.

  When degradation is not considered, Li-ion consistently achieves higher operational profit than LPCAES in the day-ahead market across all analyzed market years. This is mainly driven by its higher round-trip efficiency and higher assumed C-rates, which enable more effective exploitation of hourly price differences.

- **SQ2: What is the relationship between the sizing of short- and long-duration storage systems and the profitability of hybrid power plants across multiple electricity markets?**

  Storage sizing, expressed through energy capacity and C-rate, strongly affects operational profitability. Higher C-rates increase power capability and allow the system to capture more value during periods with large price differences. Larger energy capacities enable more energy shifting over time.

  Without considering degradation, operational profits generally increase with both C-rate and energy capacity, as additional flexibility allows greater participation in price differences across time. However, the extra benefit of increasing storage size depends on market price levels.

  Although participation in the aFRR market increases total profits compared to day-ahead-only operation, it has little impact on the relative comparison between technologies. Since the maximum reserve capacity is identical across configurations and both technologies can provide it, given that ramping requirements for aFRR are not implemented in EMERGE, aFRR revenues are nearly identical across storage sizes and technologies.

  Across all analyzed market years, Li-ion remains more profitable than LPCAES when degradation effects are neglected. This profitability gap widens with increasing storage capacity, primarily due to the higher round-trip efficiency of Li-ion systems.

- **SQ3: How does the degradation characteristics of short- and long-duration storage affect profitability and the dispatch strategy of hybrid power plants?**

  Including degradation changes both operational outcomes and long-term economic results. For Li-ion batteries, the cycle-dependent degradation model introduces a marginal cost per unit of energy throughput. As a result, the battery is only dispatched when expected revenues exceed both efficiency losses and degradation costs. This creates a profitability threshold and will lead to more selective cycling during high-value periods.

  Marginal degradation costs increase with absolute power flow. For a fixed C-rate, larger energy capacities imply higher power ratings and therefore higher throughput, which increases total degradation costs.

  When degradation is considered, the relative performance of Li-ion and LPCAES becomes year-dependent. Under moderate price conditions (2023 and 2024), LPCAES can become more profitable than Li-ion at larger capacities and the same C-rate when the lower efficiency of LPCAES is outweighed by the degradation costs of Li-ion. In this case, the additional degradation costs associated with higher Li-ion throughput reduce its net profit more than the efficiency disadvantage reduces the profit of LPCAES. In contrast, under high-price conditions (2022), the efficiency advantage of Li-ion outweighs its marginal degradation costs, and Li-ion remains more profitable at higher capacities.

  LPCAES is modeled without cycle-dependent degradation costs and is therefore primarily limited by its lower round-trip efficiency. Its dispatch is not constrained by marginal cycling costs and is better suited for longer-duration energy shifting.

  From a long-term investment perspective, degradation influences Net Present Value (NPV). Higher cycling intensity accelerates the accumulation of Equivalent Full Cycles, potentially shortening the effective lifetime of Li-ion systems and affecting replacement timing and overall project value. When evaluated using NPV, smaller configurations often appear more attractive due to lower CAPEX requirements, especially when degradation reduces the incremental benefit of larger systems.

  NPV results are highly sensitive to assumptions regarding discount rate, market conditions, and the technology-specific CAPEX assumptions. In particular, LPCAES CAPEX and efficiency assumptions remain uncertain due to its lower Technology Readiness Level, whereas Li-ion cost data are based on more mature technologies. Therefore, degradation modeling and investment assumptions are decisive in determining which technology is economically preferable.

By answering the sub-questions, the MRQ can be addressed as follows:

The profitability of hybrid power plants integrating short-duration (Li-ion) or long-duration (LPCAES) storage is highly context-dependent and driven by market conditions, storage sizing (energy capacity and C-rate), degradation, and investment assumptions.

Without degradation, Li-ion generally performs better due to its higher efficiency and power capability. When degradation is included, results become year-dependent: LPCAES can outperform Li-ion under moderate price conditions at larger sizes, while Li-ion remains superior in high-price years.

Therefore, there is no universally superior technology; the economically preferred option depends on the specific market environment and system configuration. However, further research is required to better quantify the impact of uncertain market developments, participation in additional electricity markets, and long-term investment assumptions on this comparison.

6.2. Recommendations

Based on the results and identified limitations, several directions for future research are recommended:

- **Inclusion of stochastic price modeling and risk measures:** The current analysis assumes perfect foresight of market prices. Future work should incorporate price uncertainty and forecasting errors within a stochastic optimization framework, including risk measures such as Conditional

Value-at-Risk (CVaR), to evaluate the robustness of dispatch strategies and profitability under realistic operating conditions.

- **Participation in additional markets:** Extending the analysis to include additional ancillary service markets (FCR and mFRRda) would provide deeper insight into the effects of multi-market participation on cycling intensity, degradation, and overall profitability. In addition, ramping characteristics for the aFRR market and imbalance settlement mechanisms should be incorporated to ensure a more realistic representation of operational constraints and imbalance-related financial uncertainty.
- **Technology cost development, offshore integration and long-term modeling:** Future work should evaluate potential cost reductions for LPCAES due to technological learning and scaling, and assess the economic impact of deploying Li-ion systems offshore. Since investment costs strongly depend on location and maturity level, these factors can significantly affect the comparative results between both technologies. For the NPV calculations, EMERGE could be run over a longer time horizon than one year to capture the cumulative effect of daily capacity degradation. This would allow the model to better account for the gradual daily loss in the capacity of Li-ion batteries and the associated reduction in profits over time.
- **Wind farm modeling assumptions and wake effects:** The wind generation profiles applied in this study were based on openly accessible datasets to ensure transparency and reproducibility. Nevertheless, the simplified representation of the wind farm, without explicitly modeling wake interactions, limits the precision of the results. Applying dedicated wake modeling tools such as FLORIS or PyWake would allow turbine-turbine interactions and layout-specific losses to be captured more accurately, thereby improving the precision of calculated energy production, revenues, and resulting NPV values in business case analyses.

Further research along these lines is necessary to evaluate the long-term economic role of short- and long-duration storage technologies in hybrid power plants under evolving electricity market conditions.

Cover Image

Adapted from:
De Volkskrant, *Onze Noordzeewind is geld waard*, 2015. Accessed: 2025-10-27. [Online]. Available: https://www.volkskrant.nl/nieuws-achtergrond/onze-noordzeewind-is-geld-waard~b8381e5eb/.

Bibliography

[1] Netherlands Enterprise Agency (RVO). “New offshore wind farms.” Accessed: 2025-10-09. (2025), [Online]. Available: https://english.rvo.nl/topics/offshore-wind-energy/new-offshore-wind-farms.

[2] M. van Klimaat en Groene Groei, *Actieplan windenergie op zee en overzicht maatregelen vraagstimulering*, Sep. 2025.

[3] R. Zhu, K. Das, O. Lindberg, P. E. Sørensen, and A. D. Hansen, “Optimal offering and operation strategy for hybrid power plants in hour-ahead mFRR energy activation markets with guaranteed service provision,” *International Journal of Electrical Power and Energy Systems*, vol. 169, p. 110 795, 2025. DOI: 10.1016/j.ijepes.2025.110795.

[4] J. P. Murcia Leon, H. Habbou, M. Friis-Møller, M. Gupta, R. Zhu, and K. Das, “HyDesign: a tool for sizing optimization of grid-connected hybrid power plants including wind, solar photovoltaic, and lithium-ion batteries,” *Wind Energy Science*, vol. 9, pp. 759–776, Apr. 4, 2024. DOI: 10.5194/wes-9-759-2024.

[5] K. Dykes, J. King, N. DiOrio, R. King, V. Gevorgian, D. Corbus, N. Blair, K. Anderson, G. Stark, C. Turchi, and P. Moriarty, “Opportunities for Research and Development of Hybrid Power Plants,” National Renewable Energy Laboratory, Tech. Rep. NREL/TP-5000-75026, May 2020.

[6] IEA Wind Technology Collaboration Programme, “IEA Wind Task 50: Annual Report 2021,” International Energy Agency (IEA), Tech. Rep., 2022.

[7] K. Das, A. D. Hansen, J. P. Murcia Leon, R. Zhu, M. Gupta, J.-A. Pérez-Rúa, Q. Long, D. V. Pombo, A. Barlas, T. Gocmen, A. Sogachev, M. Koivisto, N. A. Cutululis, and P. E. Sørensen, “Research Challenges and Opportunities of Utility-Scale Hybrid Power Plants,” *Wiley Interdisciplinary Reviews: Energy and Environment*, vol. 14, no. 1, e70001, 2025. DOI: 10.1002/wene.70001.

[8] W. Gorman, A. Mills, M. Bolinger, R. Wiser, N. G. Singhal, E. Ela, and E. O’Shaughnessy, “Motivations and options for deploying hybrid generator-plus-battery projects within the bulk power system,” *The Electricity Journal*, vol. 33, no. 2, p. 106 739, 2020. DOI: 10.1016/j.tej.2020.106739.

[9] A. Selänniemi, M. Hellström, and M. Björklund-Sänkiaho, “Long-Duration Energy Storage—A Literature Review on the Link between Variable Renewable Energy Penetration and Market Creation,” *Energies*, vol. 17, no. 15, p. 3779, Jul. 2024. DOI: 10.3390/en17153779. [Online]. Available: https://doi.org/10.3390/en17153779.

[10] International Energy Agency (IEA), *ETP Clean Energy Technology Guide*, 2024.

[11] International Renewable Energy Agency (IRENA), *Electricity Storage and Renewables: Costs and Markets to 2030*, 2017.

[12] A. Attarha, N. Amjady, S. Dehghan, and B. Vatani, “Adaptive Robust Self-Scheduling for a Wind Producer With Compressed Air Energy Storage,” *IEEE Transactions on Sustainable Energy*, vol. 9, no. 4, pp. 1659–1671, Oct. 2018. DOI: 10.1109/TSTE.2018.2806444.

[13] S. Ghavidel, M. Jabbari Ghadi, A. Azizivahed, J. Aghaei, L. Li, and J. Zhang, “Risk-Constrained Bidding Strategy for a Joint Operation of Wind Power and CAES Aggregators,” *IEEE Transactions on Sustainable Energy*, vol. 11, no. 1, pp. 457–466, 2020. DOI: 10.1109/TSTE.2019.2895332.

[14] H. Khaloie, A. Anvari-Moghaddam, J. Contreras, J.-F. Toubeau, P. Siano, and F. Vallée, “Offering and bidding for a wind producer paired with battery and CAES units considering battery degradation,” *International Journal of Electrical Power & Energy Systems*, vol. 136, p. 107 685, 2022. DOI: 10.1016/j.ijepes.2021.107685.

[15] A. A. S. de la Nieta, J. Contreras, and J. P. S. Catalão, “Optimal Single Wind Hydro-Pump Storage Bidding in Day-Ahead Markets Including Bilateral Contracts,” *IEEE Transactions on Sustainable Energy*, vol. 7, no. 3, pp. 1284–1294, Jul. 2016. DOI: 10.1109/TSTE.2016.2544704.

[16] E. Ghanaee, M. Chazarra, S. Castaño-Solis, J. I. Pérez-Díaz, D. Fernández-Muñoz, and J. Nájera, "Optimal Scheduling of a Hybrid Wind–Battery Power Plant in the Day-Ahead and Reserve Markets Considering Battery Degradation Cost," in *2024 International Conference on Smart Energy Systems and Technologies (SEST)*, IEEE, 2024, pp. 1–8. DOI: 10.1109/SEST61601.2024.10694289.

[17] K. Poplavskaya, J. Lago, and L. de Vries, "Effect of market design on strategic bidding behavior: Model-based analysis of European electricity balancing markets," *Applied Energy*, vol. 270, p. 115 130, 2020. DOI: 10.1016/j.apenergy.2020.115130.

[18] TenneT, *Market roles*, Accessed: 2025-06-28, 2025. [Online]. Available: https://www.tennet.eu/nl-en/market-roles.

[19] ETPA, *Spot Markets*, Accessed: 2025-06-28, n.d. [Online]. Available: https://www.etpa.nl/knowledge-base/markets/spot-markets.

[20] EPEX SPOT, *Basics of the Power Market*, Accessed: 2025-06-28, n.d. [Online]. Available: https://www.epexspot.com/en/basicspowermarket.

[21] D. R. Biggar and M. R. Hesamzadeh, *The Economics of Electricity Markets*. Hoboken, NJ: Wiley-IEEE Press, 2014, p. 432, ISBN: 9781118775721.

[22] M. Karami, E. Berschauer, P. Hille, and Z. Marijanovic, *A turning point in electricity trading: Day Away switches to 15-minute products*, Accessed: 2025-06-28, May 2025. [Online]. Available: https://www.next-kraftwerke.com/energy-blog/day-ahead-switch-15-min.

[23] S. Pfenninger-Lee, *Modelling Energy Systems - 5. Power markets and mixed-integer programming*, Accessed: 2025-06-28, n.d. [Online]. Available: https://www.modelling-energy-systems.org/basics/markets-milp.

[24] ETPA, *The Merit Order*, Accessed: 2025-06-28, n.d. [Online]. Available: https://www.etpa.nl/knowledge-base/markets/the-merit-order.

[25] T. Brown and L. Reichenberg, "Decreasing market value of variable renewables can be avoided by policy action," *Energy Economics*, vol. 100, p. 105 354, 2021. DOI: 10.1016/j.eneco.2021.105354.

[26] S. de Boer, *The Dutch electricity sector – part 2: How do the different electricity markets work?* Accessed: 2025-06-26, May 2024. [Online]. Available: https://www.rabobank.com/knowledge/d011424506-the-dutch-electricity-sector-part-2-how-do-the-different-electricity-markets-work.

[27] TenneT, *Market Types*, Accessed: 2025-06-29, 2024. [Online]. Available: https://www.tennet.eu/market-types.

[28] ETPA, *Intraday Market Auction*, Accessed: 2025-06-28, n.d. [Online]. Available: https://www.etpa.nl/knowledge-base/markets/intraday-market-auction.

[29] ETPA, *Balancing Market*, Accessed: 2025-06-26, 2024. [Online]. Available: https://www.etpa.nl/knowledge-base/markets/balancing-market.

[30] TenneT TSO GmbH, *Imbalance Pricing System*, Oct. 2024.

[31] Next Kraftwerke GmbH, *What are Ancillary Services?* Accessed: 2025-07-01, n.d. [Online]. Available: https://www.next-kraftwerke.com/knowledge/ancillary-services#system-services-for-frequency-maintenance.

[32] TenneT TSO B.V., *FCR Manual for BSPs: Requirements and procedures for supply of FCR*, version V3.3, Mar. 2022.

[33] Rabobank. "The Dutch Electricity Sector – Part 4: Changing electricity markets present opportunities and risks for businesses and households." Accessed: 2025-07-02. (2023), [Online]. Available: https://www.rabobank.com/knowledge/d011430987-the-dutch-electricity-sector-part-4-changing-electricity-markets-present-opportunities-and-risks-for-businesses-and-households.

[34] TenneT TSO B.V., *Manual aFRR for BSPs: Rules and procedures for aFRR delivery*, Apr. 2025.

[35] TenneT TSO B.V., *Handboek/productinformatie Noodvermogen voor BSPs*, Apr. 2025.

[36] J. Figgener, B. Tepe, F. Rücker, I. Schoeneberger, C. Hecht, A. Jossen, and D. U. Sauer, "The influence of frequency containment reserve flexibilization on the economics of electric vehicle fleet operation," *Journal of Energy Storage*, vol. 53, p. 105 138, Sep. 2022. DOI: 10.1016/j.est.2022.105138.

[37] K. Gicevskis and O. Linkevics, "The Role of Decentralized Electrode Boiler in Ancillary Services and District Heating: A Feasibility Assessment," *Latvian Journal of Physics and Technical Sciences*, vol. 2023, no. 5, 2023. DOI: 10.2478/lpts-2023-0029.

[38] D. A. Elalfy, E. Gouda, M. F. Kotb, V. Bureš, and B. E. Sedhom, "Comprehensive review of energy storage systems technologies, objectives, challenges, and future trends," *Energy Strategy Reviews*, vol. 54, p. 101 482, 2024. DOI: 10.1016/j.esr.2024.101482.

[39] M. B. Kebede, N. Rao, H. Wang, N. L. Panwar, Y. T. Mersha, and E. K. Tadesse, "A comprehensive review of stationary energy storage devices for large scale renewable energy sources," *Journal of Energy Storage*, vol. 47, p. 103 647, 2022. DOI: 10.1016/j.est.2022.103647.

[40] A. M. Rabi, J. Radulovic, and J. M. Buick, "Comprehensive Review of Compressed Air Energy Storage (CAES) Technologies," *Thermo*, vol. 3, no. 1, pp. 104–126, 2023. DOI: 10.3390/thermo3010008.

[41] Y. Arellano-Prieto, E. Chavez-Panduro, P. S. Rossi, and F. Finotti, "Energy storage solutions for offshore applications," *Energies*, vol. 15, no. 17, p. 6153, 2022. DOI: 10.3390/en15176153.

[42] L. Frías-Paredes and M. Gastón-Romeo, "A new methodology to easy integrate complementarity criteria in the resource assessment process for hybrid power plants: Offshore wind and floating PV," *Energy Conversion and Management: X*, vol. 26, p. 100 938, 2025. DOI: 10.1016/j.ecmx.2025.100938.

[43] E. M. Gouda, Y. Fan, M. Benaouicha, T. Neu, and L. Luo, "Review on Liquid Piston technology for compressed air energy storage," *Journal of Energy Storage*, vol. 43, p. 103 111, 2021, ISSN: 2352-152X. DOI: 10.1016/j.est.2021.103111.

[44] X. Han, L. Lu, Y. Zheng, X. Feng, Z. Li, J. Li, and M. Ouyang, "A review on the key issues of the lithium ion battery degradation among the whole life cycle," *eTransportation*, vol. 1, p. 100 005, 2019. DOI: 10.1016/j.etran.2019.100005.

[45] H. Adenusi, G. A. Chass, S. Passerini, K. V. Tian, and G. Chen, "Lithium Batteries and the Solid Electrolyte Interphase (SEI)—Progress and Outlook," *Advanced Energy Materials*, vol. 13, no. 10, p. 2 203 307, 2023. DOI: 10.1002/aenm.202203307.

[46] W. Cole, V. Ramasamy, and M. Turan, "Cost Projections for Utility-Scale Battery Storage: 2025 Update," National Renewable Energy Laboratory, Golden, CO, Tech. Rep. NREL/TP-6A40-93281, Jun. 2025. [Online]. Available: https://www.nrel.gov/docs/fy25osti/93281.pdf.

[47] D. Buhagiar, T. Sant, R. N. Farrugia, L. Aquilina, D. Farrugia, and F. M. Strati, "Small-scale Experimental Testing of a Novel Marine Floating Platform with Integrated Hydro-pneumatic Energy Storage," *Journal of Energy Storage*, vol. 24, p. 100 774, 2019. DOI: 10.1016/j.est.2019.100774.

[48] D. Buhagiar, T. Sant, and R. N. Farrugia, "Hydro-Pneumatic Energy Storage," in *Encyclopedia of Energy Storage*, L. F. Cabeza, Ed., vol. 2, Oxford: Elsevier, 2022, pp. 218–235. DOI: 10.1016/B978-0-12-819723-3.00077-9.

[49] M. Houwing, B. de Jager, B. Klootwijk, and I. G. Aparicio, "Optimizing Hybrid Power Plants: Revenue Growth and Grid Efficiency via Multi-Market Participation," TNO, Petten, The Netherlands, Tech. Rep. TNO 2024 R11911, Dec. 2024, TNO Public.

[50] B. Klootwijk, M. Houwing, J. Fatou Gómez, D. Ntagkras, and I. González-Aparicio, "Optimised Sizing and Dispatch of Hybrid Power Plants: IJmuiden Ver Gamma as a Case Study," TNO, Petten, The Netherlands, Tech. Rep. TNO 2024 R12196, Dec. 2024.

[51] Renewables.ninja, Accessed: 2024. [Online]. Available: https://www.renewableninja.org.

[52] I. Staffell and S. Pfenninger, "Using bias-corrected reanalysis to simulate current and future wind power output," *Energy*, vol. 114, pp. 1224–1239, 2016. DOI: 10.1016/j.energy.2016.08.068.

[53] ENTSO-E, *Transparency platform*, Accessed: 2024. [Online]. Available: https://transparency.entsoe.eu/.

[54] B. Xu, A. Oudalov, A. Ulbig, G. Andersson, and D. S. Kirschen, "Modeling of Lithium-Ion Battery Degradation for Cell Life Assessment," *IEEE Transactions on Smart Grid*, vol. 9, no. 2, pp. 1131–1140, 2018. DOI: 10.1109/TSG.2016.2578950.

[55] S. D. Downing and D. F. Socie, "Simple rainflow counting algorithms," *International Journal of Fatigue*, vol. 4, no. 1, pp. 31–40, 1982.

[56] S. Zhu, C. Li, P. Ruan, S. Zhou, J. Li, S. Luo, M. Li, and Q. Zhang, "State of health and remaining useful life estimation of lithium-ion battery based on parallel deep learning methods," *International Journal of Electrochemical Science*, vol. 20, p. 100 988, 2025. DOI: 10.1016/j.ijoes.2025.100988.

[57] J. Berk and P. DeMarzo, *Corporate Finance: The Core*, 4th ed. Pearson, 2017, European Edition, ISBN: 9781292158464.

[58] Government of the Netherlands (Rijksoverheid). "Windenergiegebied Nederwiek." Accessed: 2025-10-17. (2025), [Online]. Available: https://windopzee.nl/onderwerpen/waar-staan-komen-windparken/windenergiegebied-nederwiek/.

[59] Netherlands Enterprise Agency (RVO), *Participatieplan Project Net op zee Nederwiek 1*, Jan. 2023.

[60] Netherlands Enterprise Agency (RVO). "Wind op zee - Nederwiek (zuid) kavel I-B." Accessed: 2025-10-17. (2025), [Online]. Available: https://www.rvo.nl/onderwerpen/bureau-energieprojecten/lopende-projecten/woz-nederwiek-zuid-kavel-i-b.

[61] International Energy Agency and OECD Nuclear Energy Agency, *Projected Costs of Generating Electricity 2020*. Paris: OECD Publishing, 2020. DOI: 10.1787/ae0b5d7b-en.

[62] European Central Bank, "Energy price developments in and out of the COVID-19 pandemic - from commodity prices to consumer prices," *ECB Economic Bulletin*, no. 4, Jun. 2022, Accessed: 11 February 2026. [Online]. Available: https://www.ecb.europa.eu/press/economic-bulletin/articles/2022/html/ecb.ebart202204_01~7b32d31b29.en.html.

A

A.1. The Offshore Wind Energy Roadmap

The Offshore Wind Energy Roadmap details the development and planning of future offshore wind farms in The Netherlands [1]. The case study discussed in Section 3.4 focuses specifically on the *Nederwiek (zuid) kavel I–B* site with 1 GW capacity, see Figure A.1

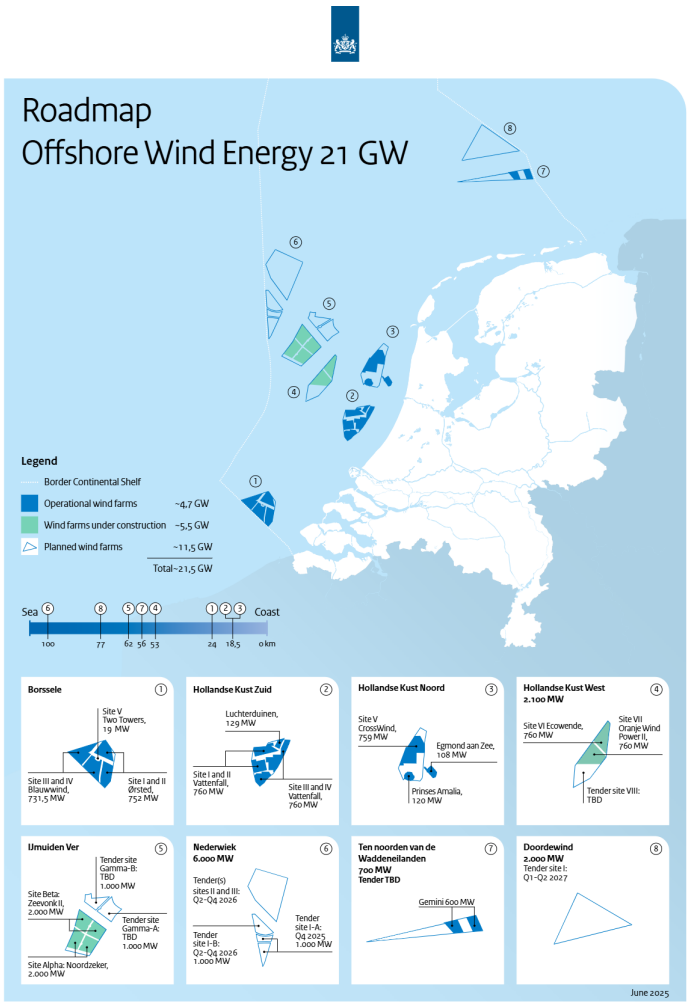

Figure A.1: The Offshore Wind Energy Roadmap of the Government of the Netherlands [1].

B

B.1. Additional results of Section 4.2

Figure B.1 compares the operational profits of the wind park combined with Li-ion battery storage and LPCAES, both participating in the day-ahead and aFRR markets, based on input data for 2022.

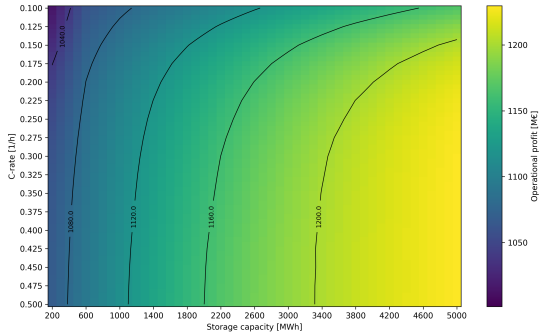

(a) Operational profits of a wind park combined with Li-ion battery storage, excluding marginal degradation, with participation in both the day-ahead and the aFRR markets.

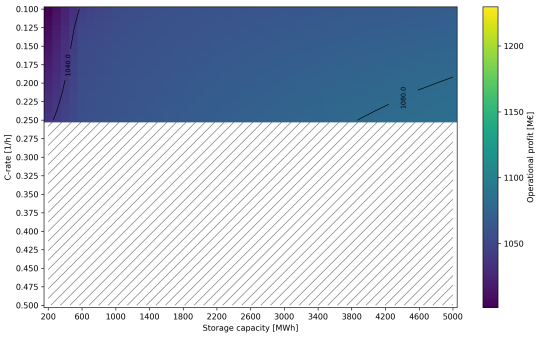

(b) Operational profits of a wind park combined with LCPAES, excluding marginal degradation, with participation in both the day-ahead and the aFRR markets.

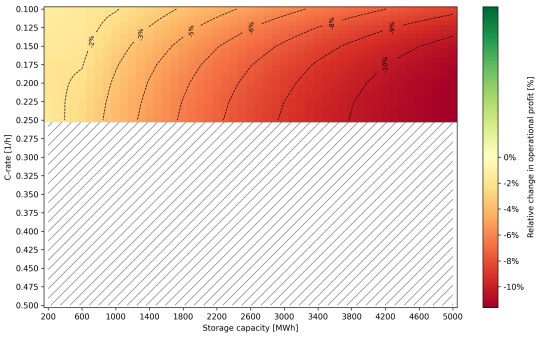

(c) Relative change in operational profits of LPCAES, compared to Figure B.1a, excluding marginal degradation costs, with participation in both the day-ahead and the aFRR markets.

Figure B.1: Operational profits (million €) and relative profit change (%) of a 1 GW wind farm combined with Li-ion battery storage and LPCAES for different storage capacities and C-rates in 2022.

Figure B.2 presents the same analysis based on input data for 2023.

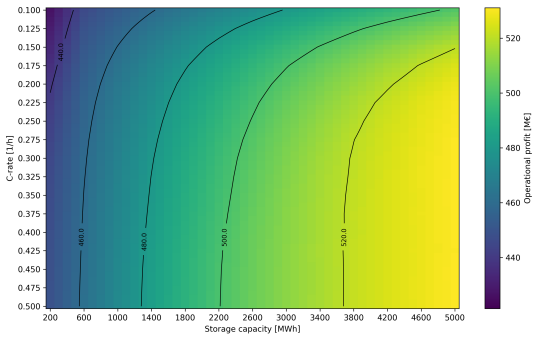

(a) Operational profits of a wind park combined with Li-ion battery storage, excluding marginal degradation, with participation in both the day-ahead and the aFRR markets.

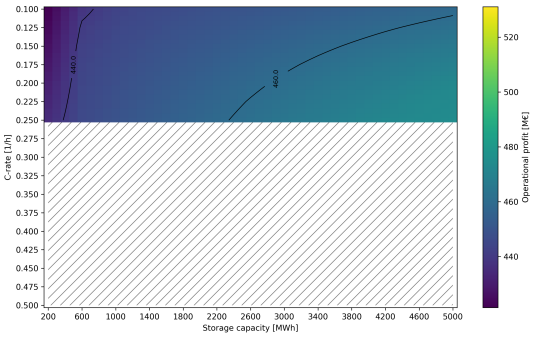

(b) Operational profits of a wind park combined with LPCAES, excluding marginal degradation, with participation in both the day-ahead and the aFRR markets.

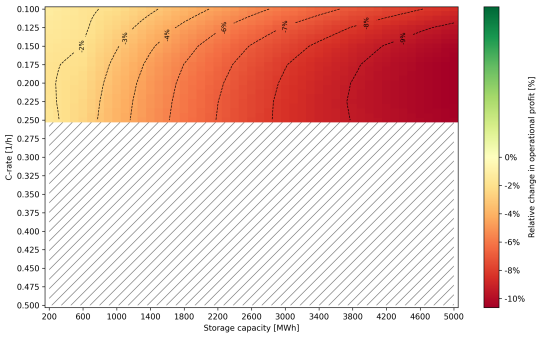

(c) Relative change in operational profits of LPCAES, compared to Figure B.2a, excluding marginal degradation costs, with participation in both the day-ahead and the aFRR markets.

Figure B.2: Operational profits (million €) and relative profit differences (%) of a 1 GW wind farm combined with Li-ion battery storage and LPCAES for different storage capacities and C-rates in 2023.

The qualitative patterns are consistent with those obtained for the input year 2024. An interpretation of these results is provided in Section 4.2.

C

C.1. Additional results of Section 4.3.1

Figure C.1 illustrates the impact of different End-of-Life (EoL) State of Health (SoH) thresholds on the operational profits of the 1 GW wind park combined with the same battery configurations, using weather and market data from 2024.

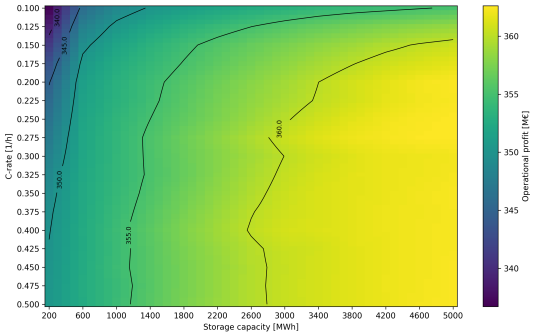

(a) Operational profits (million €) of a wind park combined with Li-ion battery storage with marginal degradation costs, with daily capacity degradation, and with participation in both the day-ahead and the aFRR markets. The EoL threshold is set at 80% SoH.

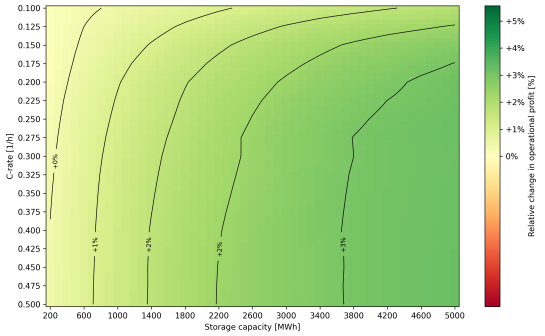

(b) Relative change in operational profits (%) for an EoL threshold of 70% SoH, compared to the 80% SoH case in Figure C.1a.

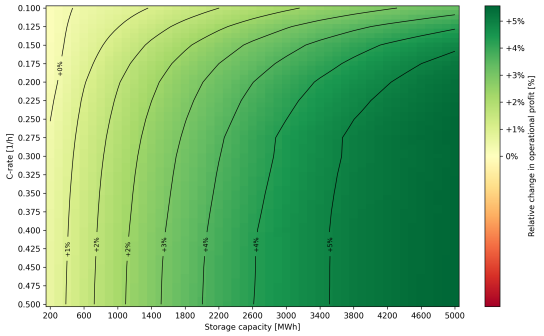

(c) Relative change in operational profits (%) for an EoL threshold of 60% SoH, compared to the 80% SoH case in Figure C.1a.

Figure C.1: Relative change in operational profits (%) in 2024 of a 1 GW wind farm combined with Li-ion battery storage for different configurations participating in both the day-ahead and aFRR markets, including marginal degradation costs and daily capacity degradation, evaluated at different End-of-Life (EoL) State of Health (SoH) thresholds, compared to the reference case shown in Figure C.1a.

For the different input years, the estimated battery lifetimes and corresponding lifetime EFC values are presented in Figure C.2.

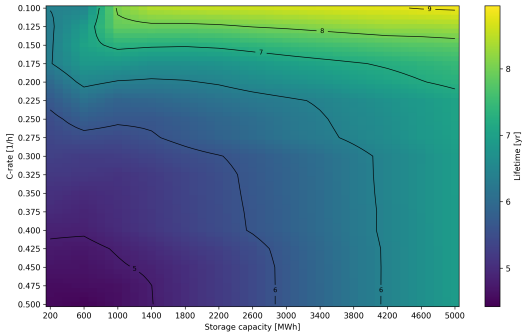

(a) Battery lifetimes with End-of-Life defined at 70% State of Health in 2022.

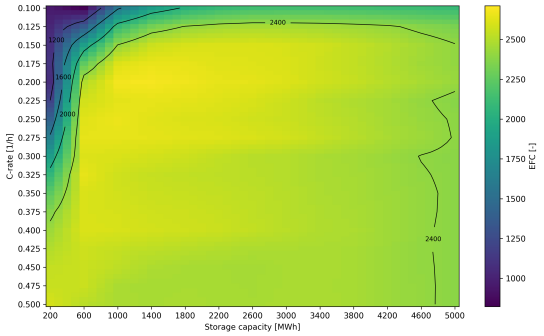

(b) Equivalent Full Cycles with End-of-Life defined at 70% State of Health in 2022.

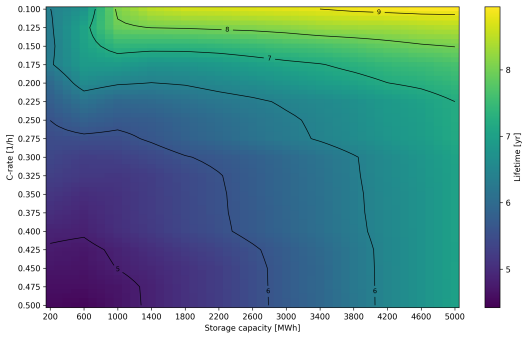

(c) Battery lifetimes with End-of-Life defined at 70% State of Health in 2023.

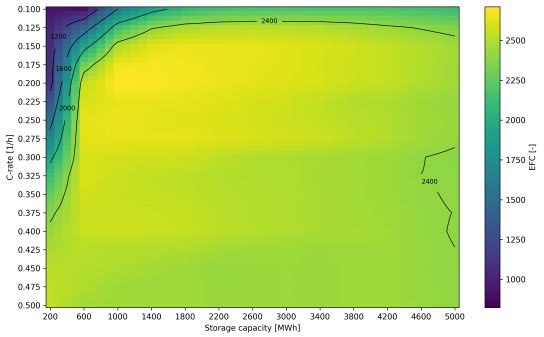

(d) Equivalent Full Cycles with End-of-Life defined at 70% State of Health in 2023.

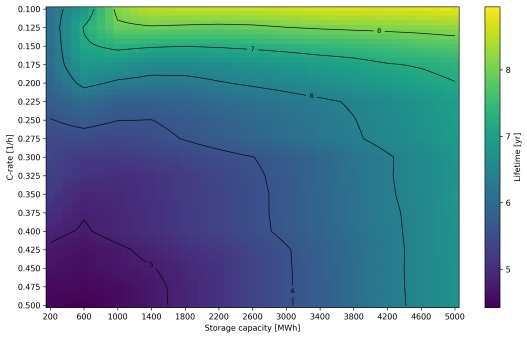

(e) Battery lifetimes with End-of-Life defined at 70% State of Health in 2024.

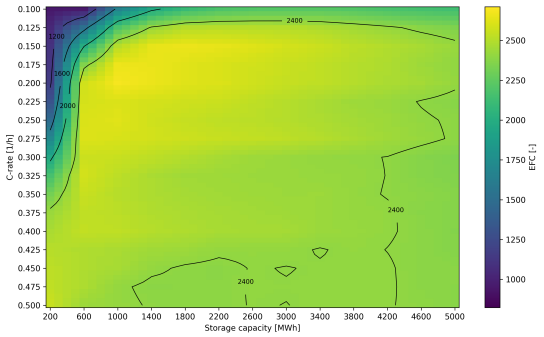

(f) Equivalent Full Cycles with End-of-Life defined at 70% State of Health in 2024.

Figure C.2: Estimated battery lifetimes for different storage capacities and C-rates in 2022, 2023, and 2024, assuming an End-of-Life (EoL) State of Health (SoH) threshold of 70%. The corresponding total number of Equivalent Full Cycles (EFC) for each SoH threshold is also presented as a function of storage capacity and C-rate. The simulations are performed for a 1 GW wind farm combined with Li-ion battery storage, including marginal degradation costs, daily degradation, and with participation in both the day-ahead and aFRR markets.

An interpretation of the results presented in this Section is provided in Section 4.3.1.

D

D.1. Additional results of Section 4.3.2

Figure D.1 presents the Net Present Value (NPV) analysis of the wind farm combined with Li-ion battery storage, based on input data from 2022.

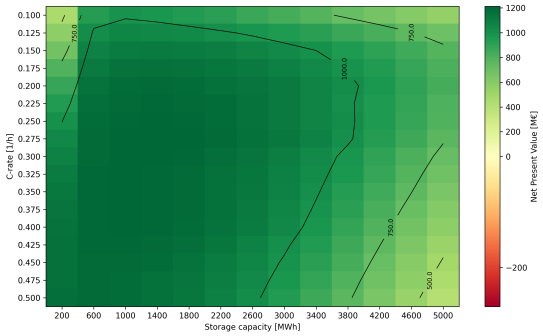

(a) NPV for wind with Li-ion storage, with $r = 5\%$

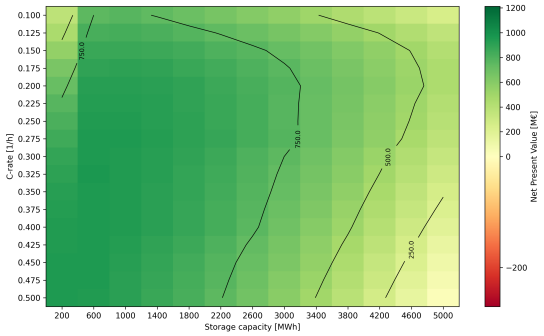

(b) NPV for wind with Li-ion storage, with $r = 7\%$

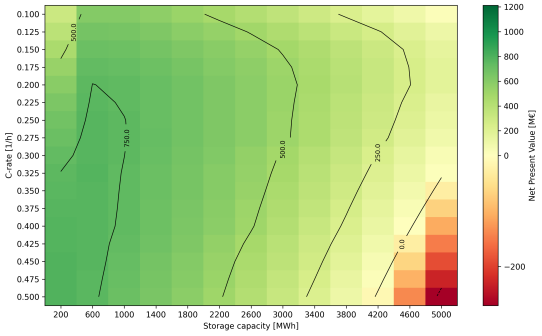

(c) NPV for wind with Li-ion storage, with $r = 9\%$

Figure D.1: Net Present Value (NPV) analysis of a 1 GW wind farm with Li-ion storage across different energy capacities and C-rates, including marginal degradation costs and daily degradation, participation in day-ahead and aFRR markets, based on 2022 data and evaluated at various discount rates.

Figure D.2 shows the NPV analysis of the wind farm combined with Li-ion battery storage, based on input data from 2023. Figure D.3 illustrates the NPV analysis of the wind farm combined with LPCAES, based on input data from 2022. Finally, Figure D.4 presents the NPV analysis of the wind farm combined with LPCAES, based on input data from 2023.

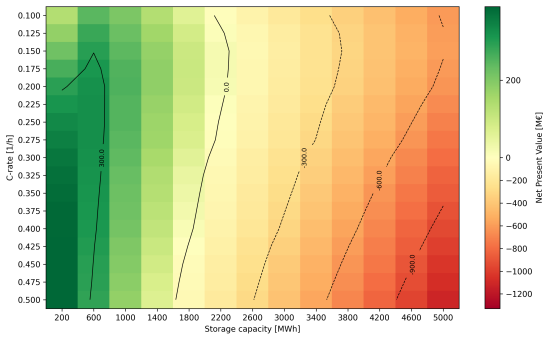

(a) NPV for wind with Li-ion storage, with $r = 5\%$

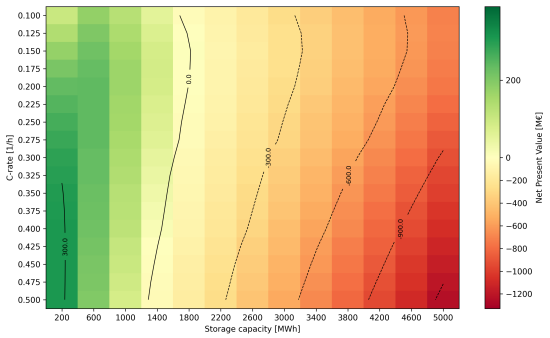

(b) NPV for wind with Li-ion storage, with $r = 7\%$

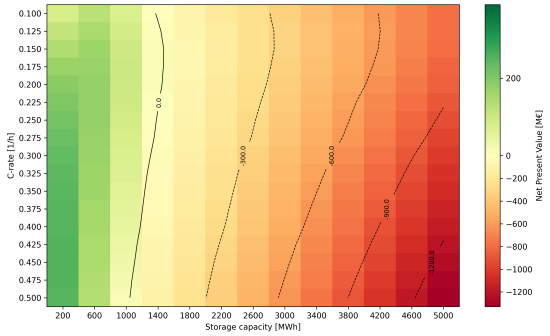

(c) NPV for wind with Li-ion storage, with $r = 9\%$

Figure D.2: Net Present Value (NPV) analysis of a 1 GW wind farm with Li-ion storage across different energy capacities and C-rates, including marginal degradation costs and daily degradation, participation in day-ahead and aFRR markets, based on 2023 data and evaluated at various discount rates.

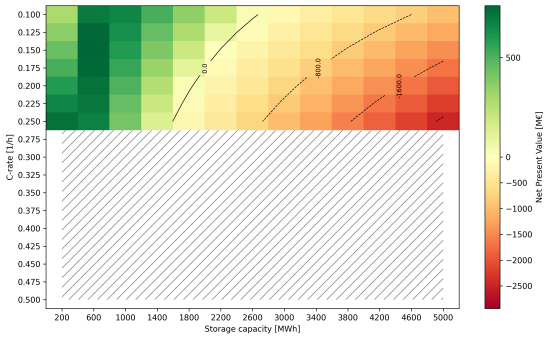

(a) NPV for wind with LPCAES, with $r = 5\%$

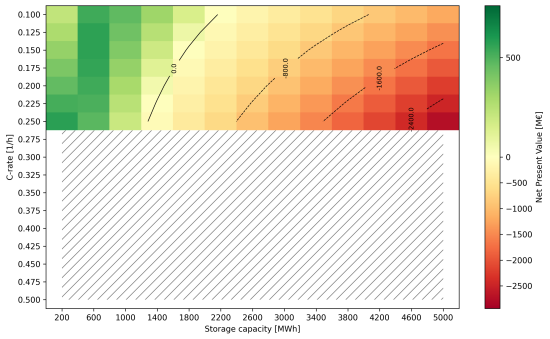

(b) NPV for wind with LPCAES, with $r = 7\%$

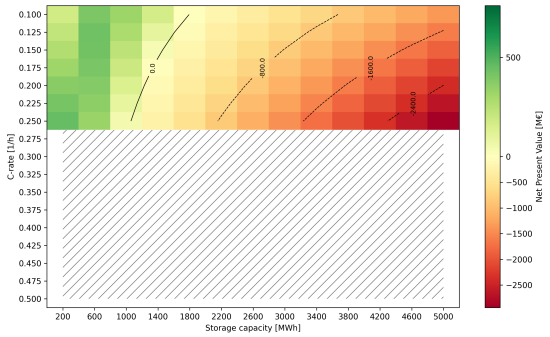

(c) NPV for wind with LPCAES, with $r = 9\%$

Figure D.3: Net Present Value (NPV) analysis of a 1 GW wind farm with LPCAES storage across different energy capacities and C-rates, with participation in day-ahead and aFRR markets, based on 2022 data and evaluated at various discount rates.

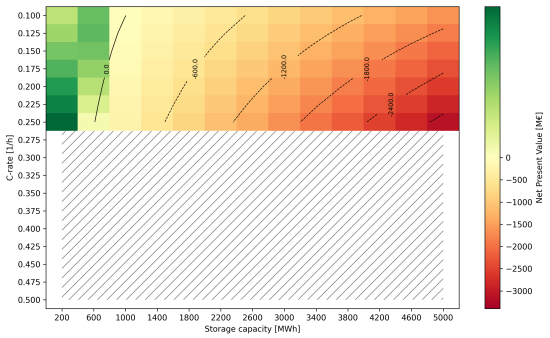

(a) NPV for wind with LPCAES, with $r = 5\%$

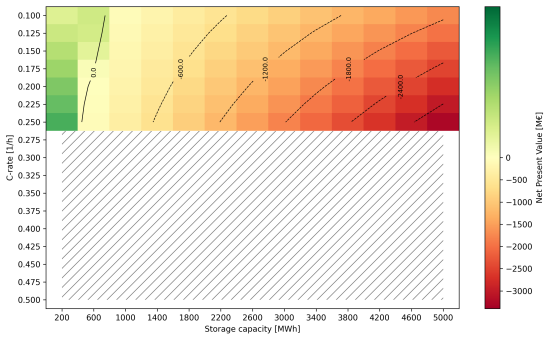

(b) NPV for wind with LPCAES, with $r = 7\%$

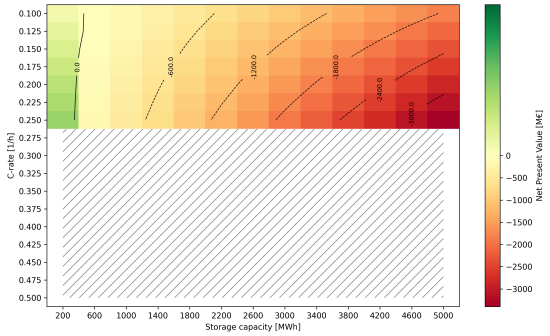

(c) NPV for wind with LPCAES, with $r = 9\%$

Figure D.4: Net Present Value (NPV) analysis of a 1 GW wind farm with LPCAES storage across different energy capacities and C-rates, with participation in day-ahead and aFRR markets, based on 2023 data and evaluated at various discount rates.

An interpretation of the results presented in this Section is provided in Section 4.3.2.